(2)

Systematic Studies on the Mixed-Valence States of Perovskite-Type Transition-Metal Complexes $Cs_2Au_2X_6$ (X=Cl, Br, I)

A Thesis

Submitted to

Kyoto University

for the Degree

of

Doctor of Science

by

Hiroshi Kitagawa

December, 1991

The author is thankful to Professor Tsuyoshi Murao (University of Osaka Prefecture) for his valuable discussions.

The author wishes to express his indebtedness to Professor Tsuyoshi Nakajima (Kyoto University) for his help to the XPS measurement.

The author wishes to express his indebtedness to Professor Hiroshi Sakai(Hiroshima University), Professor Yutaka Maeda (Kyoto University), Dr. Makoto Seto(Japan Atomic Energy Research Institute) for their help to the ^{197}Au Mössbauer measurement.

The author wishes to express his indebtedness to Mr. Fujitsugu Amita(Kyoto University) and Professor Masaru Nakahara(Kyoto University) for their help to the electrical conductivity under high pressure.

The author wishes to express his indebtedness to Dr. Takumi Kikegawa(National Laboratory for High Energy Physics), Dr. Osamu Shimomura(National Institute for Researches in Inorganic Materials), and Mr.Hirohiko Sato(Kyoto University) for their help to the structure analysis under high pressure.

The author wishes to express his indebtedness to Professor Nobuo Mori(The University of Tokyo), Dr.Hiroki Takahashi(The University of Tokyo), and Mr.Yasushi Okayama(The University of Tokyo) for their help to the electrical conductivity measurement under high pressure.

The author thanks Professor Yoshitami Ajiro(Fukui University) and Hikomitsu Kikuchi(The University of Tsukuba) for helping with the ESR measurements.

The author thanks Professor Keisaku Kimura(Himeji Institute of Technology) and Shunji Bando (Institute for molecular Science) for helping with the XPS measurements.

The author expresses his appreciation from the bottom of his heart to Drs.Masako Tanaka, Naohilo Watanabe(Kyushu Institute of Technology),Hisashi Togasi(Institute of Chemistry and Technology),Iwao Mogi(Institute for Material Research, Tohoku University),Kazuya Suzuki(Tokyo institute of Technology), Shoichi Kutsumizu(University of Gifu) and in specialty Dr. Nobuyuki Matsushita(University of Tokyo) for their helpful discussions and continuous encouragement.

Thanks are given to all the members of laboratory of Professor Gunji Saito for their encouragement and various discussions.

The author gives his thanks to Professor Tadaoki Mitani, Dr.Hiroshi Okamoto and Dr.Shuuji Asaka(Institute for Molecular Science) for their encouragement.

Finally, the author would like to express his heartfelt thanks to his parents and his fiancée Kaori Maruyama for continuous helping and encouragement.

Contents

CHAPTER 1

General Introduction

Mixed-valence compounds play an important role in many field. Although the major matter of the subject has been in chemistry, its importance has become increasingly clear in solid state physics, biology, materials science, and geology. Extensive investigation in the field of molecular metals has demonstrated that mixed valency is a prerequisite for high electrical conductivity. The electron-transfer properties of certain mixed-valence metalloproteins are important in biological processes.

'Mixed valency' has been used to describe inorganic or metal-organic compounds in which a given element is present in more than one level of oxidation. In the past, compounds in which an element occurs in different valency states has gone by various names, the terms 'non-integral oxidation state', oscillating valency', or 'mixed-oxidation state'. A classification scheme presented by Robin and Day[1] in a

landmark review distinguishes three different classes of materials:

Class I Compounds in which the valency states occupy different crystallographic sites and are too distant from each other to allow electron interaction.

Class II Compounds in which electron exchange among inequivalent sites takes place as a thermally activated process.

Class III a Compounds in which itinerant electrons are delocalized between atoms within discrete polynuclear cluster ions.

Class III b Compounds in which itinerant electrons are delocalized between atoms on identical crystallographic sites.

Robin and Day maintain that the compounds must be sufficiently ionic to enable the assignment of discrete oxidation states or to ascribe on-going electron delocalization to an interaction that involves predominantly the atoms whose valencies are under discussion. This picture excludes materials where covalency or metallic bonding effects between the constituent atoms are thought to render impossible the decision on how many valence shell

electrons are to be assigned to each atom. On the other hand, it is known that in intermetallic rare earth materials the existence of localized states leaves the valence concept still valid and the Robin-Day classification scheme may be extended to include these materials. The question whether the electronic configuration is seen as static, intermediate, or fluctuating depends largely on the inherent time scale of the observation method. It must be admitted that the Robin-Days mixed-valence concept is valid still now, but as described above their classification has its limits. In order to create a new concept of a mixed valency, we need to investigate the boundary region of class Ⅰ-Ⅱ or Ⅱ-Ⅲ.

Cesium gold chloride $Cs_2Au_2Cl_6$ is known as a three-dimensional halogen-bridged mixed-valence system, which is considered to be the boundary region of classⅡ-Ⅲ. In this case, we may observe transient states from class Ⅱ to class Ⅲ by means of an external perturbation such as an application of pressure.

This compound was first prepared by Wells in 1922.[2] It was described as astonishingly jet black in color, from which a metal-metal interaction was considered to exist. So this compound was expected to be an Au^{I}-Au^{III} mixed-valence compound, though the formal oxidation state of gold appeared to be + Ⅱ from the empirical formula $CsAuCl_3$. The crystal

structure was determined by Elliott and Pauling[3,4] in the 1930s (Figure 1). They investigated it by X-ray powder photograph and magnetic susceptibility measurements in order to obtain information regarding the valence state of the gold. Four possible structure types for $CsAuCl_3$ were considered which are reminiscent of the today's Robin-Day mixed-valence concept.

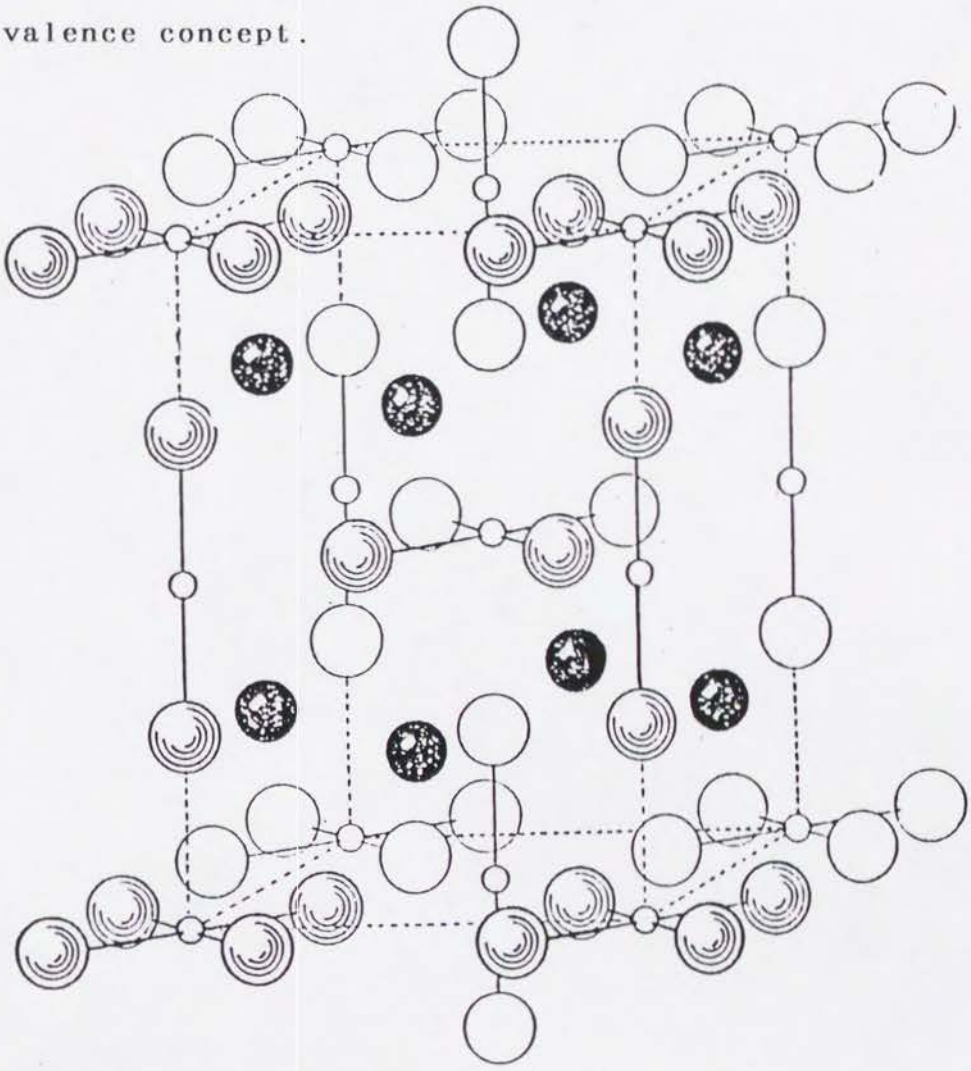

Fig.1 The atomic arrangement in tetragonal crystals of $Cs_2AuAuCl_6$. Large full circles represent cesium atoms, large open circles chlorine atoms, and small circles gold atoms.[4]

(1) *Each heavy metal atom may be bivalent and not attached by covalent bonds to other heavy metal atoms.*

(2) *Both heavy metal atoms may be bivalent, the two being joined by a covalent bond forming the group.*

(3) *One heavy metal atom may be univalent and the other trivalent.*

(4) *Each heavy metal atoms may resonate between a univalent and a trivalent state*

It is surprising that they had this idea in 1934, in view of the fact that chemists in those days had not both a term and a concept of "mixed valency".

Subsequently, much work on $Cs_2Au_2Cl_6$ have been done (e.g., high-pressure conductivity,[5] single crystal X-ray diffraction,[6] high-pressure neutron diffraction,[7] high-pressure single crystal X-ray diffraction,[8] high-pressure Mössbauer,[9] Mössbauer[10] and X-ray absorption near-edge structure (XANES).[11] On the other hand, to our knowledge, there has been little work on $Cs_2Au_2Br_6$ or $Cs_2Au_2I_6$.

Several years ago the author made a target on this mixed-valence system from motives of the followings. The author has been interested in the similarity of the crystal structure between this system and the mixed-valence perovskite-type bismuth(Ⅲ,Ⅴ) oxide $BaBiO_3$ which is a parent compound of the superconducting oxide $Ba(PbBi)O_3$. In those days $Ba(PbBi)O_3$ became of interest as an exotic

superconductor from the phenomena that in spite of a low carrier concentration and a low density of states a superconducting transition is at high temperature above 10 K, and that the origin of a superconductor-semiconductor transition was not established.[12,13] In $Ba(PbBi)O_3$ the bismuth valence state has been considered as a very important factor for a comprehension of its physical properties. The insulating state of $BaBiO_3$ was explained by the charge disproportionation of the bismuth cations (+Ⅳ into +Ⅲ and +Ⅴ) which couples to lattice deformation or the stabilization of a commensurate charge-density wave. To our interest, a possibility of an usual superconducting state, which results from condensation of bipolarons, is postulated under a strongly coupled electron-phonon system.[14] These bipolarons can be thought of as localized Cooper-pairs that are stable as long as the deformation-induced mutual attraction exceeds the mutual Coulomb repulsion.
According to the model, Cooper-pairs formation due to the condensation of bipolarons occurs under some electron-phonon coupling constant λ, while in the large λ limit bipolarons formation occurs (Figure 2). In this model the insulating $BaBiO_3$ is regarded as an on-site bipolaronic state where bipolarons form a three-dimensional lattice and localize at $Bi^{Ⅲ}$ site. We may regard $CsAuX_3$ as a bipolaronic insulator such as $BaBiO_3$. Is the possibility of superconducting

state of this type present in $CsAuX_3$?

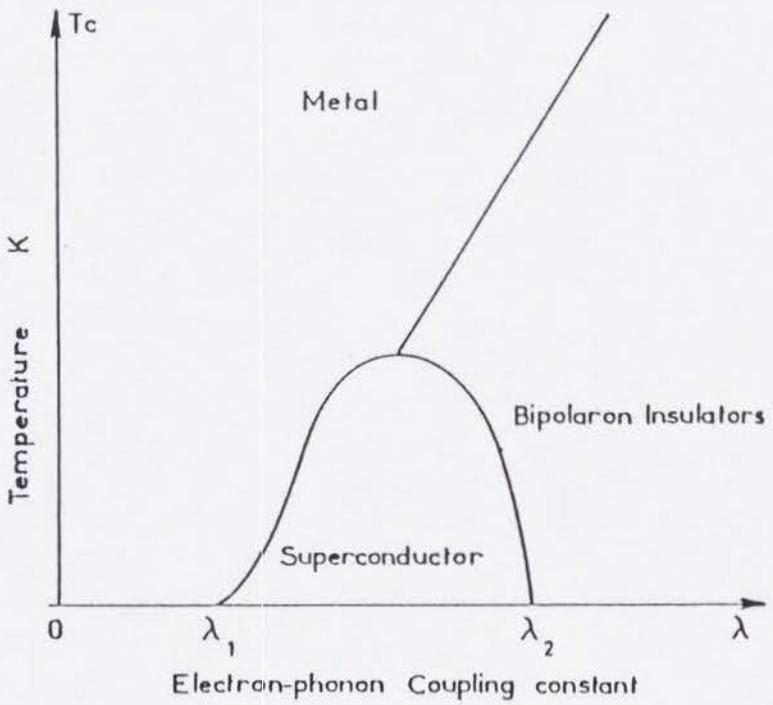

Fig.2 Phase diagram as a function of electron-phonon coupling strength.[14]

The author also has been interested in a three dimensionality. $Cs_2Au_2X_6$ is a rare three-dimensional halogen-bridged mixed-valence system.

These twenty years halogen-bridged one-dimensional mixed-valence complexes analogous to Wolffram's Red Salt have been investigated intensively from the viewpoints of physics and chemistry as a model of one-dimensional electrons system[15] and recently they become of interest of the

relaxation process from the photo-excited state from a dynamical behavior of lattice-relaxed excitations such as a soliton or a polaron.[16-19] On the other hand, there has been little work on the three-dimensional system. Therefore, researches on material and physical-property are indispensable for this system. As described in Chapter 2, there is an anisotropy in the three-dimensional -X-Au-X-Au- networks, which is expected to cause an anisotropic charge-transfer interaction. It is interesting to investigate the relationship between the anisotropy of the crystal structure and that of the electronic structure.

This salt can be characterized by metal-complex-ion assembly. The linear $[Au^{I}X_2]^-$ and square-planar $[Au^{III}X_4]^-$ complex ions are stacked alternately and the three-dimensional crystal structure is formed. An application of pressure may effect on the metal-complex-ion assembly as an useful external perturbation.

An application of pressure is an appropriate tool for probing the electronic structure widely and consequently, which can alter physical properties owing to the consequent changes in the lattice parameter and the energy of the various interactions between electrons or between electron and phonon. Under high pressure, interactions between metal complex ions $[Au^{I}X_2]^-$ and $[Au^{III}X_4]^-$ such as the charge-transfer interaction is

expected to become large. Therefore, as the pressure is increased, the nature as a condensed matter play more important role in the solid-state properties than that of each of component complex ions.The high-pressure experiments is of great interest in revealing the various properties in this system. Interrante *et al.*[20] measured electrical conductivities of various one-dimensional halogen-bridged mixed-valence complexes under high pressure. As is shown in Figure 3, the conductivity is enormously enhanced at high pressure with values at ~ 100 Kbar pressure as high as 2 $\Omega^{-1}cm^{-1}$. This observation was explained with the aid of the schematic energy level diagram in Figure 4, which shows the anticipated changes in the M dz^2 and halogen pz energy levels as the M^{II}--- X distance decreases under high pressure.

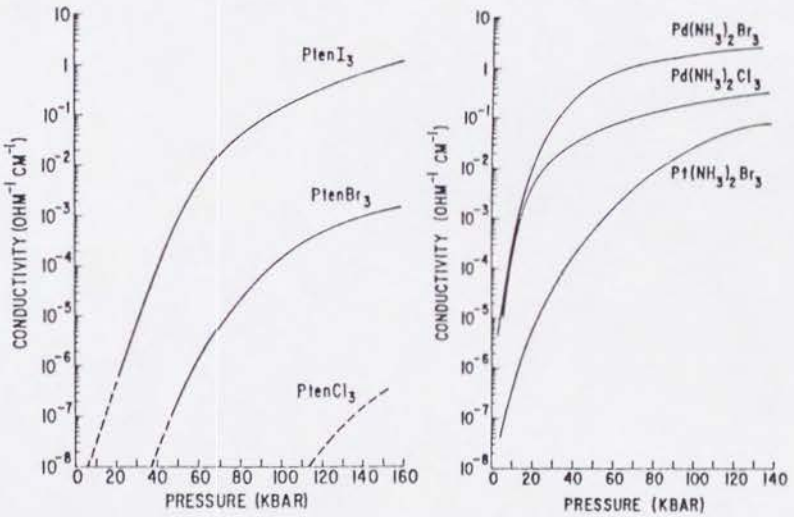

Fig.3 The conductivity of the $M(A)_nX_3$ complexes as a function of pressure.[20]

In particular, a broadening of the energy bands due to the increased M^{II}-dz^2 —halogen pz orbital overlap, along with a general merging of the two dz^2 bands as the environment about the metal ions becomes more nearly equivalent, was expected.

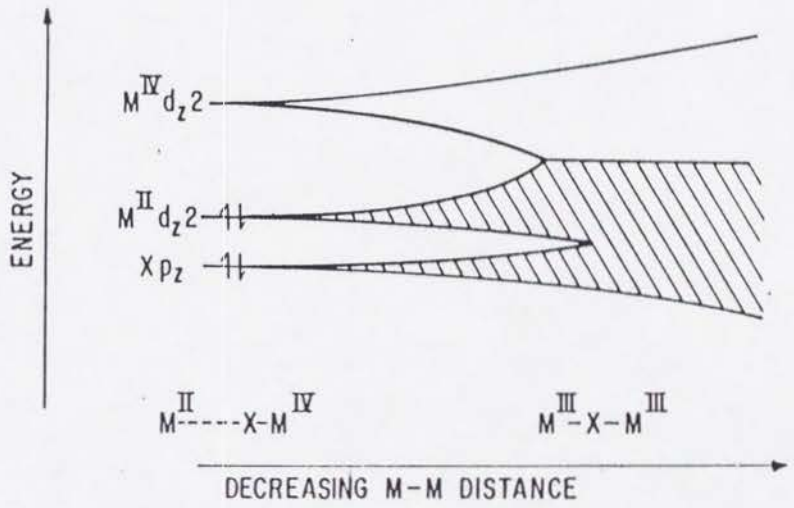

Fig. 4 Anticipated changes in the $M(A)_nX_3$ electronic structure as the M^{II}-M^{IV} distance decreases under pressure[20]

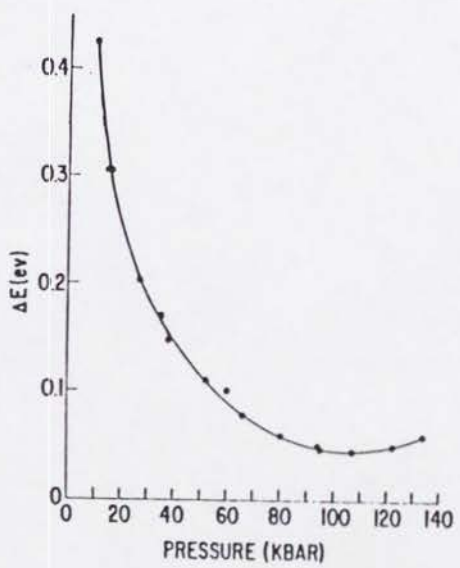

Fig.5 ΔE as a function of pressure for $Pd(NH_3)_2Br_2$.[20]

At the limit of equal metal-halogen distance, this should ultimately lead to a transition to a system with half-filled, one-dimensional metallic band. However there has been no indication of a change in sign as would be expected for the transition to a metallic state (Figure 5). This behavior is considered to arise from Peierls instability characteristic of the one-dimensional electron-lattice system. However, this instability can be suppressed by increasing the dimensionality. The three-dimensional system $Cs_2Au_2X_6$ under high pressure is of great interest in seeking the metallic-conduction behavior or superconductivity.

From these interests described above, the author has performed a series of investigation on $Cs_2Au_2X_6$.
In the course of the present study, the author has concentrated on the systematic investigation for the mixed-valence states of $Cs_2Au_2X_6$ system to elucidate a relationship between the crystal and electronic structures.

In Chapter 2 the author discusses an anisotropy of the crystal structure. Chapters 3-5 deal with mixed-valence states, anisotropy of the charge-transfer interaction and optical properties in this system. Especially as to the dimensionality of electronic structure, Mössbauer spectroscopy and polarized reflectance spectroscopy have been done.

In Chapter 6, the author reports the behavior of the

electrical conductivity of $Cs_2Au_2X_6$ under pressure.

In Chapter 7, X-ray crystal analysis of $Cs_2Au_2I_6$ are presented. The author discusses the relationship between the electrons system and lattice system.

In Chapter 8, electrical properties under high pressures and low temperatures are described. Several resistance anomalies are presented.

References

1 M.B.Robin and P.Day, *Adv.Inorg.Chem.Radiochem.*,10 (1967) 247.

2 H.L.Wells, *Am.J.Sci.*,3 (1922) 315.

3 N.Elliott, *J.Chem.Phys.*,3 (1934) 419.

4 N.Elliott and L.Pauling, *J.Am.Chem.Soc.*,60 (1938) 1846.

5 R.Keller,J.Fenner and W.B.Holzapfel, *Mater.Res.Bull.*,9 (1974) 1363.

6 J.C.M.Tindemans-v.Eijndhoven and G.C.Verschoor, *Mater. Res.Bull.*,9 (1974) 1363.

7 P.Day,C.Vettier and G.Parisot, Inorg.Chem.,17 (1978) 2319.

8 W.Denner,H.Schulz and H.D'Amour, *Acta Cryst.*,A35 (1979) 360.

9 J.Stanek, *J.Chem.Phys.*,76 (1982) 2315.

10 M.Katada,Y.Uchida,K.Sato,H.Sano,H.Sakai and Y.Maeda, *Bull. Chem.Soc.Jpn.*,55 (1982) 444.

11 H.Tanino and K.Takahashi, *Solid State Commun.*,59 (1986) 825

12 D.E.Cox and A.W.Sleight, *Solid State Commun.*,19 (1976) 969.

13 T.D.Thanh,A.Koma and S.Tanaka, *Appl.Phys.*,22 (1980) 205.

14 B.K.Chakraverty, *J.Phys.(Paris) Lett.*, 40 (1979) L99.

15 H.J.Keller, "Extended Linear-chain Compounds" J.S. Miller,ed. (Plenum,New York, 1982) vol.1, p.357.

16 N.Kuroda, M.Sakai, Y.Nishina, M.Tanaka and S.Kurita, *Phys.Rev.Lett.*58 (1987) 2122.

17 N.Matsushita,N.Kojima,T.Ban and I.Tsujikawa, *J.Phys.Soc. Jpn.*,56 (1987) 3808.

18 S.Kurita, M.Haruki and K.Miyagawa, *J.Phys.Soc.Jpn.*,57 (1988) 1789.

19 H.Okamoto,K.Okaniwa,T.Mitani,K.Toriumi and M.Yamashita, *Solid State Commun.*, 77 (1991) 465.

20 L.V.Interrante, K.W.Browall and F.P.Bundy, *Inorg.Chem.*,13 (1974) 1158: L.V.Interrante and K.W.Browall, *Inorg.Chem.*, 13 (1974) 1162.: L.V.Interrante and F.P.Bundy, *J.Inorg. Nucl.Chem.*,39 (1977) 1333.

CHAPTER 2

Structural Discussion of $Cs_2Au_2X_6$ (X=Cl, Br, I) and the Mixed-Valence State of $CsAu_{0.6}Br_{2.6}$

2-1 INTRODUCTION

In this chapter, we will discuss the characteristics of the crystal structure of this mixed-valence system in which linear $[Au^{I}X_2]^-$ and square planar $[Au^{III}X_4]^-$ complexes are formed alternately. Consequently, there is an anisotropic three-dimensional $-Au^{I}-X-Au^{III}-X-$ networks which we need to take into consideration in the charge-transfer interaction between the Au^{I} and Au^{III} ions. Secondly, we will report on a new non-stoichiometric cesium bromoaurate $CsAu_{0.6}Br_{2.6}$. In order to achieve a precise characterization of this compound, we have performed a detailed investigation by X-ray powder diffraction, ESR, electrical conductivity,

XPS,[1] and Mössbauer spectroscopy.[2]

2-2 EXPERIMENTAL

Preparation of Au Compounds—(a)$Cs_2Au_2Br_6$.The jet black mixed-valence compound $Cs_2Au_2Br_6$ was prepared by a Bridgeman technique. A powdered mixture of CsBr,Au,and $CsAuBr_4$ in the stoichiometric ratio was sealed in an evacuated quartz tube with a capillary. The capsule was placed in a furnace equipped with a temperature gradient of 5 K/cm (T_{max} was about 770 K). The melting point of this compound, as measured by differential scanning calorimetry (DSC), was near 725 K. The cooling rate for growth was *ca.* 0.4 K/h. The molar ratio of Cs:Au was determined by using a Jarrel Ash AA-8200 atomic absorption and flame emission spectrophotometer at the Research Center of Instrumental Analyses of Kyoto University (Found: Au,34.1;Cs,23.6. Calc. for $Au_2Br_6Cs_2$:Au,34.6; Cs,23.3%).

(b)$CsAu_{0.6}Br_{2.6}$. This new compound $CsAu_{0.6}Br_{2.6}$ was prepared by a slow addition of CsBr(0.72 g) dissolved in absolute ethanol to $KAuBr_4$ $2H_2O$(1.50 g) dissolved in absolute ethanol and cooling. A jet black product precipitated rapidly and almost quantitatively. It was washed with cold ethanol and dried *in vacuo*. The molar

ratios of Cs:Au were determined by the method mentioned above. The molar ratios of Br were determined by energy-dispersive fluorescence X-ray analyses using a Rigaku Ultra-Trace System at the Environment Preservation Center, Kyoto University. The variation in x and y for $CsAu_xBr_y$ between baches prepared in this manner is small ($0.55<x<0.65$, $2.5<y<2.7$). All measurements recorded in this and the following chapters were performed for the sample with x=0.6, y=2.6 (Found:Au,25.7;Br,44.8;Cs,28.9. $Au_{0.6}Br_{2.6}Cs$ requires Au,25.8;Br,45.2;Cs,29.0%).

X-Ray Diffraction—The phase identification of each compound was made with an X-ray diffractometer with monochromatic CuKα radiation. The lattice parameters were determined by least-squares fits to the measured positions of the high-angle reflections.

ESR Spectroscopy—The ESR measurements were performed on powdered samples using a JEOL X-band spectrometer with a 100 kHz field modulation. Variable temperature from 3.7 K to 300 K was provided by means of a flowing-gas cryostat system (Oxford Instruments ESR-900). The temperature of the sample was measured by AuFe-normal silver thermocouple positioned near the sample. Calibration of g-values was based on dpph (diphenypicrylhydrazyl)(g=2.0036).

Electrical Conductivity—The d.c. electrical conductivity measurements were performed on polycrystalline samples with a quasi four-probe method. Samples were prepared by pressing powdered under pressure of 0.3 GPa into cylindrical pellets, 5 mm in diameter and typically 0.6 mm in thickness.

2-3 CRYSTAL STRUCTURE AND ITS ANISOTROPY of $Cs_2Au_2X_6$

The crystal structure of $Cs_2Au_2Cl_6$ is a distorted perovskite with square planar $[Au^{III}Cl_4]^-$ and linear $[Au^{I}Cl_2]^-$ complex ions, with space group *I4/mmm* (tetragonal, a=7.495(1), C=10.880(2)Å, Z=2).[3] As reported by Brauer and Sleater,[4] the powder X-ray diffraction patterns of $Cs_2Au_2Br_6$ and $Cs_2Au_2I_6$ show these two compounds to be isostructural with $Cs_2Au_2Cl_6$. Hence the compounds $Cs_2Au_2Br_6$ and $Cs_2Au_2I_6$ have been indexed to *I4/mmm*. Our very recent single crystal X-ray analysis of $Cs_2Au_2I_6$[5] shows it to belong to the tetragonal space group *I4/mmm*, with a=8.284(1), c=12.092(2)Å, and Z=2.

The crystal structure of $Cs_2Au_2Cl_6$ can be characterized by distorted corner-sharing $AuCl_6$ octahedra which form chains in the directions of a_1+a_2, a_1-a_2, and c, where the Tetragonal unit cell is (a_1, a_2, c), as shown in

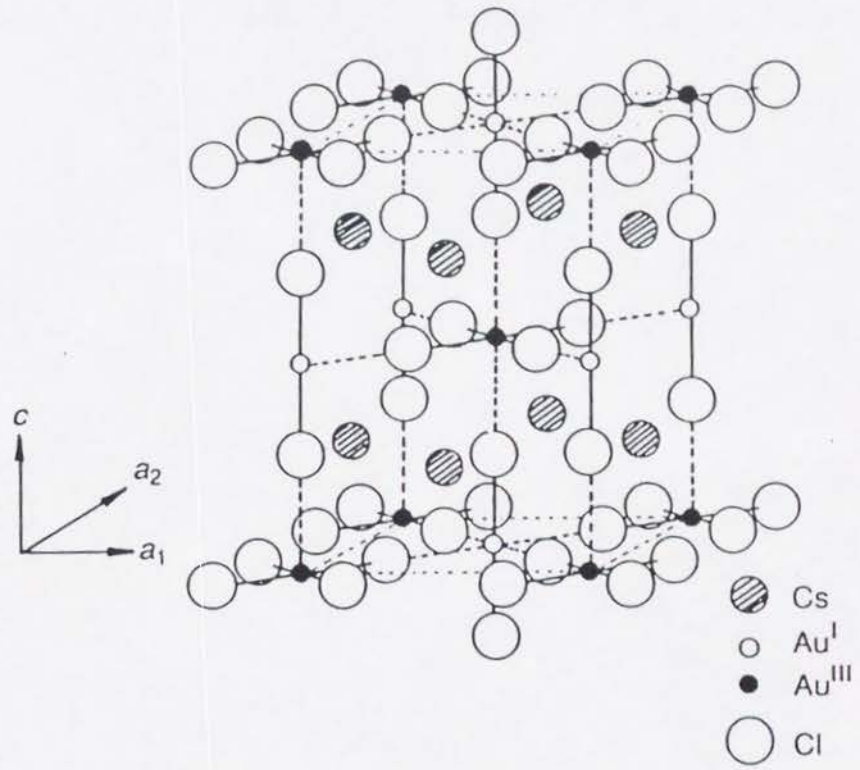

Fig. 1 Crystal structure of $Cs_2Au^IAu^{III}Cl_6$ (space group $I4/mmm$)[3,6]

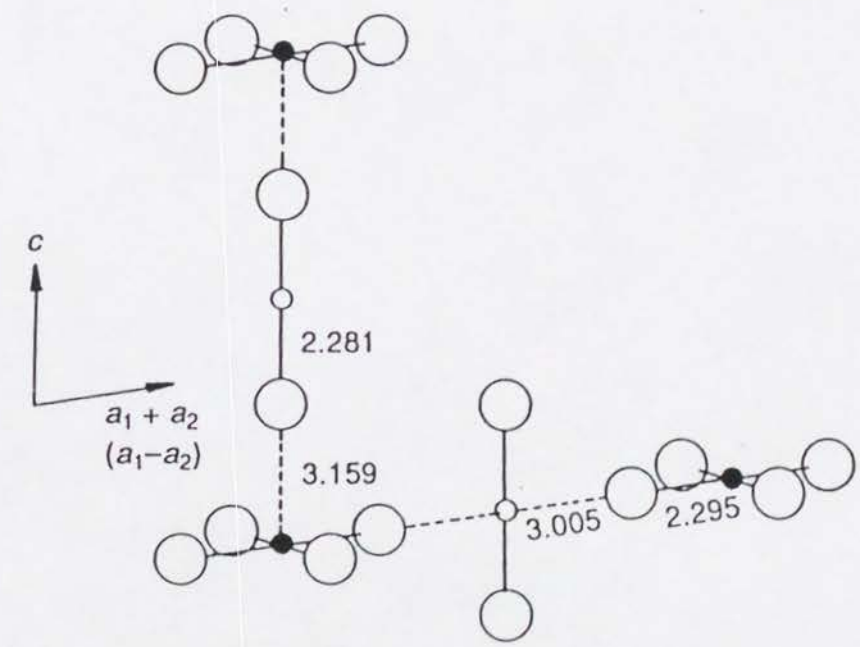

Fig. 2 Anisotropic AuCl chains in $Cs_2Au^IAu^{III}Cl_6$[6]

Figure 1. The $Au^{I}Cl_6$ octahedra are contracted in the c direction, on the other hand the $Au^{III}Cl_6$ ones are elongated in the c direction. The volume of $Au^{I}Cl_6$ octahedron (27.46 $Å^3$) is larger than that of $Au^{III}Cl_6$ one (22.18 $Å^3$). Hence the breathing-mode-type atomic distortion of $AuCl_6$ octahedra is present in this mixed-valence system. This distortion is analogous to that of the mixed-valence bismuth (Ⅲ-Ⅴ) oxide $BaBiO_3$ which is the parent compound of the Cu-free high-T_c superconducting oxides, $(Ba,K)BiO_3$ and $(Ba,Rb)BiO_3$ ($T_c \sim 30$ K), and $Ba(Pb,Bi)O_3$ ($T_c \sim 13$ K).[6-8] By analogy with these 3-D superconductors, the following correspondence may occur: $Cs^{+} \Leftrightarrow Ba^{2+}$, $Au^{I}, Au^{III} \Leftrightarrow Bi^{III}, Bi^{V}$ and $X^{-} \Leftrightarrow O^{2-}$.[9] The insulating state of $BaBiO_3$ was explained as the result of a commensurate charge-density wave (CCDW) involving the ordering of Bi^{III} and Bi^{V} into distinct crystallographic sites.[10] Therefore, the structure of $Cs_2Au_2X_6$ might be regarded as frozen in a soft mode of perovskite structure, resulting in a CCDW and a displacive modulation of the halogen positions. In recent years halogen-bridged one-dimensional M^{II}-M^{IV} mixed-valence complexes of Pt, Pd, and Ni analogous to Wolffram's Red Salt have been investigated intensively from the viewpoints of physics and chemistry as a model of one-dimensional electrons system.[11,12] On the other hand, there has been little work on the three-dimensional halogen-bridged mixed-

valence complexes [*e.g.* $Rb_2Au_2X_6$(X=Br or I),[13] $K_2Au_2I_6$,[14] PtI_3,[15] and Pt_3I_8.[16]]. Among the three-dimensional halogen-bridged mixed-valence complexes, $Cs_2Au_2X_6$ is a rare mixed-valence system in which three-dimensional —M—X—M—X— networks are orthogonal to each other. The three-dimensional networks in $Cs_2Au_2Cl_6$ are not isotropic but anisotropic, being $\cdots Cl\text{-}Au^{I}\text{-}Cl\cdots Au^{III}\cdots$ in the c direction and $\cdots Au^{I}\cdots Cl\text{-}Au^{III}\text{-}Cl\cdots$ in the a_1a_2 plane. In many halogen-bridged one-dimensional mixed-valence complexes of Pt, Pd, and Au, the bridging halogen ions lie closer to the more highly oxidized metal cations, as is realized in the a_1a_2 plane of $Cs_2Au_2Cl_6$. It seems strange that the bridging halogen anions lie closer to the Au^{I} cations in the networks of c direction. Also that the Au^{I}-Cl distance (2.281 Å) is shorter than the Au^{III}-Cl (2.295 Å). In general, as the oxidation state of a metal cation increases, the metal-ligand bond length becomes shorter. This implies that the covalency of the $Cl\text{-}Au^{I}\text{-}Cl$ bonds is rather high and that some d-s mixing[17] is present in the valence orbitals in spite of the d^{10} complex ion. If the electron pair occupying the d_{z^2} orbital of the free ion are put into the $(1/\sqrt{2})(5d_{z^2}-6s)$ orbital, the ligand anion can approximate more closely to the Au ion due to the promotion of electron density from the d_{z^2} to the s orbital which causes a significant reduction in the magnitude of the repulsion

between the metal d_{z^2} and the ligand p_z orbitals. The d-s mixing is important for the analyses of ^{197}Au Mössbauer spectra and we will discuss it in Chapter 4.[2]

Figure 2 shows a part of the three-dimensional networks in $Cs_2Au_2Cl_6$. From a structural point of view in $Cs_2Au_2Cl_6$, we consider that the charge-transfer interaction between Au^{I} and Au^{III} through the bridging halogens would be stronger in the networks in the a_1a_2 plane than those in the c direction. This consideration is due to the following reasons.

1) The $Au^{I}\cdots Au^{III}$ distance (5.300 Å) in the networks in the a_1a_2 plane is shorter than that (5.440 Å)in the networks in the c direction.

2) The ratio $p = |d_1-d_2|/(d_1+d_2)$, where d_1 and d_2 are the Au^{I}-X and Au^{III}-X distances, respectively, is an indication of the deviation of the bridging halogen ion from the midpoint between the Au^{I} and Au^{III} sites. As the charge-transfer interaction becomes stronger, the difference of the oxidation states between Au^{I} and Au^{III} decreases and then the ratio p decrease. The value of p in the networks of the a_1a_2 plane (0.13) is smaller than that in the networks of the c direction (0.16).

3) The $Au^{I}\cdots Cl$ distance (3.005 Å) in the networks of the a_1a_2 plane is shorter than the $Au^{III}\cdots Cl$ distance (3.159 Å) in the networks of the c direction.

4) As mentioned above, in many halogen-bridged one-

dimensional mixed-valence complexes, the bridging halogen ions lie to the more highly oxidized metal cations, as in the networks in the a_1a_2 plane. This shows that the more highly oxidized metal cations possess unoccupied acceptor orbitals. As pointed out by Robin and Day,[18] the d_{z^2} orbital of the $[Au^{I}Cl_2]^-$ ion and the $d_{x^2-y^2}$ orbital of $[Au^{III}Cl_4]^-$ ion are orthogonal in the networks of the c direction. On the other hand, those orbitals in the networks of the a_1a_2 plane have nonzero overlap. They considered that the donor and acceptor orbitals were the d_{z^2} orbital of the $[Au^{I}Cl_2]^-$ ion and the $d_{x^2-y^2}$ orbital of $[Au^{III}Cl_4]^-$ ion, respectively. However, the overlap between those orbitals is considered to be small, and both the d_{z^2} orbitals of the $[Au^{I}Cl_2]^-$ and the $[Au^{III}Cl_4]^-$ ions are occupied. Therefore, we consider that the charge-transfer interaction in $Cs_2Au_2Cl_6$ is mainly between the donor $d_{x^2-y^2}$ orbital of $[Au^{I}Cl_2]^-$ ion and the acceptor $d_{x^2-y^2}$ orbital of $[Au^{III}Cl_4]^-$ ion in the networks of the a_1a_2 plane.

5) The intervalence charge-transfer absorption spectra have been observed for the halogen-bridged one-dimensional mixed-valence gold complexes AuX_2(DBS) (X=Cl or Br, DBS= dibenzyl sulfide)[19] which possess networks analogous to those in the a_1a_2 plane of $Cs_2Au_2Cl_6$. Recently, Janiak and Hoffmann have carried out band-structure calculations on AuX_2(DBS) by using the extended-Hückel method.[20] They

consider that the intervalence charge-transfer transition occurs between the $d_{x^2-y^2}$ orbitals of Au^{I} and Au^{III}. We have systematically investigated the anisotropic charge-transfer interaction in $Cs_2Au_2X_6$ by changing the bridging halogen X from Cl to I as a method for modifying the interaction and details on this will be reported in Chapter 3 (XPS study)[1] Chapter 4 (Mössbauer study)[2] and Chapter 5 (polarized reflectance spectroscopy).

2-4 Powder X-ray Diffraction Profiles of Cs-Au-Br mixed-valence system

The powder X-ray diffraction profile was obtained at room temperature for the $Cs_2Au_2Br_6$ compound prepared by Bridgeman technique. It is similar to that obtained by other workers[4] for the same compound prepared by thermal decomposition of $CsAuBr_4$. Their work indicated that the compound crystallizes with a structure isomorphous with that of Wells salt, $Cs_2Au_2Cl_6$, leading to the conclusion that Br_6 coordination octahedra of Au^{I} and Au^{III} (*i.e.* $Au^{I}Br_6$ and $Au^{III}Br_6$) are crystallographically non-equivalent. In the profile obtained, each doublet (*e.g.*[(002),(110)],[(112),(200)]) is due to the difference between the $Au^{I}\cdots Au^{III}$ distances in the a_1a_2 plane ($d_{a_1a_2}$ = 5.44 Å) and the z direction (d_c = 5.57 Å). The

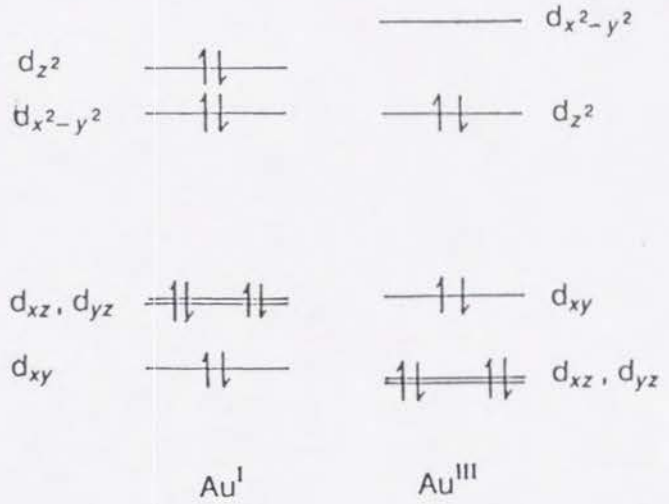

Fig. 3 Schematic energy-level diagram for 5d orbitals of Au^{I} and Au^{III} in $Cs_2Au_2X_6$

presence of weak superstructure reflections (*e.g.*(103),(301)) indicates that the Br atoms are shifted from the symmetrical position between the Au atoms. The intensities of the powder lines of $Cs_2Au_2Br_6$ were calculated by assuming tetragonal space group *I4/mmm*, with a=7.69 Å, C=11.38 Å, Z=2, using the atomic scattering factors given by ref.21 and the positional parameters reported for $Cs_2Au_2Cl_6$[3].

No absorption correction was applied. A typical observed diffraction profile and the calculated profile of the tetragonal phase $Cs_2Au_2Br_6$ are shown in Figure 4. All the reflections present are indicative of single phase and do not contradict the distorted perovskite structure with space group *I4/mmm*. The agreement between observation and calculation shows that $Cs_2Au_2Br_6$ possesses the similar anisotropic MX networks to those of $Cs_2Au_2Cl_6$. The $Cs_2Au_2Br_6$ compounds prepared by the Bridgeman technique is, therefore, considered to be a Robin-Day class II [22] mixed-

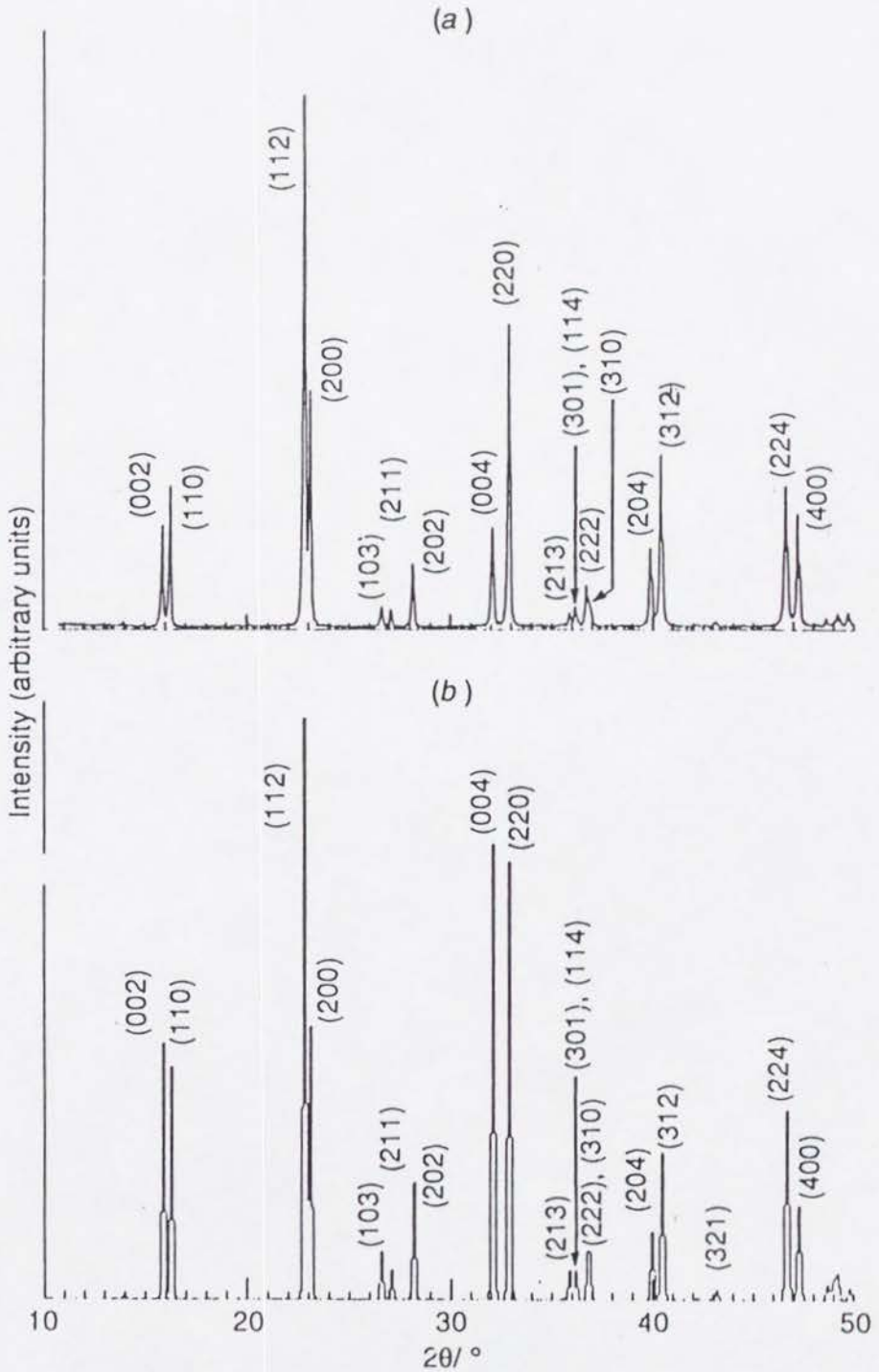

Fig. 4 Powder X-ray diffraction profiles of $Cs_2Au^{I}Au^{III}Br_6$: (*a*) observed, (*b*) calculated on the space group *I*4/*mmm*. The numbers indicate the indices of the Bragg reflections

valence compound.

The powder X-ray diffraction profile obtained at room temperature for the compound $CsAu_{0.6}Br_{2.6}$ differs significantly from that of the tetragonal phase. The small number of very sharp peaks indicates the high symmetry of the structure. Weak superstructure reflections were not observed. The intensities of the powder lines were calculated by assuming cubic lattice, *Pm*3*m* space group, a=5.46 Å, Z=1 (the cubic perovskite structure with the Cs atoms on the lattice sites of Sr, the Au atoms on the sites of Ti, and the Br atoms on the sites of O in strontium titanate $SrTiO_3$.). The same values of atomic scattering factors as those in $Cs_2Au_2Br_6$ were used. A typical observed diffraction profile and the calculated profiles of the compound $CsAu_{0.6}Br_{2.6}$ are shown in Figure 5. In Figure 5(b) each of the Cs, Au, and Br sites is full occupancy, while in Figure 5(c) occupancies of the Cs, Au, and Br sites are 1.00, 0.60, and 0.87, respectively. As shown in Figure 5(a) and 5(c), the observed diffraction profile can be quantitatively reproduced, taking into account the vacancies of the Au and Br sites. This agreement is consistent with the presence of Au and Br vacancies found by atomic absorption analyses. No existence of weak superstructure reflections in the observed diffraction pattern indicates the simple cubic perovskite structure in which the Au and Br vacancies distribute

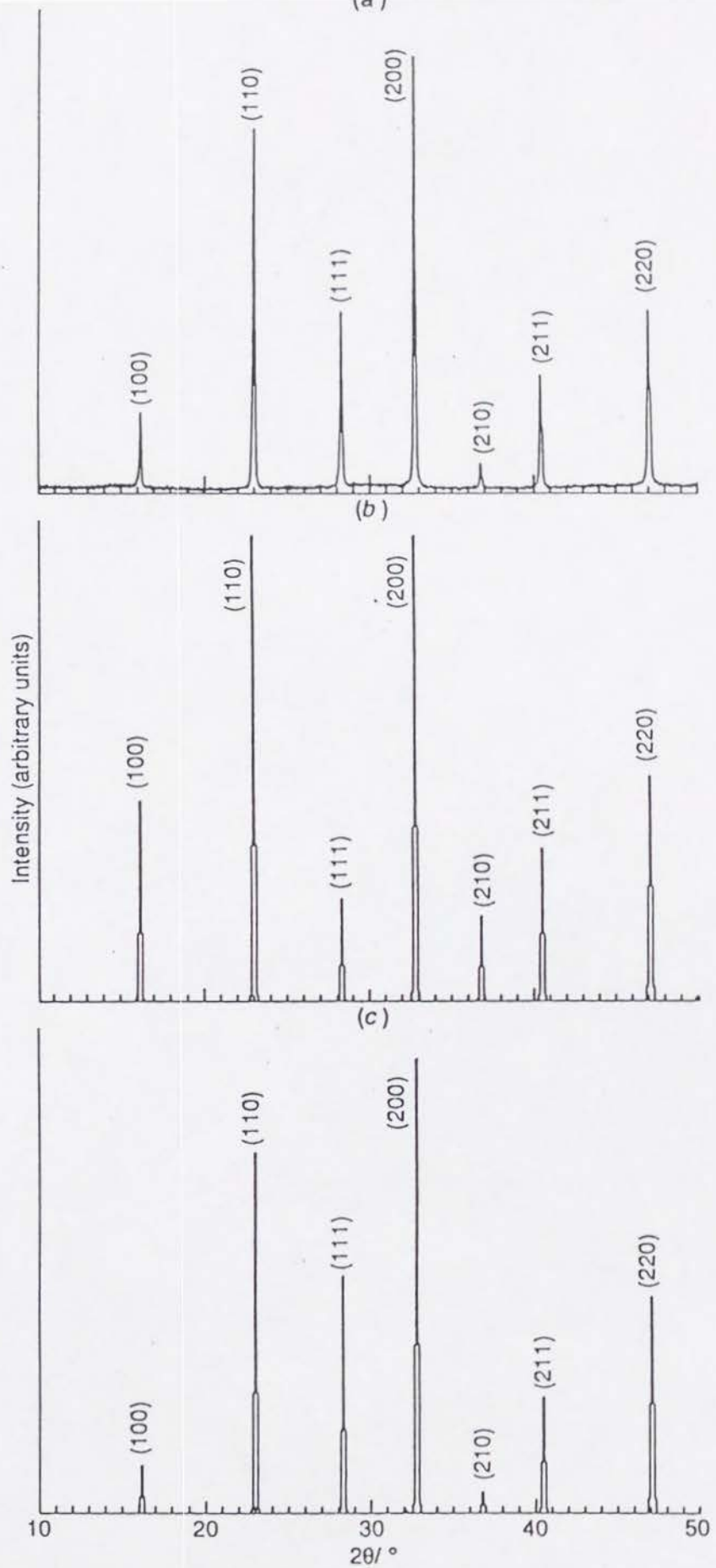

Fig. 5 Powder X-ray diffraction profiles of $CsAu_{0.6}Br_{2.6}$: (*a*) observed, (*b*) calculated on the space group *Pm3m* with full occupancies for the Cs, Au, Br sites, and (*c*) calculated based on the space group *Pm3m* with occupancies 1.00, 0.60, 0.87 for the Cs, Au, Br sites, respectively

randomly for B and X sites of ABX_3, respectively. Therefore any larger unit cell than the ABX_3 perovskite unit cell with a=5.46 Å can be neglected. From these results, we can conclude that the cubic phase compound $CsAu_{0.6}Br_{2.6}$ is a single phase with cubic perovskite structure (Cubic lattice, space group *Pm*3*m*, a=5.462(2) Å, Z=1.). This means that the $AuBr_6$ octahedra are crystallographically equivalent. In connection with the cubic phase compound $CsAu_{0.6}Br_{2.6}$, the following should be mentioned. The Au^{III} compound $Cs_{1.6}(Au^{III}Br_4)(Br_3)_{0.2}Br_{0.3}$, synthesized by Gütlich, *et al.*, crystallizes in a disordered cubic perovskite structure with a=5.475 Å.[23] However, the compositional ratio and the lattice constant differ from those of $CsAu_{0.6}Br_{2.6}$.

2-5 ESR SPECTRA OF the CUBIC PHASE

The Au^{II} valence state was hitherto unknown for Au complexes having infinite chains. Therefore, whether the gold ion in the non-stoichiometric compound $CsAu_{0.6}Br_{2.6}$ is present in a +II formal oxidation state or not is of great interest. A Au^{II} complex has one unpaired electron due to the $5d^9$ configuration. Since naturally occurring gold consists of 100% ^{197}Au, which has a nuclear spin of 3/2, solutions of Au^{II} complexes would be expected to give rise

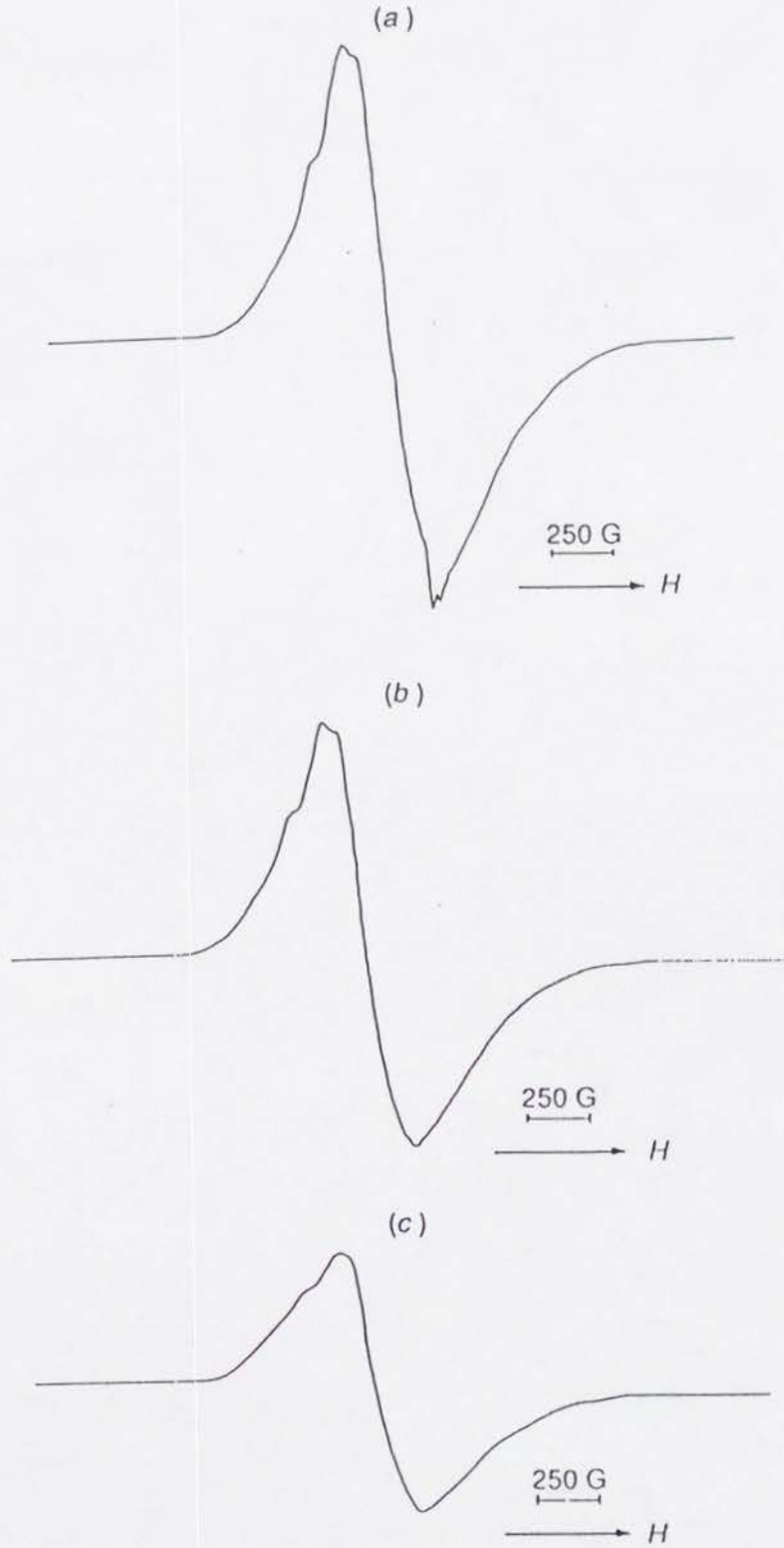

Fig. 6 Powder ESR spectra of $CsAu_{0.6}Br_{2.6}$ observed at (*a*) 3.7, (*b*) 77 and (*c*) 290 K

to electron spin resonance spectra consisting of four equally separated and equally intense lines. A solid complex would also be expected to display paramagnetic behavior. To investigate the oxidation state of Au in $CsAu_{0.6}Br_{2.6}$, ESR measurements were carried out.

In the solid state the spectrum consisting of one broad line. The observed X-band ESR spectra of the cubic phase compound $CsAu_{0.6}Br_{2.6}$ at 3.7, 77, and 290 K are shown in Figure 6. The observed g value is constant(=2.12) in this temperature range and is close to the free spin value (see below). The breadth of the ESR absorption line, ΔH (peak-to-peak width), is temperature independent (ΔH = 315 G).

The compound $CsAu_{0.6}Br_{2.6}$ has a cubic perovskite structure, in which a large part of Au ions are considered to be in a cubic field (sixfold coordination). In such a field, the orbital ^2D state ($5d^9$) splits into an orbital doublet $\Gamma_3(^2E_g)$ and an orbital triplet $\Gamma_5(^2T_{2g})$, the former being the lower in energy. In the ground state Γ_3 (^2E_g), there is no first-order contribution arising from the spin-orbit interaction to the g value. Therefore the observed g value is expected to be close to the free spin value. The spin-lattice relaxation time τ_1 is also expected to be long. However the breadth of the ESR absorption line is considerably larger than one would expect, and is considered to be caused by the non-stoichiometry, an

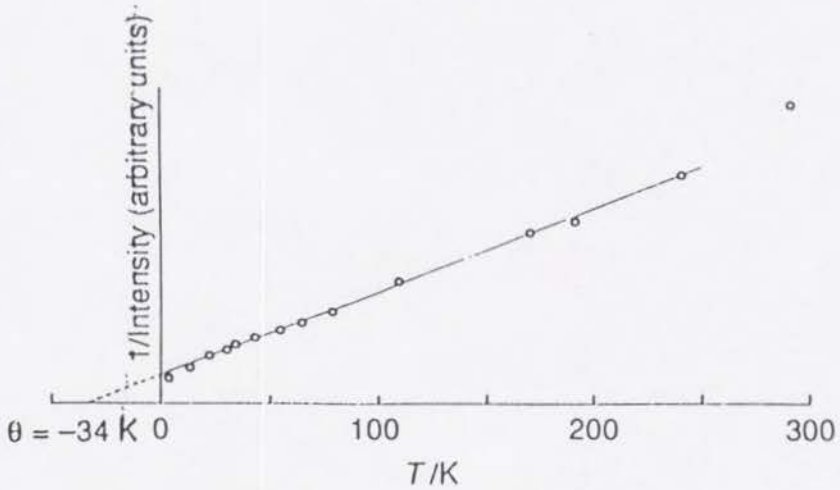

Fig. 7 The reciprocal of the ESR signal intensity of $CsAu_{0.6}Br_{2.6}$ as a function of temperature

the magnetic dipoles. As shown in Figure 7, the ESR intensity (*i.e.* spin susceptibility) of $CsAu_{0.6}Br_{2.6}$ follows Curie-Weiss law with Θ = -34 K. The large negative Weiss constant implies antiferromagnetic interaction between the Au ions. Despite this, the antiferromagnetic transition does not take place on cooling to 3.7 K, probably due to the dilute random spin system. It should be noted that the critical concentration of the diluted three-dimensional Heisenberg-type antiferromagnet, at the temperature at which the magnetic phase transition becomes zero, is 60 %.[24] In the case of $CsAu_{0.6}Br_{2.6}$, the proportion of Au occupancy is 60 %.

2-6 ELECTRICAL CONDUCTIVITY OF THE CUBIC PHASE

For $CsAu_{0.6}Br_{2.6}$, a thermally activated semiconducting behavior was observed in the temperature range 300-240 K. The electrical conductivity at room temperature of $CsAu_{0.6}Br_{2.6}$ is *ca.* 10^{-4} Scm^{-1}, whereas that of $Cs_2Au_2Br_6$ is *ca.* 10^{-8} Scm^{-1}. The activation energy *Ea*, where $\sigma = \sigma_0 \exp(-Ea/k_BT)$, is 0.36 eV (between 300-240 K) for $CsAu_{0.6}Br_{2.6}$, whereas that is 0.46 eV (between 373-270 K) for $Cs_2Au_2Br_6$.

From the powder X-ray diffraction, the Au sites in the crystal structure of $CsAu_{0.6}Br_{2.6}$ are indistinguishable. The ESR spectra and the considerable increase of electrical conductivity due to the partially oxidation were observed for $CsAu_{0.6}Br_{2.6}$. This behavior is analogous to that of $K_2Pt(CN)_4Br_{0.3}\cdot n(H_2O)$[25] which is a class Ⅲ mixed-valence system, according to the Robin-Day classification.[22] Accordingly, it can be concluded that the cubic phase $CsAu_{0.6}Br_{2.6}$ is also a class Ⅲ mixed-valence system.

2-7 CONCLUSIONS

From a structural point of view, we have discussed the anisotropy in the three-dimensional MX-networks of the mixed-valence system $Cs_2Au_2X_6$. The present structural study

and the results of physical measurements for the cubic phase $CsAu_{0.6}Br_{2.6}$ are consistent with 'class-Ⅲ mixed-valence compounds' according to the classification of Robin and Day. From the ESR experimental results, the oxidation state Au^{II} is present in $CsAu_{0.6}Br_{2.6}$.

References

1 H.Kitagawa,N.Kojima,and T.Nakajima,*J.Chem.Soc.,Dalton Trans.*,1991,3121.

2 H.Kitagawa,N.Kojima,and H.Sakai,*J.Chem.Soc.,Dalton Trans.*,1991,3211.

3 J.C.M.Tindemans-v.Eijndhoven and G.C.Verschoor,*Mater.Res. Bull.*,1974,9,1667.

4 G.Brauer and G.Sleater,*J.Less-commom Met.*,1970,21,283.

5 N.Matsushita,H.Kitagawa,and N.Kojima, unpublished work.

6 A.W.Sleight,J.L.Gillson,and P.E.Bierstedt,*Solid State Commun.*1975,17,27.

7 L.F.Mattheiss,E.M.Georgy,and D.W.Jhonson Jr.,*Phys.Rev.B*, 1988,37,3745.

8 R.J.Cava,B.Batlogg,J.J.Krajewski,R.C.Farrow,L.W.Rupp Jr., A.E.White,K.T.Short,W.F.Pevk Jr.,and T.Y.Kometani,*Nature*, 1988,332,814

9 I.Tsujikawa,*Jpn.J.Appl.Phys.,Series 1*,1988, Superconducting Materials,155;N.Kojima,H.Kitagawa,T.Ban, F.Amita,and M.Nakahara,*Solid State Commun.*,1990,73,743.

10 D.E.Cox and A.W.Sleight,*Solid State Commun.*,1976,19,969.

11 H.J.Keller,in 'Extended Linear-chain Compounds,' ed.J.S.Miller,Plenum,New York,1982,vol.1,p.357.

12 K.Nasu, *J.Phys.Soc.Jpn.*, 1983, 52, 3865; 1984, 53, 302; 1984, 53, 427.

13 J.Strähle, J.Gelinek, and M.Kölmel, *Z.anorg.allg.Chem.*, 1979, 456, 241.

14 J.Strähle, J.Gelinek, and M.Kölmel, and A.-M.Nemecek, *Z. Naturforsch.*, 1979, 34b, 1047.

15 G.Thiele, M.Steiert, D.Wagner, and H.Wochner, *Z.anorg.allg. Chem.*, 1984, 516, 207.

16 G.Thiele, W.Weigl, and H.Wochner, *Z.anorg.allg.Chem.*, 1986, 539, 1986.

17 L.E.Orgel, *J.Am.Chem.Soc.*, 1958, 80, 4186.

18 M.B.Robin and P.Day, *Adv.Inorg.Chem.Radiochem.*, 1967, 10, 363.

19 H.Tanino, K.Takahashi, M.Tajima, M.Kato, and T.Yao, *Phys.Rev.B*, 1989, 38, 8327.

20 C.Janiak and R.Hoffmann, *Inorg.Chem.*, 1989, 28, 2743.

21 'International Tables for X-Ray Crystallography,' Kynoch Press, Birmingham, 1974, vol.IV.

22 M.B.Robin and P.Day, *Adv.Inorg.Chem.Radiochem.*, 1967, 10, 247.

23 P.Gütlich, B.Lehnis, K.Romhild, and J.Strähle, *Z.Naturforsch.*, 1982, 37b, 550.

24 T.Oguchi and T.Obokata, *J.Phys.Soc.Jpn.*, 1969, 27, 1111.

25 'Extended Linear-chain Compounds,' ed.J.S.Miller, Plenum, New York, 1982, vol.1 and vol.2.

CHAPTER 3

X-Ray Photoelectron Spectroscopic Study of the Mixed-Valence States in $Cs_2Au_2X_6$ (X=Cl, Br, I)

3-1 INTRODUCTION

The technique of X-ray photoelectron spectroscopy (XPS) has been suggested to be an appropriate tool for probing the electronic structure of mixed-valence compounds.[1] Halogen-bridged one-dimensional M^{II}-M^{IV} mixed-valence complexes of Pt, Pd, and Ni have been investigated intensively from the viewpoints of physics and chemistry as a model of one-dimensional system,[2,3] and XPS has been employed.[4-6] On the other hand, to our knowledge, little XPS work on the Au^{I}-Au^{III} mixed-valence complexes has been done.[7,8] In the preceding chapter[9] we have mentioned an important feature that there are anisotropic three-dimensional -X-Au^{I}-X-Au^{III}- networks in

the structure of Cs-Au-X mixed-valence system and also reported on a new non-stoichiometric cesium bromoaurate, $CsAu_{0.6}Br_{2.6}$ (cubic phase of Cs-Au-Br system). The purposes of the present study were systematically to investigate the mixed-valence states in $Cs_2Au_2X_6$ by changing the bridging halogen X from Cl to I as a method for modifying the anisotropic charge-transfer interaction between Au^{I} and Au^{III} through the bridging halogen, to investigate the gold valence state in the cubic phase of the Cs-Au-Br system, and to investigate the oxidation states in halogeno complexes of Au^{I} and Au^{III}, by means of XPS measurements.

3-2 EXPERIMENTAL

Preparation of Au Compounds—(a)$Cs_2Au_2Cl_6$.The mixed-valence compound $Cs_2Au_2Cl_6$ was prepared by the same method as described in ref.10 (Found:Au,44.9;Cs,30.7. Calc.for $Au_2Cl_6Cs_2$:Au,45.2;Cs,30.5%).

(b)$Cs_2Au_2Br_6$.The mixed-valence compound $Cs_2Au_2Br_6$ was prepared by the same method as described in the preceding chapter.[9]

(c)$CsAu_{0.6}Br_{2.6}$.The non-stoichiometric cesium bromoaurate $CsAu_{0.6}Br_{2.6}$ was prepared by the same method as described in the preceding chapter.[9]

(d)$Cs_2Au_2I_6$. An aqueous solution of CsI was slowly added to an aqueous solution of $H[AuCl_4]\cdot 4H_2O$ at ice-bath temperature. The black compound $Cs_2Au_2I_6$ was formed. This compound was filtered off, washed with a dilute hydroiodic acid, and then dried in a vacuum desiccator for several days (Found:Au,27.6;Cs,18.7.Calc.for $Au_2I_6Cs_2$:Au,27.7;Cs,18.7%).

(e)$Cs[AuCl_4]$. A saturated aqueous solution of CsCl was added to a dilute HCl solution of $H[AuCl_4]\cdot 4H_2O$ at ice-bath temperature. The yellow complex $Cs[AuCl_4]\cdot nH_2O$ was immediately formed. This was filtered off, washed with cold water, and then dried in a vacuum desiccator for several days. In this manner, the anhydrous complex $Cs[AuCl_4]$ was obtained.

(f)$Cs[AuBr_4]$. An aqueous solution of CsBr was slowly added to a dilute HCl solution of $H[AuCl_4]\cdot 4H_2O$ at ice-bath temperature. The red-brown complex $Cs[AuBr]_4$ was formed. filtered off, washed with cold water, and then dried in a vacuum desiccator for several days.

(g)$[Bu^n_4N][AuX_4]$(X=Cl,Br,or I). These salts were prepared by the methods described in the literature[11,12] (Found:C, 32.90;H,6.25;Cl,24.3;N,2.40. Calc.for $C_{16}H_{36}AuCl_4N$:C,33.05; H,6.25;Cl,24.4;N,2.40%. Found:C,25.55;H,4.75;Br,42.4;N,1.75. Calc.for $C_{16}H_{36}AuBr_4N$:C,25.30;H,4.80;Br,42.1;N,1.85%. Found: C,20.30;H,3.75;I,53.3;N,1.50. Calc.for $C_{16}H_{36}AuI_4N$:C,20.30; H,3.80;I,53.6;N,1.50%).

(h)[Bu^n_4N][AuX_2](X=Cl,Br,or I). The bromide and iodide were prepared by the methods of Baunstein and Clark.[13] For the preparation of [Bu^n_4N][$AuCl_2$], their method was modified. We used phenylhydrazinium chloride ($PhNHNH_2HCl$) in an anhydrous ethanol solution of hydrogen chloride instead of in absolute ethanol (Found:C,37.45;H,7.10;Cl,13.7;N,2.75. Calc. for $C_{16}H_{36}AuCl_2N$:C,37.65;H,7.10;Cl,13.9;N,2.75%. Found:C, 31.95;H,6.00;Br,26.6;N,2.30. Calc.for $C_{16}H_{36}AuBr_2N$:C,32.05; H,6.05;Br,26.7;N,2.35%. Found:C,27.65;H,5.25;I,36.9;N,1.95. Calc.for $C_{16}H_{36}AuI_2N$:C,27.70;H,5.25;I,36.6;N,2.00%).

(i) AuCl,AuI. Gold(I) chloride and iodide were prepared by the methods described in the literature.[14]

X-Ray Analysis—Powder X-ray diffraction profiles were obtained at room temperature for all compounds mentioned above. Each profile is in good agreement with the calculated one from previous X-ray work.[14,16]

X-Ray Photoelectron Spectra—The X-ray photoelectron spectra were obtained on DuPont ESCA 650B electron spectrometer (Shimazu Seisakusho), the source vacuum being $\sim 10^{-7}$ Torr, with a Mg-Kα X-ray source (1253.6 eV) at room temperature. Binding energies were measured relative to the C1s peak (285.0 eV) due to hydrocarbon contamination which built up slowly on the surface under these operating

conditions or to the C1s peak (285.3 eV) for alkyl carbon in tetranbuthylammonium gold halides, in agreement with previous work.[17,18]

3-3 XPS SPECTRA OF MIXED-VALENCE COMPOUNDS $Cs_2Au_2X_6$

The observed binding energies of Au 4f region are given in Table 1. Figure 1 shows the XPS spectra of this region for $Cs_2Au_2X_6$(X=Cl,Br,or I). As can be seen, the observed spectra for $Cs_2Au_2Cl_6$ and $Cs_2Au_2Br_6$ can be resolved into signals for Au^{I} and Au^{III}, the latter ionizing at the higher energy. The intensity of Au^{III} signal is a little smaller than that of Au^{I}, probably due to the partial decomposition (Au^{III} is partially reduced to Au^{I}) caused by the X-ray beam. For $Cs_2Au_2I_6$ the two Au sites were not satisfactorily resolved, though it is obvious from its powder[19] and our single crystal[20] X-ray analyses that two sites are present. This doublet is very broad having a half-maximum (fwhm) of approximately 2.6 eV. The doublets of $[Bu^{n}_{4}N][AuI_2]$, AuI, and $[Bu^{n}_{4}N][AuI_4]$ are much narrower having widths of about 1.8 eV. The broad peak observed for $Cs_2Au_2I_6$ can be attributed to the contributions from both Au^{I} and Au^{III} sites giving rise to two overlapping signals separated by about 0.9 eV. According to our very recent work[21] using a VG ESCA MKII electron

Table 1 Binding energies (eV) for the 4f region of gold

	$4f_{\frac{5}{2}}$		$4f_{\frac{7}{2}}$	
Compound	Au^{III}	Au^{I}	Au^{III}	Au^{I}
$Cs_2Au_2Cl_6$ [a,b]	90.0	88.2	86.5	84.7
AuCl [a,b]		88.5		84.8
$[NBu^n_4][AuCl_2]$ [a,c]		88.3		84.7
$[NEt_4][AuCl_2]$ [d]		—		84.8
$[NBu^n_4][AuCl_4]$ [a,c]	91.0		87.4	
$Cs[AuCl_4]$ [a,b]	91.4		87.7	
$[NEt_4][AuCl_4]$ [d]	—		87.6	
$Cs_2Au_2Br_6$ [a,b]	89.4	88.2	85.8	84.6
$CsAu_{0.6}Br_{2.6}$ [a,b]	90.1		86.5	
$[NBu^n_4][AuBr_2]$ [a,c]		88.5		84.9
$[NEt_4][AuBr_2]$ [d]		—		84.3
$[NBu^n_4][AuBr_4]$ [a,c]	90.8		87.2	
$Cs[AuBr_4]$ [a,b]	90.6		87.0	
$[NEt_4][AuBr_4]$ [d]	—		86.7	
$Cs_2Au_2I_6$ [a,b]	88.4		84.8	
$Cs_2Au_2I_6$ [a,b]	89.1	88.2	85.5	84.6
AuI [a,b]		88.3		84.6
$[NBu^n_4][AuI_2]$ [a,c]		88.6		85.0
$[NEt_4][AuI_2]$ [d]		—		84.3
$[NBu^n_4][AuI_4]$ [a,c]	88.5		84.9	
$[NEt_4][AuI_4]$ [d]	—		84.3	

[a] Binding energies are accurate to ± 0.15 eV. [b] Binding energies corrected by comparison with C 1s energy set at 285.0 eV for the hydrocarbon contamination. [c] Binding energies corrected by comparison with C 1s energy set at 285.3 eV for alkyl carbon in $[NBu^n_4]^+$. [d] From ref. 18. As more than one datum is given in ref. 18, the values quoted are averages. Binding energies are corrected by comparison with the C 1s energy set at 285.3 eV for alkyl carbon in $[NEt_4]^+$. Binding energies of $4f_{\frac{5}{2}}$ are not given in ref. 18.

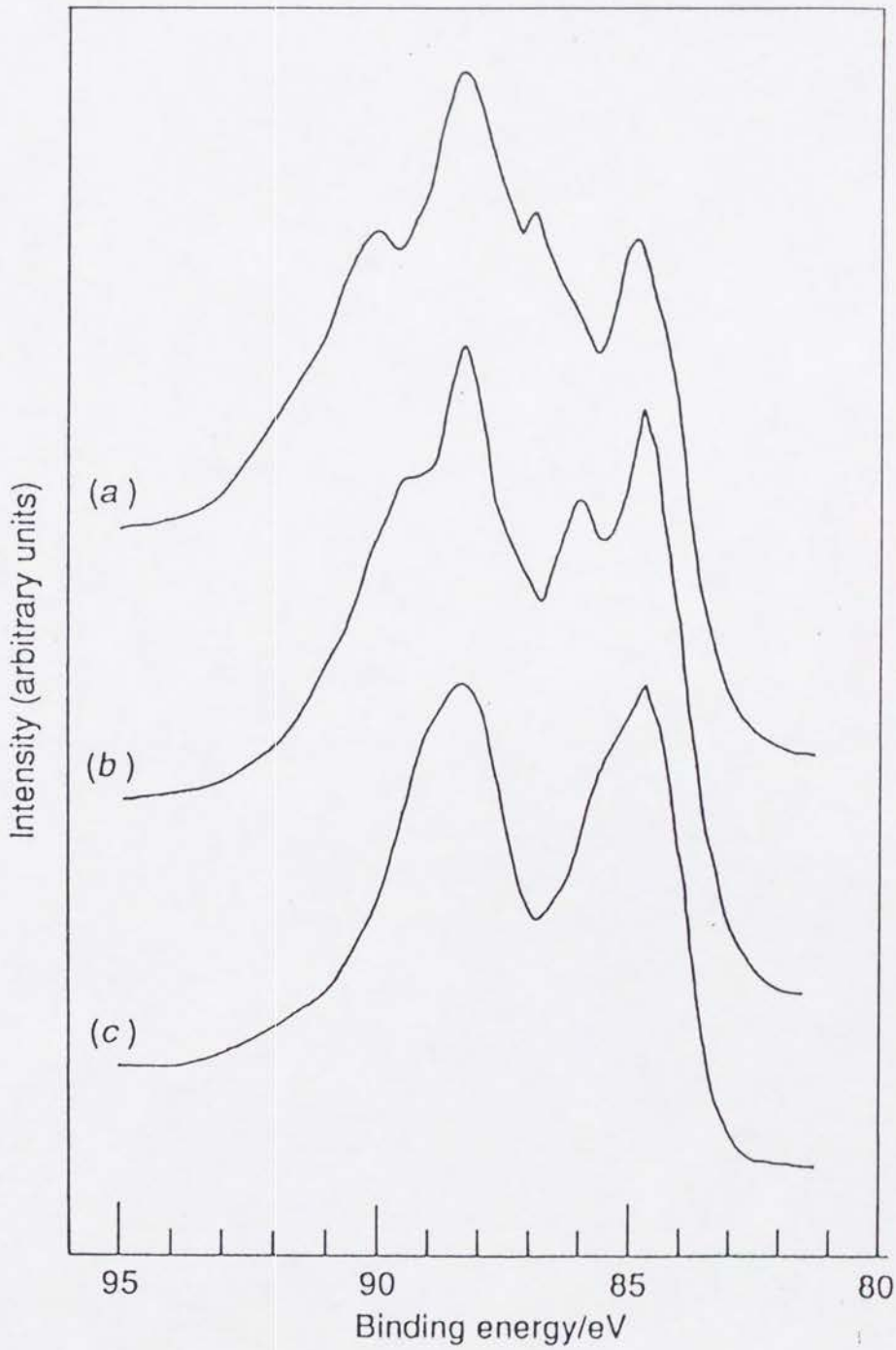

Fig. 1 The XPS spectra in the Au 4f region of the mixed-valence compounds (*a*) $Cs_2Au_2Cl_6$, (*b*) $Cs_2Au_2Br_6$ and (*c*) $Cs_2Au_2I_6$

spectrometer, the XPS spectrum for $Cs_2Au_2I_6$ could be resolved into signals for Au^{I} and Au^{III}, shown in Table 1. Thus, it is obvious that two oxidation states of Au^{I} and Au^{III} exist in $Cs_2Au_2I_6$. Figure 1 also shows that the difference in binding energy of the 4f signal between Au^{I} and Au^{III} decreases in the series $Cs_2Au_2Cl_6 \rightarrow Cs_2Au_2Br_6 \rightarrow Cs_2Au_2I_6$. This may be explained as follows. As the covalency of the $-Au^{I}-X-Au^{III}-X-$ bonds increases in the order X=Cl→Br→I, the charge-transfer interaction between the electronic state of Au^{I} and that of Au^{III} through the bridging halogen becomes stronger.

The binding energies $4f_{5/2}$ and $4f_{7/2}$ of Au^{III} in $Cs_2Au_2X_6$ decrease in the order X=Cl>Br>I, while those of Au^{I} signal are constant in going from X=Cl to X=I. This shows that the valence 5d orbital population of Au^{I} remains unchanged from X=Cl to I.

In the preceding chapter[9], we referred to the crystal structures of $Cs_2Au_2X_6$ (X=Cl, Br, or I), in which there are anisotropic three-dimensional $-X-Au^{I}-X-Au^{III}-$ networks. Therefore, also in the charge-transfer interaction between Au^{I} and Au^{III} through the bridging halogen X, it can be considered that there should be some anisotropy. We suppose that the charge-transfer interaction should be stronger in the xy plane (⊥c axis) than in the z direction(//c axis), because $5d_{x^2-y^2}$ orbital of the $[Au^{III}Cl_4]^-$ ion is unfilled in

contrast to $5d_{z^2}$ orbital which is filled. The charge-transfer interaction is considered to arise mainly from an overlap between $5d_{x^2-y^2}$ orbitals of Au^{I} and Au^{III} through p orbitals of the bridging halogens. On this basis, the lack of a shift in binding energy of the Au^{I} signal of $Cs_2Au_2X_6$ from X=Cl to X=I can be explained as follows.

The decrease and the increase of the valence $5d_{x^2-y^2}$ orbital population of Au^{I} occur simultaneously in going from $Cs_2Au_2Cl_6$ to $Cs_2Au_2I_6$. The former and the latter are due to the increase of the strength of the charge-transfer interaction and to the increase of the strength of the ligand-to-metal electron σ donation in the xy plane, respectively. The experimental result that the binding energies $4f_{5/2}$ and $4f_{7/2}$ of Au^{I} signal are constant in going from $Cs_2Au_2Cl_6$ to $Cs_2Au_2I_6$ can be explained by assuming that the increase and the decrease of the valence orbital population of Au^{I} in going from $Cs_2Au_2Cl_6$ to $Cs_2Au_2I_6$ are compensated.

Figure 2 shows the XPS spectra of Au 4f region for $Cs_2Au_2Cl_6$ and the control complexes, $[Bu^{n}_{4}N][AuCl_2]$ and $[Bu^{n}_{4}N][AuCl_4]$. The binding energies $4f_{7/2}$ and $4f_{5/2}$ of Au^{I} signal in $Cs_2Au_2Cl_6$ are almost equal to those of the Au^{I} chloro complex. On the other hand, there is a significant difference between the binding energy of Au^{III} signal of $Cs_2Au_2Cl_6$ and that of the Au^{III} chloro complex, the former

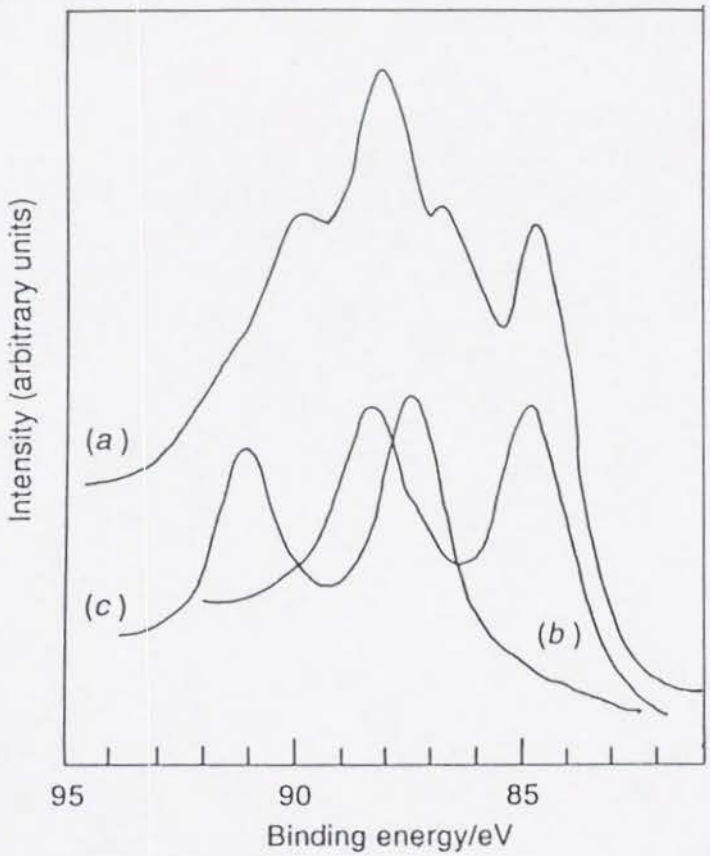

Fig. 2 The XPS spectra in the Au 4f region of (*a*) $Cs_2Au_2Cl_6$, (*b*) $[NBu^n_4][AuCl_2]$ and (*c*) $[NBu^n_4][AuCl_4]$

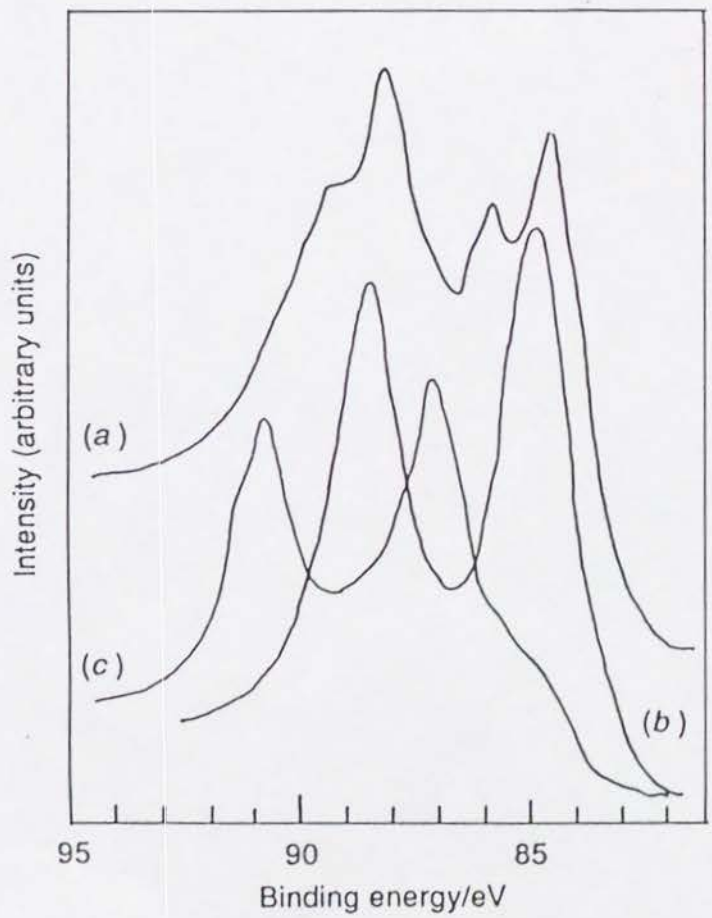

Fig. 3 The XPS spectra in the Au 4f region of (*a*) $Cs_2Au_2Br_6$, (*b*) $[NBu^n_4][AuBr_2]$ and (*c*) $[NBu^n_4][AuBr_4]$

being 1.0 eV smaller. These behaviors of Au^{I} and Au^{III} signals are interpreted as follows. When the linear $[Au^{I}Cl_2]^-$ and the square planar $[Au^{III}Cl_4]^-$ are stacked alternately and three-dimensional -X-Au^{I}-X-Au^{III}- networks are formed, the charge-transfer from Au^{I} to Au^{III} through the bridging halogen Cl and the ligand-to-metal electron σ donation from the ligand halogen Cl in $[Au^{III}Cl_4]^-$ to Au^{I} occurs in the xy plane. The lack of a difference in binding energy of Au^{I} between $Cs_2Au_2Cl_6$ and the Au^{I} chloro complex suggests that the quantity of the charge-transfer from Au^{I} to Au^{III} in the xy plane is equal to that of that (ligand-to-metal electron σ donation) in the xy plane from the ligand Cl in $[Au^{III}Cl_4]^-$ to Au^{I}. On the other hand, the difference in binding energy of Au^{III} between $Cs_2Au_2Cl_6$ and the Au^{III} chloro complex suggests that the amount of electronic charge flow into Au^{III} is larger than that of electronic charge flow from Au^{III}. The charge flow into Au^{III} is mainly caused by the charge transfer from Au^{I} through the bridging halogen Cl in the xy plane and by the ligand-to-metal electron σ donation in the z direction from the ligand halogen Cl in $[Au^{I}Cl_2]^-$ to Au^{III}. The charge outflow from Au^{III} is caused only by the increase of Au^{III}-Cl distance in $[Au^{III}Cl_4]^-$ in the xy plane." However, we consider the amount of the charge outflow caused by removal of halogen from Au^{III} is small. The difference in the binding energy of Au^{III} between $Cs_2Au_2Cl_6$

and the Au^{III} chloro complex supports this consideration.

However, Robin and Day[22] suggested that the intervalence charge-transfer transition from a filled d_{z^2}-orbital of Au^{I} to the unfilled $d_{x^2-y^2}$-orbital of Au^{III} should occur in the xy plane, but reported that the intervalence charge-transfer absorption band in $Cs_2Au_2Cl_6$ was observed with light polarized parallel to the c axis. Their result is a puzzle for us. In order to elucidate this problem, the detailed measurements of polarized reflectance spectra in $Cs_2Au_2X_6$ (X=Cl,Br,and I) are indispensable and discussed in Chapter 5.

Also in the case of $Cs_2Au_2Br_6$ (Figure 3), a difference in the binding energy of Au^{III} signal between $Cs_2Au_2Br_6$ and the Au^{III} bromo complex but no difference in the binding energy of Au^{I} one between $Cs_2Au_2Br_6$ and the Au^{I} bromo complex were observed. Explanations for this behavior are similar to those in $Cs_2Au_2Cl_6$ described above. The observed difference in the

When $[Au^{I}Cl_2]^-$ and $[Au^{III}Cl_4]^-$ are stacked alternately, the ligand Cl in $[Au^{III}Cl_4]^-$ co-ordinates to Au^{I} and then the electronic charge in Au^{I} is transferred to Au^{III} by the charge-transfer interaction. Here the valence of Au in $[Au^{III}Cl_4]^-$ would change from +3 to $+(3-\beta)$ $(0<\beta<1)$. Hence the Au^{III}-Cl distance for $[Au^{III}Cl_4]^-$ in the mixed-valence compound $Cs_2Au_2Cl_6$ would be longer than that in the Au^{III} chloro complex $[AuCl_4]^-$.

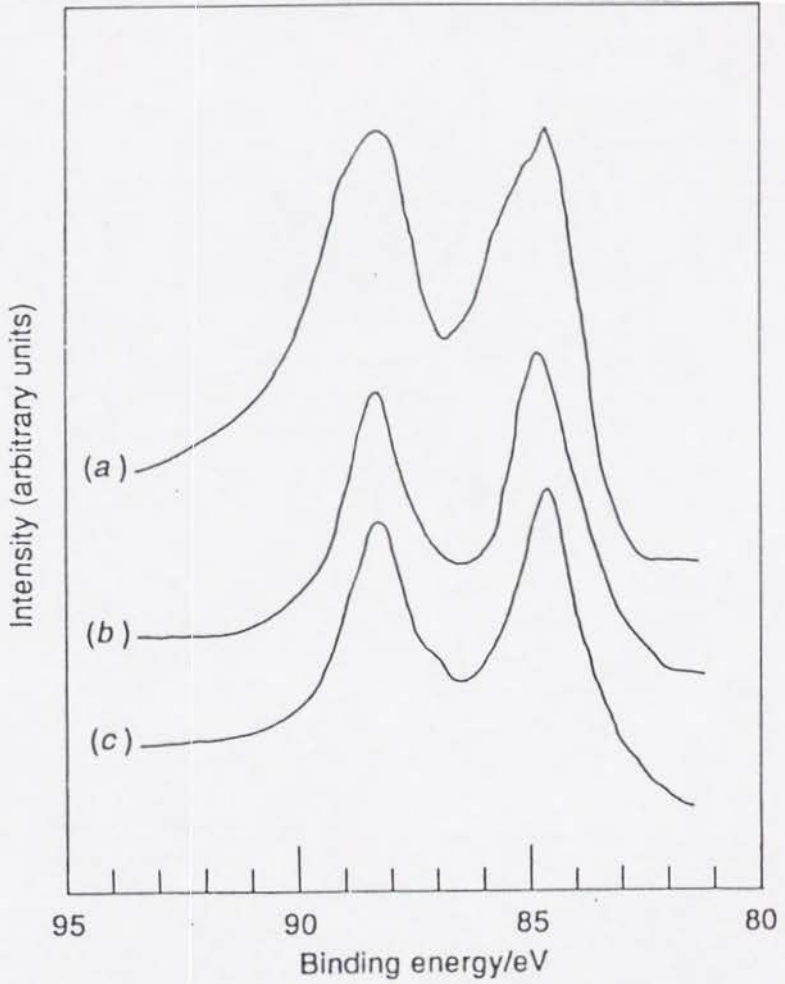

Fig. 4 The XPS spectra in the Au 4f region of (*a*) $Cs_2Au_2I_6$, (*b*) $[NBu^n_4][AuI_2]$ and (*c*) $[NBu^n_4][AuI_4]$

binding energy of Au^{III} is 1.4 eV. The charge-transfer interaction in $Cs_2Au_2X_6$ (X=Cl, Br, and I) will be evaluated below using the XPS results.

As an indication of the strength of the charge-transfer interaction,

We adopted

$$\Gamma = \delta(M)/\delta(S),$$

$\delta(M)$ is the difference in binding energy of Au4f signal between Au^{I} and Au^{III} in $Cs_2Au_2X_6$ and $\delta(S)$ is the difference in binding energy of this signal between $[AuX_2]^-$ and $[AuX_4]^-$. If we imagine a hypothetical state with $\Gamma = 1$,

there is no interaction between Au^{I} and Au^{III} (Robin-Day class I mixed-valence system [22]). If $\Gamma = 0$, the oxidation states of Au^{I} and Au^{III} are indistinguishable and that is +II (Robin-Day class III mixed-valence system[22]).

From the values in Table 1, we obtain

$$\Gamma (X=Cl) = 0.64$$

and $$\Gamma (X=Br) = 0.55,$$

where the binding energies of Au4f signal used for calculating δ (S) are the average value of listed complexes.

This indicates that the charge-transfer interaction in $Cs_2Au_2Br_6$ is stronger than that in $Cs_2Au_2Cl_6$. In the case of $Cs_2Au_2I_6$ (Figure 4), the value Γ cannot be estimated because of no difference in binding energy of Au4f signal between $[Bu^{n}_{4}N][AuI_2]$ and $[Bu^{n}_{4}N][AuI_4]$.

3-4 XPS SPECTRA OF Au^{III} HALOGENO COMPLEXES

Figure 5 shows the XPS spectra of Au^{III} halogeno complexes. It is immediately noticed that the binding energy of Au4f signal in $[Au^{III}X_4]^-$ is shifted to lower energy in the order X=Cl→Br→I. This behavior can be explained as follows. A decrease in the binding energy of Au4f electrons is caused by an increase of Au 5d population. Considering $5d6s6p^2$ hybridization, the increase in the covalency of the Au^{III}-X

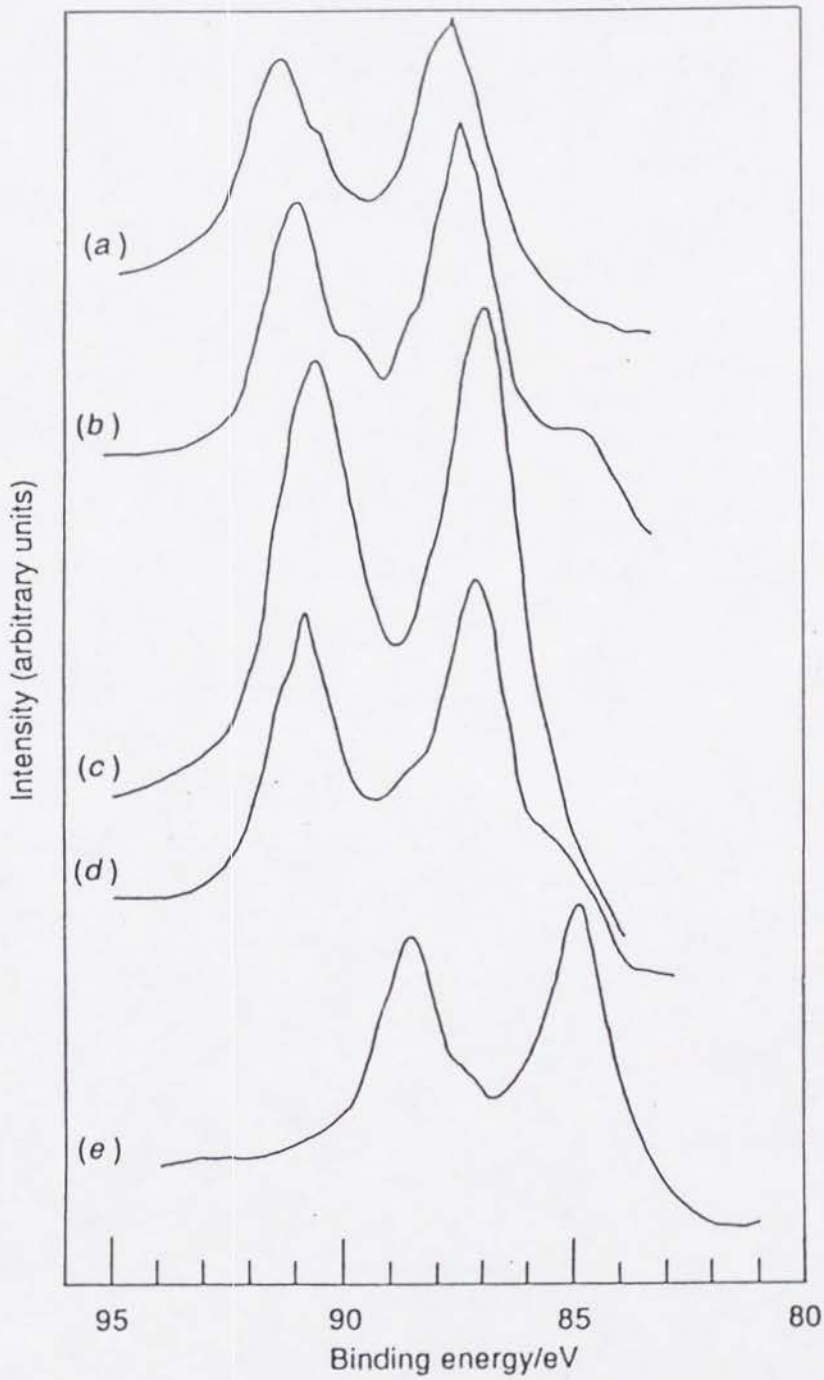

Fig. 5 The XPS spectra in the Au 4f region of the halogenogold(III) complexes (*a*) $Cs[AuCl_4]$, (*b*) $[NBu^n_4][AuCl_4]$, (*c*) $Cs[AuBr_4]$, (*d*) $[NBu^n_4][AuBr_4]$ and (*e*) $[NBu^n_4][AuI_4]$

bond in the order X=Cl→Br→I causes an increase of $5d_{x^2-y^2}$ population. As can be seen from Figure 4, the binding energy of the Au4f signal in $[Bu^n_4N][AuI_4]$ is almost equal to that of $[Bu^n_4N][AuI_2]$. From this, the amount of the charge transfer from I^- to $5d_{x^2-y^2}$ of Au^{III} is expected to be considerably large. Therefore, the oxidation state of Au in $[Bu^n_4N][AuI_4]$ is close to Au^I. The atomic Au $5d_{x^2-y^2}$ population of molecular orbitals in $[Bu^n_4N][AuI_4]$ is considered to be close to 2.0.

3-5 XPS SPECTRA OF Au^I HALOGENO COMPLEXES

On the other hand, the binding energies of Au^I halogeno complexes are constant despite changing halogen ion X^- in $[AuX_2]^-$ and AuX (Figure 6). Au^I complexes have linear two co-ordinate stereochemistry much more commonly than complexes of Cu^I or Ag^I. Whether $6s6p_z$ hybridization or $5d_{z^2}6s6p_z$ hybridization in such a linear co-ordination is favorable for Au^I has been discussed in many papers.[23-27] The electronic charge of halogen would be transferred mainly to 6s or $6p_z$ orbital of Au^I. The amount of this charge transfer (the ligand-to-metal electron σ donation) is expected to increase in the order Cl→Br→I for X in $[AuX_2]^-$. However the 6s or 6p orbital contribution to the

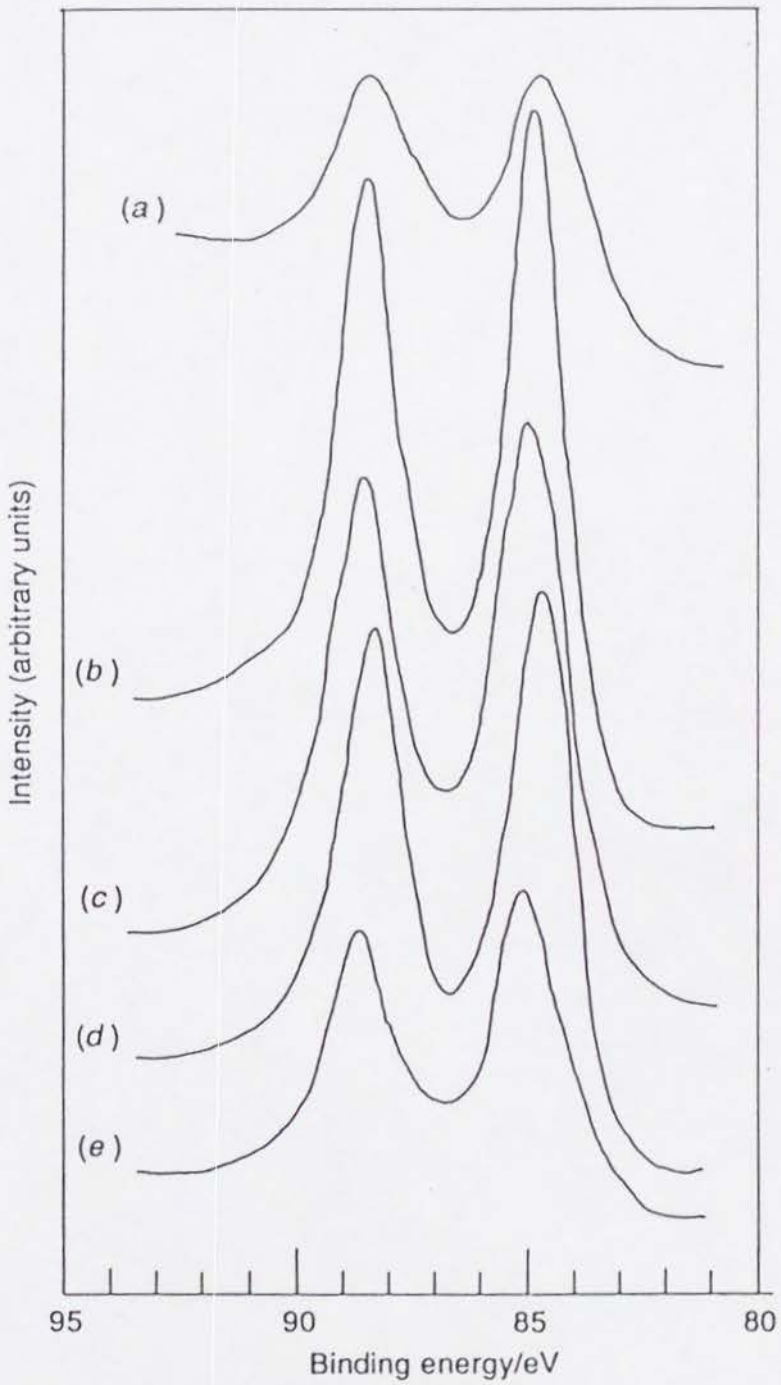

Fig. 6 The XPS spectra in the Au 4f region of the halogenogold(I) complexes (*a*) $[NBu^n_4][AuCl_2]$, (*b*) AuCl, (*c*) $[NBu^n_4][AuBr_2]$, (*d*) AuI and (*e*) $[NBu^n_4][AuI_2]$

shielding of the 4f electrons from the nucleus is smaller than the 5d-orbital one. It is, therefore, difficult to estimate the 6s or $6p_z$ population by XPS measurement of the Au 4f region. We suppose ^{197}Au Mössbauer spectroscopy might be a more useful tool for probing the electronic structure of 6s or $6p_z$ level.

3-6 XPS SPECTRUM OF THE CUBIC PHASE $CsAu_{0.6}Br_{2.6}$

Figure 7 shows the spectrum of the cubic phase of Cs-Au-Br system $CsAu_{0.6}Br_{2.6}$. In contrast to the tetragonal phase

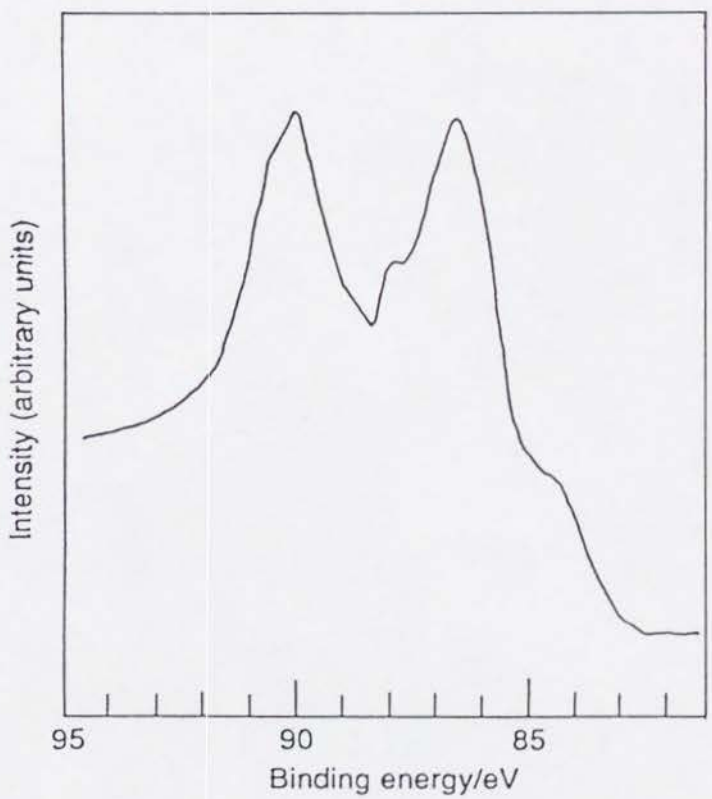

Fig. 7 The XPS spectrum in the Au 4f region of the cubic phase $CsAu_{0.6}Br_{2.6}$

$Cs_2Au_2Br_6$, only one doublet structure was observed. The discernible shoulders to lower energy of each of $4f_{7/2}$ and $4f_{5/2}$ signals are due to the partial decomposition to Au^{I} caused by the X-ray beam, since the $4f_{7/2}$ and $4f_{5/2}$ binding energies of the shoulder are almost equal to those of Au^{I} signal for $[Bu^{n}_{4}N][AuBr_2]$. This phenomenon was also observed for $[Bu^{n}_{4}N][AuX_4]$(X=Cl,Br,or I). From only one doublet structure of this spectrum having a fwhm approximately equal to that of the spectrum in the Au^{I} or Au^{III} complex, the oxidation state of Au in the cubic phase is expected to be almost homogeneous. However, from its compositional ratio and binding energies of Au 4f, the oxidation state of Au is supposed to be close to Au^{III} rather than expectative Au^{II} state and a puzzle requiring further research.

3-7 CONCLUSIONS

X-ray photoelectron spectra were recorded to investigate the mixed-valence states of $Cs_2Au_2X_6$ (X=Cl,Br,or I) for the first time. The difference between the oxidation states of Au^{I} and Au^{III} decreases in the order X=Cl→Br→I. Because the charge-transfer interaction in the xy plane becomes stronger in this order. In the cubic phase $CsAu_{0.6}Br_{2.6}$ the oxidation state of Au is considered to be almost homogeneous.

References

1 P.A.Cox,R.G.Egdell,and A.F.Orchard in 'Mixed-Valence Compounds,'ed.D.B.Brown,D.Reidel,Dordrecht,The Netherlands,1982,p.475.

2 H.J.Keller,in 'Extended Linear-chain Compounds,' ed.J.S.Miller,Plenum,New York,1982,vol.1,p.357.

3 K.Nasu,*J.Phys.Soc.Jpn.*,1983,52,3865;1984,53,302; 1984,53,427.

4 D.Cahen and J.E.Lester,*Chem.Phys.Lett.*,1973,18,108.

5 M.Yamashita,N.Matsumoto,and S.Kida,*Inorg.Chim.Acta*,1978, 31,L381;M.Yamashita,I.Murase,and I.Ikemoto, *Bull.Chem.Soc.Jpn.*,1985,58,2697.

6 J.-M.Bret,P.Castan,and J.-P.Laurent,*J.Chem.Soc.Dalton Trans.*,1984,1975.

7 H.Schmidbauer,A.Wohlleben,F.E.Wagner,D.F.Van de Vondel, and G.P.Van de Kelen,*Chem.Ber.*,1977,110,2758.

8 N.Kojima,H.Kitagawa,T.Nakajima,T.Ban,and I.Tsujikawa, Proceedings of the 25th International Conference on Coordination Chemistry,Nanjing,1987,A2-197.

9 H.Kitagawa,N.Kojima,N.Matsushita,T.Ban,and I.Tsujikawa, *J.Chem.Soc.,Dalton Trans.*,1991,3115.

10 J.C.M.Tindemans-v.Eijndhoven and G.C.Verschoor,*Mater.Res.*

Bull.,1974,9,1667.

11 W.R.Mason,Ⅲ,and H.B.Gray,*Inorg.Chem.*,1968,7,55.

12 J.L.Ryan,*Inorg.Chem.*,1969,8,2058.

13 P.Braunstein and R.J.H.Clark,*J.Chem.Soc.,Dalton Trans.*, 1973,1845.

14 M.O.Faltens and D.A.Shirley,*J.Chem.Phys.*,1970,53,4249.

15 JCPDS Powder Diffraction File.

16 P.Braunstein,A.Müller,and H.Bogge,*Inorg.Chem.*,1986,25, 2104.

17 J.R.Blackburn,R.Nordberg,F.Stevie,R.G.Allridge,and M.M. Jones,*Inorg.Chem.*,1970,9,2374.

18 A.McNeillie,D.H.Brown,W.E.Smith,M.Gibson,and L.Watson, *J.Chem.Soc.,Dalton Trans.*,1980,767.

19 G.Brauer and G.Sleater,*J.Less-Common Met.*,1970,21,283.

20 N.Matsushita,H.Kitagawa,and N.Kojima, unpublished work.

21 XPS spectra for $Cs_2Au_2I_6$ were obtained using VG Scientific ESCA LAB MKⅡ system at Institute for Molecular Science.

22 M.B.Robin and P.Day,*Adv.Inorg.Chem.Radiochem.*,1967,10, 247.

23 L.E.Orgel,*J.Am.Chem.Soc.*,1958,80,4186.

24 R.J.Puddephatt,ed.,'The Chemistry of Gold,' Elsevier, Amsterdam,1978,Vol.16,p.15.

25 T.K.Sham,R.E.Watson,and M.L.Perlman,*Phy.Rev.B*,1980,21, 1457.

26 J.Stanek, *J.Chem.Phys.*, 1982, 76, 2315.

27 G.A.Bowmaker, P.D.W.Boyd, and R.J.Sorrenson, *J.Chem.Soc.*, *Faraday Trans.*, *2*, 1985, 81, 1627.

CHAPTER 4

Gold-197 Mössbauer Spectroscopic Study of the Mixed-Valence States in $Cs_2Au_2X_6$ (X=Cl, Br, I)

4-1 INTRODUCTION

In this chapter we report Mössbauer data for this system, which, taken together with previously published work[1-4] and the XPS data discussed in the preceding chapter,[5] afford a useful insight into the electronic structure of these mixed-valence compounds. The 77.34 keV ^{197}Au Mössbauer resonance is very sensitive to the valence state and the chemical environment, and the Au compounds show a wide variation in quadrupole splitting and isomer shift.[6-9]

In this study we employ a method of changing the charge-transfer interaction in $Cs_2Au^{I}Au^{III}X_6$ which is the replacement of bridging halogen X=Cl>Br>I. The consequent changes in

the isomer shifts and the quadrupole splittings of the Au^{I} and Au^{III} nuclei will provide some new information about the signs of the electric field gradient at these nuclei, the hybridization scheme, and the charge-transfer interactions between Au^{I} and Au^{III}. In the preceding chapter (XPS study),[5] we showed that the charge-transfer interaction should be stronger in the xy plane ($\perp$ c-axis) than in the z direction (//c-axis). The main purpose of this study is to discuss the changes in the isomer shifts and quadrupole splittings of $Cs_2Au_2X_6$ (X=Cl,Br,or I) on this basis.

4-2 EXPERIMENTAL

All the compounds were prepared by the same methods described in Chapters 2[10] and 3.[5]

Mössbauer spectroscopic measurements of the 77.34 keV transition in ^{197}Au were carried out with both source and absorber cooled to 16K by using a constant-acceleration spectrometer with a NaI(Tl) scintillation counter. The data were stored in a microcomputerized 512 multichannel analyser. A ^{197}Pt source was obtained by neutron irradiation of 98% enriched platinum due to the nuclear reaction $^{196}Pt[n,\gamma]^{197}Pt$ in the Kyoto University Reactor (KUR). The velocity scale was calibrated by taking spectra of body-

centred cubic iron against a ^{57}Co source, both at room temperature. The observed spectra were analyzed by use of a computer program including folding and least-squares fitting with Lorentzian lines.

4-3 DIFFERENCE IN RECOIL-FREE FRACTIONS FOR THE Au^{I} AND Au^{III} SITES IN $Cs_2Au_2X_6$ (X=Cl,Br,I)

The observed ^{197}Au Mössbauer data, isomer shift (IS), quadrupole splitting (QS), half-width (Γ), and the intensity ratio (A^{I}/A^{III}) for the mixed-valence compounds, $Cs_2Au_2X_6$ (X=Cl,Br,or I), are given in Table 1. All IS values here are referenced to metallic gold foil. In order to refer these isomer shifts to gold in platinum, 1.20 (mm/s) have to be subtracted from the tabulated values. The observed ^{197}Au Mössbauer spectra are shown in Figure 1. A best fit is obtained with two doublets, the outer doublet with lower intensity being assigned to Au^{I}, and the inner to Au^{III}. These assignments are similar to those previously reported[1-3] for $Cs_2Au_2Cl_6$ and not similar to those[5] for $Cs_2Au_2Br_6$. In Ref. 4, the doublet at low velocity was assigned to the Au^{I}, and that at high velocity to Au^{III}. The intensity ratio of the two components A^{I}/A^{III} should be 1.0 because of the Au^{I}/Au^{III} compositional ratio in stoichiometric

Table 1. ^{197}Au Mössbauer data for the mixed-valence compounds $Cs_2Au_2X_6$ (X=Cl, Br, and I) and the cubic phase of Cs-Au-Br system $CsAu_{0.60}Br_{2.63}$

Complexes	IS (mm/s)	QS (mm/s)	Γ (mm/s)	A (%)	A^I
$Cs_2Au_2Cl_6$ (160mg Au/cm^2)[a]					
Au^I	0.03±0.05	5.06±0.05	2.04±0.08	44.9	0.
Au^{III}	1.38±0.05	0.76±0.05	2.14±0.08	55.1	
$Cs_2Au_2Br_6$ (160mg Au/cm^2)[a]					
Au^I	0.21±0.05	4.57±0.05	1.81±0.08	32.3	0.
Au^{III}	1.12±0.05	1.37±0.05	2.43±0.08	67.7	
$Cs_2Au_2I_6$ (160mg Au/cm^2)[a]					
Au^I	1.02±0.05	4.58±0.05	2.04±0.08	46.9	0.
Au^{III}	1.54±0.05	1.68±0.05	1.89±0.08	53.1	
$CsAu_{0.60}Br_{2.63}$ (100mg Au/cm^2)[a]					
	1.52±0.05	0.95±0.05	2.26±0.08	----	--

[a] The absorber thickness of Au in mg/cm^2.

$Cs_2Au_2X_6$. However, the experimental ratios are smaller than the expected ones. As is well known,[1,11,12] the unequal intensities is due to the difference in recoil-free fractions f^{I} and f^{III} for the Au^{I} and Au^{III} sites in $Cs_2Au_2X_6$. Since the Au^{I} is in two-fold (linear) ligand co-ordination and the Au^{III} in four-fold (square-planar) co-ordination,[13-15] the environment of the Au^{III} in $Cs_2Au_2X_6$ is more rigid than that of the Au^{I}. The mean-square vibrational amplitude of Au^{III} is considered, therefore, to be smaller than that of Au^{I}. The intensity ratio (A^{I}/A^{III}) for $Cs_2Au_2Cl_6$ will be discussed below using the isotropic temperature factors B obtained from the X-ray measurement.[18]

From the value of the mean-squared vibrational displacement u^2, where

$$u^2 = B/8\pi^2,$$

we obtain

$$u^2(Au^{I}) = 0.0223\ \text{Å}^2$$

and $u^2(Au^{III}) = 0.0201\ \text{Å}^2$ at 293 K,

and for the ratio of the f factors

$$f^{I}/f^{III} = \exp\{-K^2[u^2(Au^{I}) - u^2(Au^{III})]\}$$

$$= 3.7 \times 10^{-2}$$

with $K^2 = 1.5 \times 10^{3}\ \text{Å}^{-2}$ for the 77.34 keV γ-rays of ^{197}Au. In the limit of high temperatures we obtain approximately

$$f = \exp(-6E_R T/k_B\theta_D^2) \quad ; \quad T > \theta_D$$

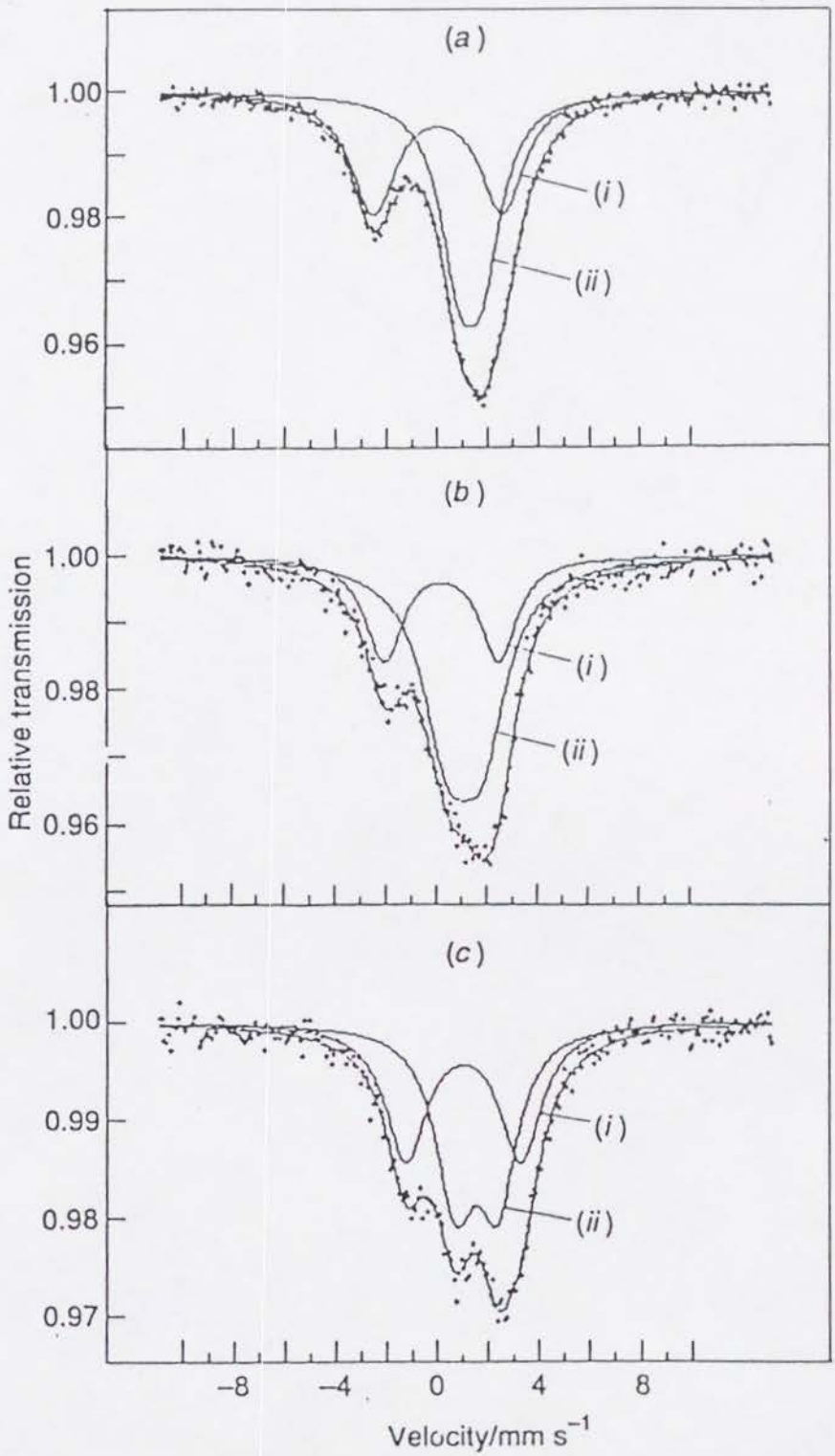

Fig. 1 Gold-197 Mössbauer spectra of the mixed-valence compounds (*a*) $Cs_2Au_2Cl_6$, (*b*) $Cs_2Au_2Br_6$ and (*c*) $Cs_2Au_2I_6$; (*i*) Au^{I}, (*ii*) Au^{II}

Debye temperatures θ_D=99 and θ_D=104 K are obtained for Au^{I} and Au^{III}, respectively. For this, E_R=16.3 × 10^{-3} eV was adopted. Debye temperatures obtained by this simple model are applicable to the low temperature approximation($T<<\theta_D$)

$$f=\exp\{(-3E_R/2k_B\theta_D)[1+(2\pi^2/3)(T/\theta_D)^2]\}$$

(f^{I}=0.034, f^{III}=0.042) f^{I}/f^{III}=0.81, may be compared with the experimental value A^{I}/A^{III}=0.82 at 16 K (Table 1). The ratio of the f factors estimated from the X-ray diffraction is in excellent agreement with the observed intensity ratio. In the case of $Cs_2Au_2Br_6$ and $Cs_2Au_2I_6$ we cannot estimate the f values because of no single crystal x-ray data.

4-4 MÖSSBAUER SPECTRA OF $Cs_2Au_2X_6$ (X=Cl,Br,I)

As can be seen from Figure 1, the valence states of Au^{I} and Au^{III} are clearly distinguishable for all the compounds. In the case of $Cs_2Au_2I_6$, we could not distinguish satisfactorily between the valence states of Au^{I} and Au^{III} by XPS,[5,16] but ^{197}Au Mössbauer spectrum can be now well resolved into these components.

Information obtained from XPS of inner shells is chemical shift only ($4f_{5/2}$ -$4f_{7/2}$ separation of a spin-orbit doublet is approximately constant~3.6 eV, regardless of the variation of the oxidation state of Au.). On the other hand, the

Mössbauer spectroscopy provides two major parameters (i.e. IS and QS), which can be related to the populations and changes in population of the valence shell orbitals. A IS relates to the total electron density on the nucleus (*i.e.* s electron density), $\rho(0)$ and a QS reflects any anisotropy in the distribution of the electron density. Therefore, the Mössbauer spectroscopy may be more suitable for detailed analysis of oxidation states than XPS of inner shells.

Figure 2 shows the isomer shifts IS^{I} and IS^{III} for the Au^{I} and Au^{III} sites in $Cs_2Au_2X_6$(X=Cl,Br,or I). The difference in the IS values between Au^{I} and Au^{III} decreases in the order X=Cl>Br>I, which implies that the oxidation states of Au^{I} and Au^{III} in $Cs_2Au_2X_6$ tend to approach the Au^{II} state in this order. This behavior suggests that the charge-transfer interaction between Au^{I} and Au^{III} becomes stronger in this order and is consistent with our XPS study.[6,16] This is mainly due to the increase in covalency of the $-Au^{I}-X-Au^{III}-X-$ bonds (the overlap of filled $5d_{x^2-y^2}$ orbitals of Au^{I} and empty $5d_{x^2-y^2}$ orbitals of Au^{III} through p_x or p_y orbitals of the bridging halogen X) in the order X=Cl<Br<I. Also as shown in Figure 2, IS^{I} increases in the order X=Cl<Br<I, while the IS^{III} decreases from X=Cl to X=Br and increases from X=Br to X=I. As shown in Figure 3, the quadrupole splitting QS^{III} increases in the order X=Cl<Br<I, on the other hand QS^{I} decreases slightly in this order. The changes of QS^{I} and

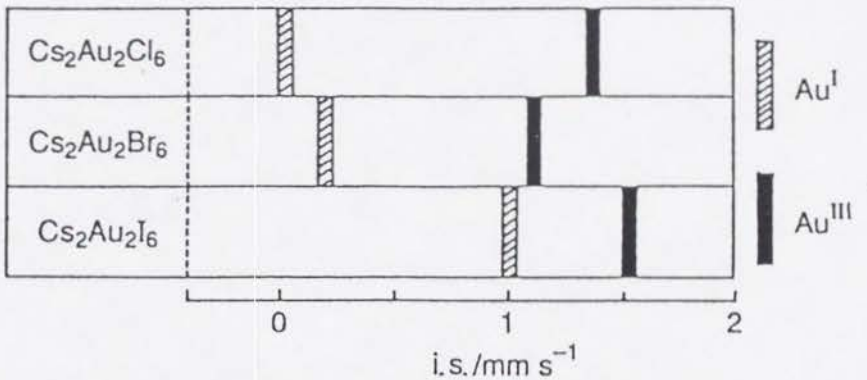

Fig. 2 Changes in the isomer shifts i.s.^{I} and i.s.^{III} for the gold-(I) and -(III) sites in $Cs_2Au_2X_6$ in going from X = Cl to I

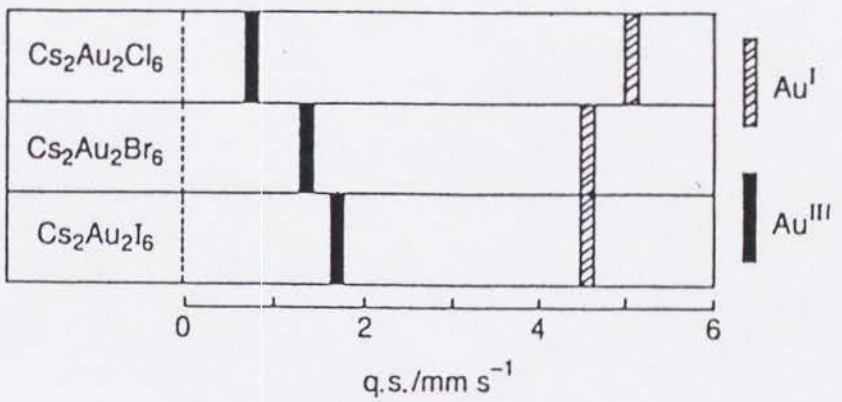

Fig. 3 Changes in the quadrupole splittings q.s.^{I} and q.s.^{III} for the gold-(I) and -(III) sites in $Cs_2Au_2X_6$ in going from X = Cl to I

QS^{III} in $Cs_2Au_2X_6$ are quite similar to the pressure-induced changes of those in $Cs_2Au_2Cl_6$ reported by J.Stanek and co-workers.[1,17] The charge-transfer interaction in $Cs_2Au_2Cl_6$ should become stronger with increasing pressure, which is consistent with the above similarity. However, their assumption that the signs of the electric field gradient (EFG) at the Au^{I} and Au^{III} sites are positive and negative, respectively, is in disagreement with ours as described in the following paragraphs. As the charge-transfer interaction in $Cs_2Au_2X_6$ becomes stronger, the QS^{III} increases, while the QS^{I} decreases. However, in the work by Katada, *et al.*,[3] based on their experimental result that the QS^{III} of $Cs_2Ag^{I}Au^{III}Cl_6$ is smaller than that of $Cs_2Au^{I}Au^{III}Cl_6$, they concluded that the interaction between two metal atoms in the 4d-5d mixed-metal compound $Cs_2Ag^{I}Au^{III}Cl_6$ is stronger than that in 5d-5d mixed-valence compound $Cs_2Au^{I}Au^{III}Cl_6$. Their conclusion is, therefore, in conflict with our discussion and, moreover, Yamada and Tsuchida[18] did not reach such a conclusion. X-Ray absorption near-edge structure (XANES) spectra[19] suggest that the oxidation state of Au^{III} in $Cs_2Ag^{I}Au^{III}Cl_6$ is almost equal to that in $[Bu^{n}_4N][Au^{III}Cl_4]$. Hence we are convinced that the charge-transfer interaction in the 4d-5d mixed-metal system is weaker than that in the 5d-5d mixed-valence system. In the preceding chapter (XPS study),[6] we showed that the charge-transfer interaction between Au^{I} and

Au^{III} should be stronger in the xy plane than in the z direction. In the following paragraphs, the changes in QS and IS in $Cs_2Au_2X_6$ (X=Cl,Br,or I) will be discussed on the basis of this view.

4-5 QUADRUPOLE SPLITTING OF Au^{I} IN $Cs_2Au^{I}Au^{III}X_6$

When the Mössbauer spectrum is a simple doublet, the quadrupole splitting QS is then given by

$$QS=(1/2)eQV_{zz}(1+\eta^{2}/3)^{1/2}$$

where e is the charge on the proton ($e>0$), Q is the nuclear quadrupole moment (+ 0.59 x $10^{-28}m^2$ for the ground state of ^{197}Au), V_{zz} is the principal component of the EFG (often designated as eq_{zz}), and η is the asymmetry parameter. For linear $[AuX_2]^-$ and square-planar $[AuX_4]^-$ ions we shall take η as zero. The concentration of negative charge on the xy plane makes the EFG positive, and that on the z axis does it negative. The sign of the EFG at Au^{I} has been discussed in many papers.[1,20-28] The sign of the EFG at Au^{I} in $KAu(CN)_2$ was determined by means of single-crystal absorber.[29] However, in the case of the halogeno complexes $[AuX_2]^-$ (X=Cl,Br,or I) the sign has not yet been determined by experiment. In the case of linear $Au^{I}(5d^{10})$ complexes, it has been considered[20,21,23,26,28,29] that ^{197}Au Mössbauer

data favor the sp hybridization scheme.# In this scheme the sign of the EFG is expected to be negative. From the viewpoint of the sp hybridization, with increasing σ-donor strength of the ligands in the order X=Cl<Br<I, the atomic $6p_z$ population (negative contribution to the EFG) of the molecular orbitals on the Au ion increases, and therefore the absolute value of the negative EFG should be expected to increase in this order. However the experimental fact is the opposite. Mössbauer measurements on $[Bu^n_4N][Au^IX_2]$(X=Cl or I) reported by Braunstein,*et al.*,[28] have shown that the QS^I (5.61 mm/s) when X=I is smaller than that (5.93 mm/s) when X=Cl. This anomalous order of IS values has also been noted for corresponding chloro- and iodo-complexes.[32] This discrepancy has been a puzzle for us. However, the SCF-MS-Xα study in $[Au^IX_2]$(X=Cl,Br,or I) reported by Bowmaker,*et al.*[31] has showed that the $6p_z$ population increases from $[AuCl_2]^-$ to $[AuI_2]^-$, but that there is a slight expansion in the $6p_z$ orbital from $[AuCl_2]^-$ to $[AuI_2]^-$ which results in a progressive decrease in the normalized EFG for the $6p_z$ orbital (The main contribution to the EFG comes from the electron density in the Au $6p_z$ orbital.). This phenomenon is

However, we note that some workers[1,22,24,26,27,29-31] have considered that the partial presence of some d-s mixing cannot be excluded.

Table 2 Gold-197 Mössbauer data (mm s^{-1})

Compound		i.s.	q.s.	Γ	Ref.
$Cs_2Au_2Cl_6$ [a]	Au^I	0.13 [b]	5.06	2.04	9
	Au^{III}	1.31 [b]	1.00	1.88	
$Cs_2Au_2Cl_6$	Au^I	−1.07(3) [c]	5.04(6)		7
	Au^{III}	0.34(2) [c]	1.17(4)		
$Cs_2Au_2Br_6$	Au^I	−1.22 [c]	3.84	1.88	10
	Au^{III}	0.54 [c]	1.72	1.90	
$Cs_2AgAuCl_6$ [d]		1.54 [b]	0	2.33	9
$Cs_2AgCuCl_6$		0.32(1) [c]	0.86(2)		7
$Cs_2AgAuBr_6$		0.42 [c]	0.99	2.18	10
$Cs_{1.5}(AuBr_4)(Br_3)_{0.2}Br_{0.3}$		0.53 [c]	0.94	2.16	10
$[NBu^n_4][AuCl_2]$		0.31(7) [c]	5.93(7)		29
$[NBu^n_4][AuI_2]$		0.30(7) [c]	5.61(7)		29
$K[AuCl_4]$		0.81 [c,e]	1.11 [f]	1.76 [e]	34
$K[AuBr_4]$		0.60 [c,e]	1.13 [f]	1.78 [d]	34
$K[AuI_4]$		0.43 [c,g]	1.28 [h]	1.92 [f]	34

[a] ±0.08 mm s^{-1}. [b] Relative to gold metal. [c] Relative to gold in platinum. [d] ±0.04 mm s^{-1}. [e] ±0.03 mm s^{-1}. [f] ±0.06 mm s^{-1}. [g] ±0.05 mm s^{-1}. [h] ±0.10 mm s^{-1}.

supposed to relate closely to the nephelauxetic series of ligands Cl < Br < I.

In the case of the mixed-valence compounds $Cs_2Au_2X_6$, QS^I decreases from X=Cl to Br and does not change from X=Br to I (Figure 3). In the order X=Cl < Br < I for $Cs_2Au_2X_6$, both the charge-transfer interaction between $5d_{x^2-y^2}$ orbitals of Au^I and Au^{III} and the σ donation of attached ligands in

$[Au^{III}X_4]^-$ into $5d_{x^2-y^2}$ orbitals of Au^I are considered to become stronger. From the XPS study for $Cs_2Au_2X_6$,[6] it is found that the valence 5d-orbital population of Au^I does not change in going from X=Cl to I. Therefore, the decrease in the valence 5d-orbital population of Au^I, which is due to the increase in the strength of the charge-transfer interaction (X=Cl<Br<I), and the increase in those of Au^I, which is due to the increase in the strength of ligand-to-metal electron σ donation (X=Cl<Br<I), compensate each other in the xy plane. On the other hand, the charge-transfer interaction in the z direction should be weak. Therefore, the decrease in QS^I from X=Cl to Br is mainly due to the slight expansion in the $6p_z$ orbital which causes a significant reduction in the magnitude of the EFG at the Au^I site. Compared with the QS^I in $[Bu^n_4N][AuCl_2]$, the value in $Cs_2Au_2Cl_6$ is small. This may be explained as follows. The Au^I-Cl distance in $Cs_2Au_2Cl_6$(2.281 Å) is longer than that in $[Bu^n_4N][AuCl_2]$ (2.257 Å).* An increase of the Au^I-Cl distance causes a slight expansion in the $6p_z$ orbital and a

* The Au^I-X distances for $[AuX_2]^-$ in the Au^I-Au^{III} mixed-valence compounds $Cs_2[AuCl_2][AuCl_4]$, $Rb_2[AuBr_2][AuBr_4]$, and $K_2[AuI_2][AuI_4]$ are longer than those in $[Bu^n_4N][AuCl_2]$, $[Bu^n_4N][AuBr_2]$, and $[Bu^n_4N][AuI_2]$, respectively.[33]

decrease of the $6p_z$ orbital population. Thus, electron density of the Au $6p_z$ orbital in $Cs_2Au_2Cl_6$, which is the main contribution to the EFG at the Au^I site, is smaller than that in $[Bu^n_4N][AuCl_2]$. The similar behavior of QS^I of $Cs_2Au_2I_6$ compared with that of $[Bu^n_4N][AuI_2]$ can be explained in the same way. The lack of a shift in QS^I from $Cs_2Au_2Br_6$ to $Cs_2Au_2I_6$ can be interpreted as follows. From $Cs_2Au_2Br_6$ to $Cs_2Au_2I_6$, the $6p_z$ population of Au^I increases, while the $6p_z$ orbital of Au^I expands slightly. The effect of the expansion in the $6p_z$ orbital on the EFG is supposed to be almost equal to the effect of the increase in the $6p_z$ population from $Cs_2Au_2Br_6$ to $Cs_2Au_2I_6$. This is consistent with the SCF-MS-Xα study.[31], in which atomic orbital populations and orbital contributions to the EFG for $[AuX_2]^-$ (X=Cl,Br,or I) were estimated. The $6p_z$ orbital of Au plays most important role in determining the magnitude and sign of the EFG. Though the atomic $6p_z$-orbital population becomes larger in the order X=Cl(0.328)<Br(0.338)<I(0.366), negative contributions of this orbital to the EFG decrease from X=Cl(-8.2 a.u.) to X=Br(-7.8 a.u.) and unchange from X=Br to X=I(-7.8 a.u.).

4-6 QUADRUPOLE SPLITTING OF Au^{III} IN $Cs_2Au_2X_6$ (X=Cl,Br,I)

Although a QS-IS correlation for Au^{III} is similar to that for Au^{I},[34] it is clear that the EFG at Au^{I} must be different in sign from that at Au^{III}. In a square-planar Au^{III} complexes, the principal component of the EFG must lie perpendicular to the xy plane ($5d_{x^2-y^2}$ hole, negative contribution to the EFG). Increasing σ donation from ligands (into $5d_{x^2-y^2}$- and $6p_{x,y}$-orbitals) will induce an increasing positive contribution to the EFG. Since the experimental $\langle r^{-3} \rangle$ values have found to be larger for 6p than for the 5d electrons, the EFG at Au^{III} is expected to be relatively small and presumably positive, and this has been confirmed for $K[Au(CN)_4]$.[10] Mössbauer measurements in $K[AuX_4]$(X=Cl,Br,or I) have shown that the QS^{III} increases in the order X=Cl(1.11) → Br(1.13) → I(1.28 mm/s).[34] In this mixed-valence system, the QS^{III} was found to increase in the order X=Cl(0.76) → Br (1.37) → I(1.68 mm/s). The QS^{III} of each of $Cs_2Au_2Br_6$ and $Cs_2Au_2I_6$ is larger than that of $K[AuBr_4]$ and $K[AuI_4]$, respectively, while QS^{III} of $Cs_2Au_2Cl_6$ is smaller than that of $K[AuCl_4]$. These trends can be explained as below. Because of a large increase in the unilateral electronic charge transfer from Au^{I} to Au^{III} in the xy plane (positive contribution to the EFG at the Au^{III} nuclei) along the series of $Cs_2Au_2Cl_6 < Cs_2Au_2Br_6 < Cs_2Au_2I_6$, the positive QS^{III} should increase along its series, in spite of an increase of the charge transfer from halogen p_z to the metal orbital (

negative contribution to the EFG). The fact that, in spite of this negative contribution, the QS^{III} of each of $Cs_2Au_2Br_6$ and $Cs_2Au_2I_6$ is larger than that of $K[AuBr_4]$ and $K[AuI_4]$, respectively, suggests that the charge-transfer interaction between Au^{I} and Au^{III} is stronger in the xy plane than in the z direction. In $Cs_2Au_2Cl_6$ the opposite relation may be explained as follows. The charge-transfer interaction in $Cs_2Au_2Cl_6$ is weaker than that in $Cs_2Au_2Br_6$ or $Cs_2Au_2I_6$. In the case of $Cs_2Au_2Cl_6$,therefore, the effect of the expansion in $5d_{x^2-y^2}$ and $6p_{x,y}$ orbitals on the EFG or the charge transfer from the halogen p_z orbital in $[AuX_2]^-$ to the Au^{III} orbital (each is negative contribution to the EFG at Au^{III}.) can not be negligible compared with transfer of electronic charge from Au^{I} to Au^{III} in the xy plane caused by the charge-transfer interaction (positive contribution to the EFG at Au^{III}).

As was noted in the previous section, the changes in the QS^{I} and QS^{III} in $Cs_2Au_2X_6$ in going from X=Cl to X=I are quite similar to the pressure-induced changes for X=Cl reported by J.Stanek.[1] From this similarity it can be considered that with increasing pressure the charge-transfer interaction in X=Cl becomes stronger in the xy plane. However, in the high-pressure Mössbauer study for $Cs_2Au_2Cl_6$, the charge-transfer interaction was not taken into account for the pressure-induced changes, though the charge-transfer interaction plays

a more important role in a mixed-valence system under high pressure than under ambient pressure. Moreover, despite the similarity of the changes of QS^{I} and QS^{III}, his conclusion that the signs of the EFG at Au^{I} and Au^{III} are positive and negative, respectively is in disagreement with ours. In his study, the pressure-induced change in QS^{I} for $Cs_2Au_2Cl_6$ was discussed on the basis of a ds-hybridization scheme for $[Au^{I}Cl_2]^-$. The hybridization scheme in complexes of Au^{I} having the d^{10}-electron configuration has been the subject of considerable discussion (5d6s *vs.* 6s6p). Recently, however, most of Mössbauer investigators favor the sp-hybridization scheme. And also, the pressure-induced change in QS^{III} for $Cs_2Au_2Cl_6$ was discussed only on the basis of a decrease in σ-donor strength of the attached ligands in $[Au^{III}Cl_4]^-$ due to the increase of the Au^{III}-Cl distances within the xy plane. Since the charge-transfer was not considered in the high-pressure study, Stanek's conclusion as to the signs of the EFG at Au^{I} and Au^{III} is the opposite of ours.

4-7 ISOMER SHIFTS OF Au^{I} and Au^{III} in $Cs_2Au_2X_6$ (X=Cl,Br,I)

The isomer shift (IS) is given by

$$IS=C\ \Delta\langle R^2\rangle\ \Delta\rho\ (0)$$

where C is a constant containing nuclear parameters(>0),

$\Delta \langle R^2 \rangle$ is the change in the square of the nuclear radius between the excited and the ground states which has been estimated[36] as + 8.6 × 10^{-3} fm^2 for ^{197}Au, and $\Delta \rho(0)$ is the difference between the contact densities of the source and the absorber. For ^{197}Au, therefore, a positive shift of IS indicates an increase in the electron density at the nucleus, $\rho(0)$. The valence-electron contribution to $\rho(0)$ is well known to be affected in two ways:

Ⓐ Increasing the s-electron population in the valence shell directly increases $\rho(0)$.

Ⓑ Occupation of p or d orbitals decreases $\rho(0)$ as a result of screening the valence and core s orbitals from the nucleus.

As is known for the highly covalent gold complexes, Au^{I} whose gold hybrid orbitals (sp hybridization) have a larger s character than those of Au^{III} (dsp^2 hybridization) yield larger isomer shifts (*i.e.* in terms of Ⓐ). From Figures 1 and 2, it was found that IS^{I} is, on the contrary, smaller than IS^{III} for each mixed-valence compound. This behavior can be explained in terms of Ⓑ (Au^{I};$5d^{10}$, Au^{III}; $5d^{8}$). The increase of IS^{I} from $Cs_2Au_2Cl_6$ to $Cs_2Au_2I_6$ is due to the increase of 6s population caused by increasing the σ-donor property of ligand halogens in $[Au^{I}X_2]^-$ groups. The decrease

of IS^{III} from $Cs_2Au_2Cl_6$ to $Cs_2Au_2Br_6$ would be attributed mainly to the increase of $5d_{x^2-y^2}$ population (*i.e.* in terms of 𝔹), and the increase of IS^{III} from $Cs_2Au_2Br_6$ to $Cs_2Au_2I_6$ mainly to the increase of 6s population (*i.e.* in terms of 𝔸).

4-8 MÖSSBAUER SPECTRUM OF THE CUBIC PHASE $CsAu_{0.6}Br_{2.6}$

Figure 4 shows the spectrum of the cubic phase of Cs-Au-Br system, $CsAu_{0.6}Br_{2.6}$. In contrast to the tetragonal phase of $Cs_2Au_2Br_6$, only a single resonance line having a rather broad half-width was observed for the cubic phase. Strangely, the IS (1.52 mm/s) is larger than IS^{III} (1.12 mm/s) for the tetragonal phase and almost equal to IS^{III} (1.54 mm/s) for $Cs_2Au_2I_6$. This suggests that the 6s population in the valence-shell molecular orbitals of Au in the cubic phase is larger than that in the corresponding orbitals of Au^{III} in the tetragonal phase. The observed half-width Γ (2.73 mm/s) is rather broader than that (2.34 mm/s) for Au foil[130 mg Au/cm^2]. The rather broad line might be due to the Br vacancies. In the system $CsAu_{0.6}Br_{2.6}$, the Au and Br vacancies are considered to be distributed in the lattice at random. Though most of Au ions are six-coordinate, some are supposed to be five- or smaller number-coordinate. In

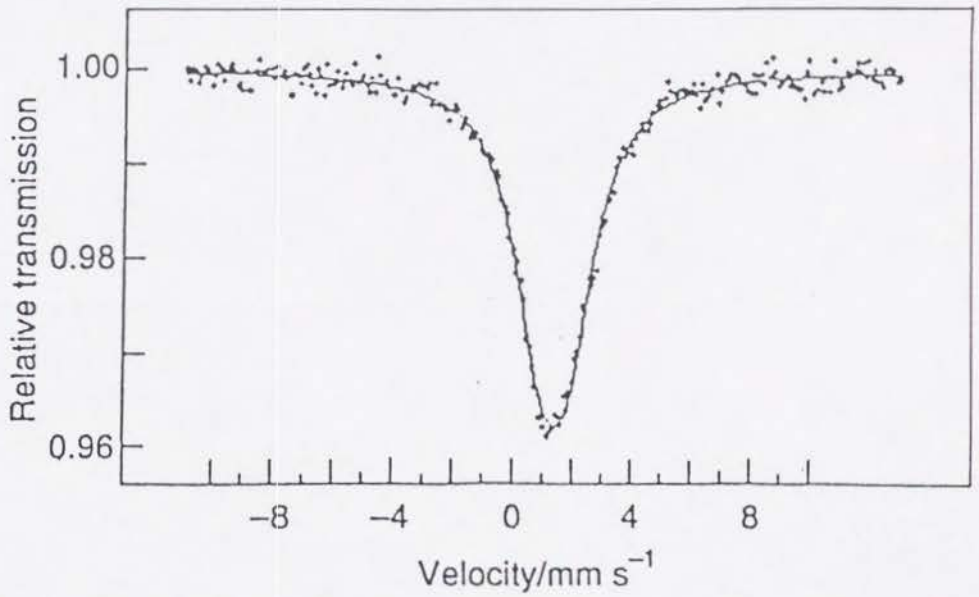

Fig. 4 Gold-197 Mössbauer spectrum of the cubic phase $CsAu_{0.6}Br_{2.6}$

general, the oxidation state of Au ions with larger co-ordinatation number is higher. Therefore the valence state of six-coordinate gold would be +Ⅲ, and that of five- or four-coordinate gold would be +Ⅱ. Injected electrons reducing the Au^{III} complex might be trapped at sites of five- or four-co-ordinate Au. Consequently, this system exhibits semiconducting behavior, in spite of moving away from half-filling by the non-stoichiometry. From mentioned above, the rather broad line-width is considered to be due to the varieties of Au sites, and this implies that the oxidation state of Au is not completely homogeneous. The randomness of the Au and Br vacancies would suppress the lattice distortion from cubic. We note that this spectrum

resembles that (IS=0.53 mm/s relative to gold in the ^{197}Pt source, QS=0.94 mm/s, Γ=2.16.) reported by Gütlich, *et al.*,[4] for $Cs_{1.6}(Au^{III}Br_4)(Br_3)_{0.2}Br_{0.3}$, but compositional ratio is different from that in our cubic phase $CsAu_{0.6}Br_{2.6}$.

4-9 CONCLUSIONS

^{197}Au Mössbauer spectra were measured to investigate the mixed-valence states of $Cs_2Au^{I}Au^{III}X_6$ (X=Cl,Br,or I). The Au^{I} and Au^{III} states were clearly distinguishable for all the compounds. In this three-dimensional mixed-valence system, as the charge-transfer interaction between Au^{I} and Au^{III} becomes stronger in the order X=Cl<Br<I, the quadrupole splitting of Au^{III} increases, while that of Au^{I} decreases from X=Cl to X=Br and does not change from X=Br to I. This behavior suggests that the interaction between Au^{I} and Au^{III} s hould be stronger in the xy plane ($\perp$ c axis) than in the z direction (//c-axis), and therefore two-dimensional correlation may be present in the charge-transfer interaction between Au ions. For the cubic phase of Cs-Au-Br system $CsAu_{0.6}Br_{2.6}$, only a single resonance line having a rather broad half-width was observed. The cubic phase would be realized by the random distribution of Br vacancies.

References

1 J.Stanek, *J.Chem.Phys.*, 1982, 76, 2315.

2 M.O.Faltens and D.A.Shirley, *J.Chem.Phys.*, 1970, 53, 4249.

3 M.Katada, Y.Uchida, K.Sato, H.Sano, H.Sakai, and Y.Maeda, *Bull.Chem.Soc.Jpn.*, 1982, 55, 444.

4 P.Gütlich, B.Lehnis, K.Romhild, and J.Strähle, *Z.Naturforsch.*, 1982, 37b, 550.

5 H.Kitagawa, N.Kojima, and T.Nakajima, *J.Chem.Soc., Dalton Trans.*, 1991, 3121.

6 H.D.Bartunik and G.Kaindl, in 'Mössbauer Isomer Shifts,' ed.G.K.Shenoy and F.E.Wagner, North Holland, Amsterdam, 1978, chapter 8b, p.515

7 R.V.Parish, in 'Mössbauer Spectroscopy Applied to Inorganic Chemistry,' ed.G.J.Long, Plenum, New York, 1984, vol.1, p.577.

8 D.B.Brown and J.T.Wrobleski, in 'Mixed-Valence Compounds,' ed.D.B.Brown, D.Reidel, Dordrecht, The Netherlands, 1982, p.243.

9 H.Eckert, in 'Mössbauer Spectroscopy Applied to Inorganic Chemistry,' ed.G.J.Long, Plenum, New York, 1987, vol.2, p.125.

10 H.Kitagawa, N.Kojima, N.Matsushita, T.Ban, and I.Tsujikawa,

J.Chem.Soc.,Dalton Trans.,1991,3115.

11 T.P.A.Viegers,J.M.Trooster,P.Brouten,and T.P.Rit, *J.Chem.Soc.,Dalton Trans.*,1977,2074.

12 H.Schmidbaur,C.Hartmann,and F.E.Wagner,*Angew.Chem.Int.Ed. Engl.*,1987,26,1148.

13 N.Elliott and L.Pauling,*J.Am.Chem.Soc.*,1938,60,1846.

14 G.Brauer and G.Sleater,*J.Less-commom Met.*,1970,21,283.

15 J.C.M.Tindemans-v.Eijndhoven and G.C.Verschoor,*Mater.Res. Bull.*,1974,9,1363.

16 N.Kojima,H.Kitagawa,T.Nakajima,T.Ban,and I.Tsujikawa, Proceedings of the 25th International Conference on Coordination Chemistry,Nanjing,1987,A2-197.

17 J.Stanek,S.S.Hafner,and H.Schulz,*Phys.Lett.*,1980,76A, 333.

18 S.Yamada and R.Tsuchida,*Bull.Chem.Soc.Jpn.*,1956,29,421.

19 H.Tanino and K.Takahashi,*Solid State Commun.*,1986,59,825.

20 H.Prosser,G.Wortmann,K.Syassen,and W.B.Holzapfel, *Z.Physik B*,1976,24,7.

21 P.G.Jones,A.G.Maddock,M.J.Mays,M.M.Muir,and A.F.Williams, *J.Chem.Soc.,Dalton Trans.*,1977,1434.

22 D.M.S.Esquivel,D.Guenzburger,and J.Danon,*Phys.Rev.B*,1979, 19,1357.

23 T.K.Sham,R.E.Watson,and M.L.Perlman,*Phys.Rev.B*,1980, 21,1457.

24 D.Guenzburger and D.E.Ellis,*Phys.Rev.B*,1980,22,4203.

25 G.M.Bancroft,T.Chan,R.J.Puddephatt,and J.S.Tse, *Inorg.Chem.*,1982,21,2946.

26 R.V.Parish,*Gold Bull.*,1982,15,51.

27 M.Sano,H.Adachi,and H.Yamatera,*Bull.Chem.Soc.Jpn.*,1982, 55,1022.

28 P.Braunstein,U.Schubert,and M.Burgard,*Inorg.Chem.*,1984, 23,4057.

29 H.Prosser,F.E.Wagner,G.Wortmann,G.M.Kalvius,and R.Wäppling,*Hyperfine Interactions*,1975,1,25.

30 L.E.Orgel,*J.Am.Chem.Soc.*,1958,80,4186.

31 G.A.Bowmaker,P.D.W.Boyd,and R.J.Sorrenson,*J.Chem.Soc., Faraday Trans.2*,1985,81,1627.

32 A.K.H.Al-Sa'ady,C.A.McAuliffe,K.Moss,R.V.Parish,and R.Fields,*J.Chem.Soc.,Dalton Trans.*,1984,491.

33 P.Braunstein,A.Müller,and H.Bögge,*Inorg.Chem.*,1986,25, 2104.

34 H.D.Bartunik,W.Porzel,R.L.Mössbauer,and G.Kaindl, *Z.Physik*,1970,240,1.

35 G.M.Kalvius and G.K.Sheny,*At.Data Nucl.Data Tables*,1974, 14,639.

CHAPTER 5

INTERVALENCE CHARGE-TRANSFER ABSORPTION

5-1 INTRODUCTION

It is well known that compounds containing an element in two different oxidation states often show unusually intense colors. This absorption, labelled intervalence charge-transfer or mixed-valence absorption band, is not observed in the spectra of mononuclear parts and is attributed to an electron transfer from one metal site to the other.

In this chapter, We will discuss characteristics of polarization in the intervalence charge-transfer absorption of $Cs_2Au_2X_6$, which represents an anisotropy of the charge-transfer interaction between Au ions.

5-2 HISTORY OF INTERVALENCE CHARGE-TRANSFER ABSORPTIONS IN $Cs_2Au_2Cl_6$ AND RELATED COMPOUNDS

In 1920, Pollard described the preparation of a "new purplish-brown triple chloride" to which he assigned the formula $(NH_4)_8Ag_3Au_4Cl_{23}$[1]. This complex, which is called Pollard salt, had been studied about the mixed-valence state from a similarity with $Cs_2Au_2Cl_6$. Since its formula appeared rather complex, a new investigation was undertaken by Wells in 1922.[2] He described it as $(NH_4)_6Ag_2Au_3Cl_{17}$. Afterward, Yamada and Tsuchida also investigated Pollard salt which they described as $(NH_4)_3AgAuCl_7$.[3] Crystal structure determination of this complex was not performed until the preliminary work in 1971 and final work in 1975, by Bowles and Hall.[4] Though there had been a discrepancy in the empirical formula of its salt for a long time, they concluded it as $(NH_4)_6Ag_2Au_3Cl_{17}$, which is the same composition as that proposed by Wells. The crystal structure is shown in Figure 1.

In 1922, Wells extended the investigation by using cesium ion instead of ammonium ion and isolated five new triple chlorides[5] :

Complexes	Color
$Cs_4ZnAu^{III}{}_2Cl_{12}$	yellow
$Cs_4HgAu^{III}{}_2Cl_{12}$	orange

$Cs_4CuAu^{III}{}_2Cl_{12}$ ----- black

$Cs_4Ag_2Au^{III}{}_2Cl_{12}$ ----- very black

$Cs_4Au^{I}{}_2Au^{III}{}_2Cl_{12}$ ----- very black

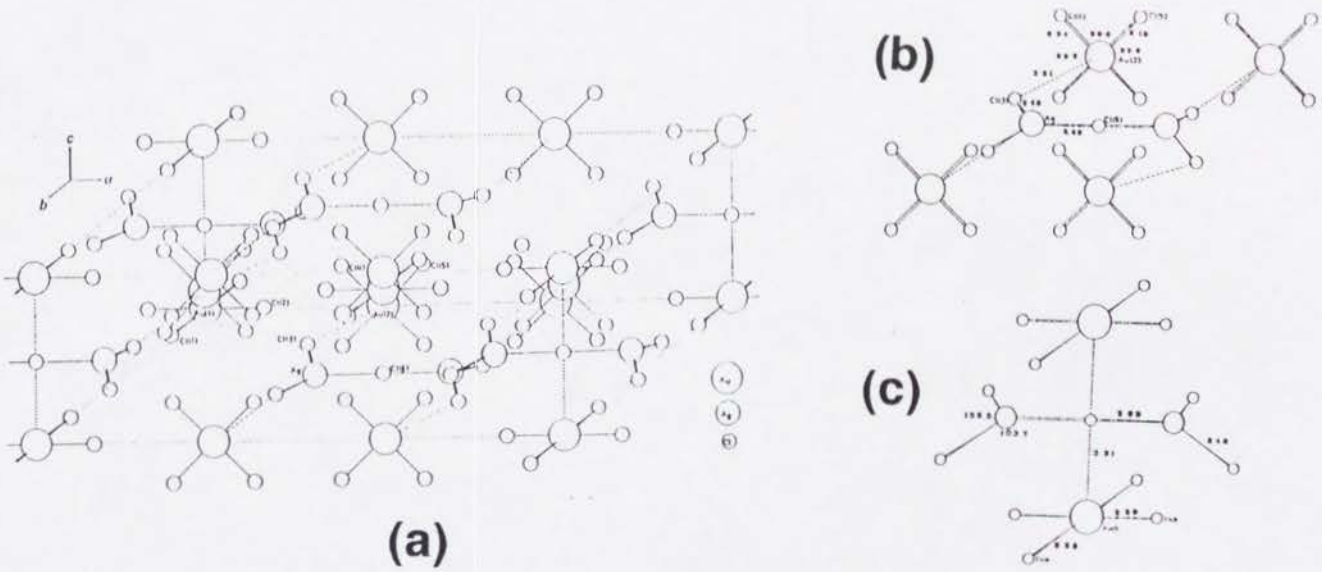

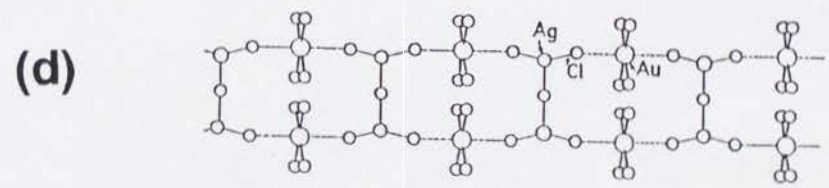

Fig.1 The crystal structure of Pollard salt $(NH_4)_6Ag_2Au_3Cl_{17}$. (a) Unit cell (b) The chains parallel to b. (c) The chains parallel to c (d) Double chains parallel to b.[4]

Wells compared the intense black color of the two salts, $Cs_4Ag_2Au^{III}{}_2Cl_{12}$ and $Cs_4Au^{I}{}_2Au^{III}{}_2Cl_{12}$, with Setterberg's very intensely colored salt $Cs_4Sb^{III}Sb^{V}Cl_{12}$[6] and noticed that the latter two each contained atoms of a metal in two valence states. He pointed out the analogy between $KFe^{II}Fe^{III}{}_2Br_9 3H_2O$ and $RbFe^{II}Fe^{III}{}_2Br_9 3H_2O$ and Prussian blue $KFe^{II}Fe^{III}(CN)_6$. Wells's explanation of the behavior of the chromophore was that "There is a constant exchange of electrons between the atoms of different valency, and that this activity of electrons affects the passage of light producing colors or opacity." In 1938, an X-ray study of crystallines $Cs_2AgAu^{III}Cl_6$ or $Cs_2Au^{I}Au^{III}Cl_6$ indicated that its structure was closely related to the perovskite structure.[7]

In 1956, the intervalence charge-transfer band in the halogen-bridged mixed-valence complexes were investigated for the first time by Yamada and Tsuchida.[3] They determined quantitatively the dichroism (Figure 2) of $[Pd^{II}(NH_3)_2Cl_2][Pd^{IV}(NH_3)_2Cl_4]$ and $Pt(en)Cl_3$. In both complexes, the optical measurement demonstrated the presence of a strong, broad absorption band at longer wavelengths than either of the component complexs. This absorption appeared in the spectral region from the visible to near-infrared, for the light polarized parallel to the needle axis (c-axis). The strong absorption band was thought to be a charge-transfer transition due to the infinite

chain as shown in Figure 3;

$$\cdots Cl-Pd^{IV}-Cl\cdots Pd^{II}\cdots Cl-Pd^{IV}-Cl\cdots$$

Wolffram's red salt, together with its corresponding bromine analogue, were also shown to contain infinite chain.

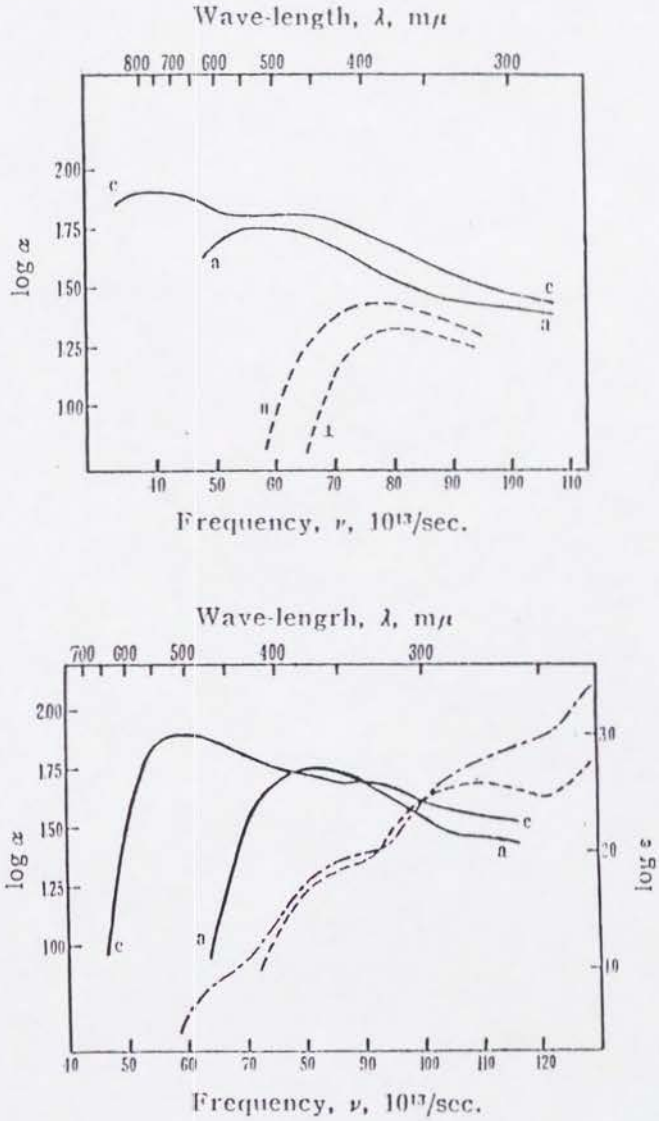

Fig.2 Absorption spectra of $[Pd^{II}(NH_3)_2Cl_2]$-$[Pd^{IV}(NH_3)_2Cl_4]$(above) and $Pt(en)Cl_3$(below)[3]

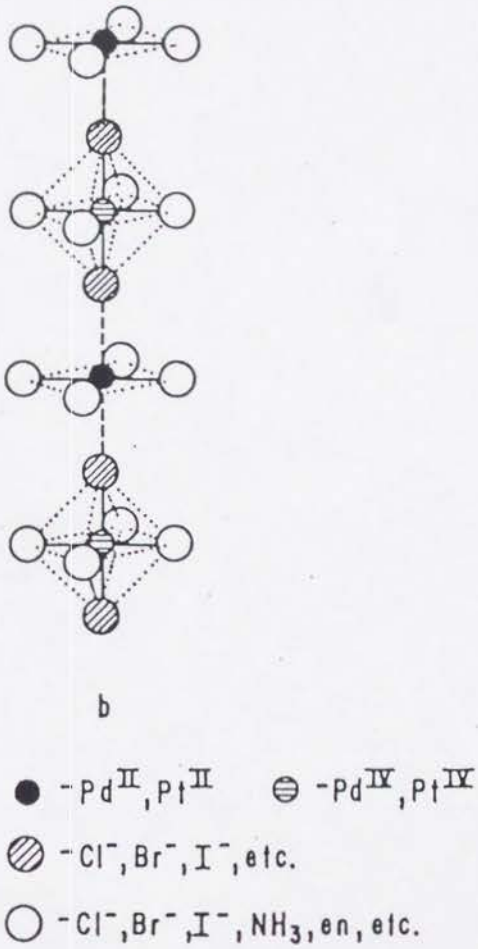

Fig.3 Chain structure in the one-dimensional halogen-bridged mixed-valence complexes

They also investigated Pollard salt.[3] An absorption band (Figure 4) at much longer wavelength than would be expected for the component complexes was observed. The new absorption band at about 18000 cm^{-1} was found to be polarized along the "c-axis".They considered that this band was a kind of

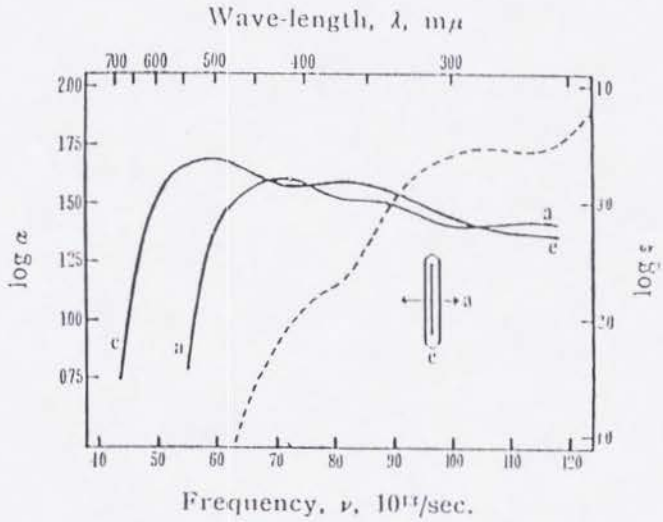

Fig.4 Absorption spectra of Pollard salt[3]

charge-transfer band and the salt might contain such an infinite chain as shown in Figure 3 along the c-axis. The "c-axis" of the salt, where they called, was the longitudinal axis of a single crystal. According to Professor S.Yamada, they did not perform the crystal structure determination of this complex.

However, many further investigators after 1956 has been failed to understand the Yamada-Tsuchida's experimental results exactly. They have thought that Yamada and Tsuchida determined the crystal axis (*i.e.*"c-axis") of this salt by

determined the crystal axis (*i.e.*"c-axis") of this salt by X-ray measurements.

Yamada and Tsuchida[3] also investigated $Cs_2AgAuCl_6$ salt as well as Pollard salt. However they could not quantitatively determined the dichroism of this salt because of too small crystals for the absorption measurement. So they made an observation with some of $Cs_2AgAuCl_6$ crystals under the microscope. The crystals showing a straight extinction were strongly dichroic. They described that "They appear almost black with the electric vector along the c-axis, and yellow with the electric vector normal to the c-axis".

A large controversial point is there in their description. This is the root of confusion. As well as the ammonium salt, they never determined the crystal axis of $Cs_2AgAuCl_6$ salt by X-ray analysis. I suppose that "the c-axis" they assigned was the longitudinal axis. From the analogy to $[Pd^{II}(NH_3)_2Cl_2][Pd^{IV}(NH_3)_2Cl_4]$ and $Pt(en)Cl_3$, they considered that absorption (i.e. black color) with the electric vector along the $\cdots Au^{III}(Cl_4)\cdots Cl\text{-}Ag^{I}\text{-}Cl\cdots Au^{III}$ chains (*i.e.*"c-axis" they called) lay at much longer wave-length than that (*i.e.* yellow color) with the electric vector normal to the chain. Because of their confusing description, many further workers have thought that the strong intervalence charge-transfer absorption appears

crystal axis (Figure 5). But, as mentioned below, it is doubtful that the "c-axis" they called was actually identical with the *true* c-axis.

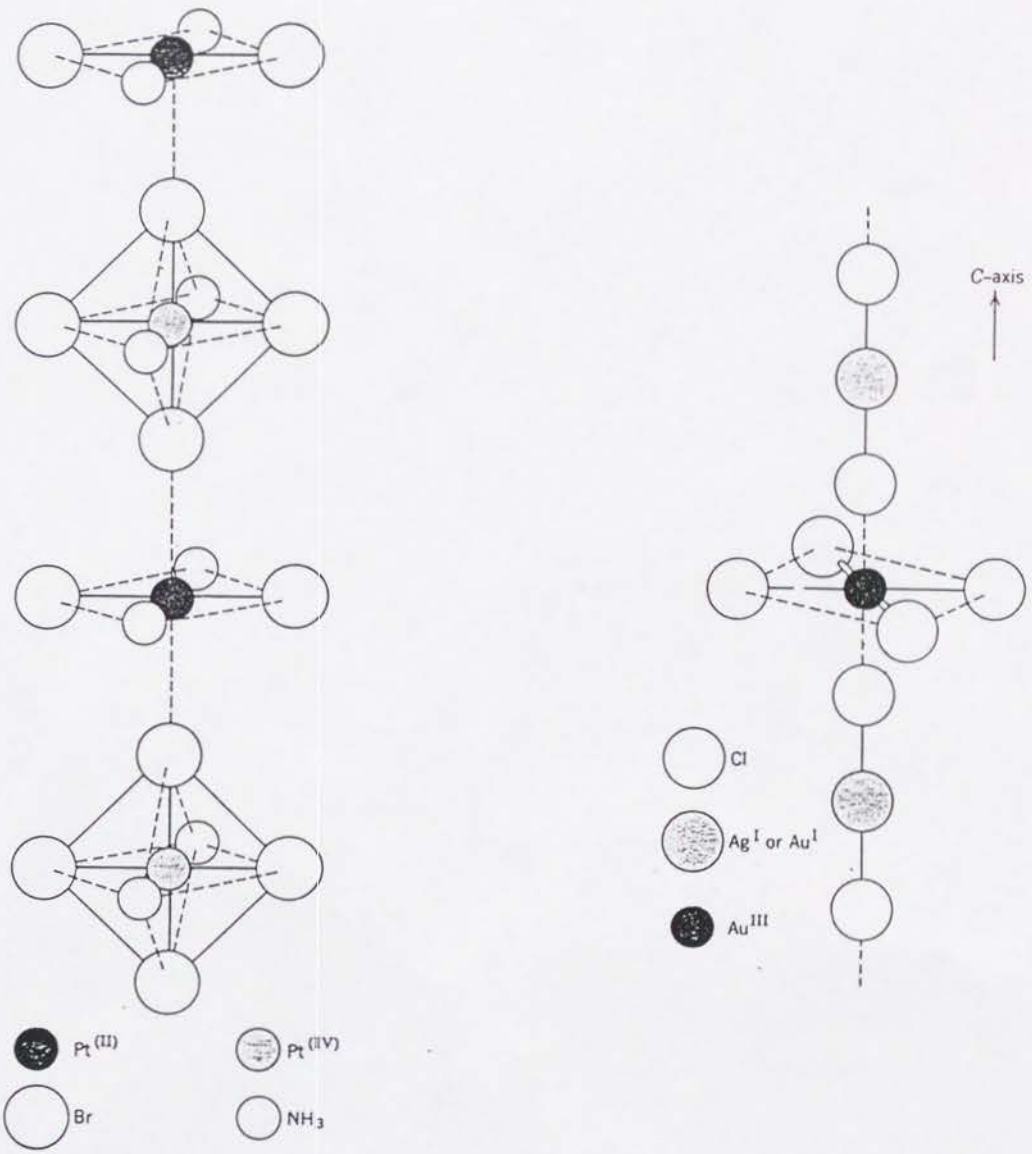

Fig. 5 Similarity in the Chain structures of the 1-D system and the c-axis of Wells salt

5-3 QUESTIONS IN PREVIOUS OPTICAL STUDIES FOR WELLS SALT

As pointed out by Robin and Day,[8] there are two relative orientations of $[Au^{I}Cl_2]^-$ and $[Au^{III}Cl_4]^-$ groups in the crystal, shown as configurations (a) and (b) in Figure 6. The configuration (a) is the networks in the c direction, while (b) is that in the ab plane. Robin and Day considered the following; In $Cs_2AuAuCl_6$, the donor and acceptor orbitals were the axially symmetrical dz^2 orbital of the $[Au^{I}Cl_2]^-$ ion and terminating in the dx^2-y^2 orbital of the $[Au^{III}Cl_4]^-$ ion, respectively. In the case of the configuration (a), the donor dz^2 and acceptor dx^2-y^2 orbitals should be diagonal. But in the case of the configuration (b), they must have a nonzero overlap. So they assumed that it was configuration (b) which was responsible for the mixed-valence absorption in $Cs_2AuAuCl_6$, and that this absorption would be polarized in the ab plane.

In 1962, Robin[9] determined the dichroism of $Cs_2AgAuCl_6$ and $Cs_2AuAuCl_6$ quantitatively. To the author's knowledge, this work has not been published. According to the Robin-Day "Mixed Valence Chemistry" review,[8] the absorption spectra of both salts showed the intervalence charge-transfer transition as a rather weak but distinct feature at 15500 cm^{-1} followed by a stronger absorption centered at 23500 cm^{-1}, having the opposite polarization. They thought that the latter band was

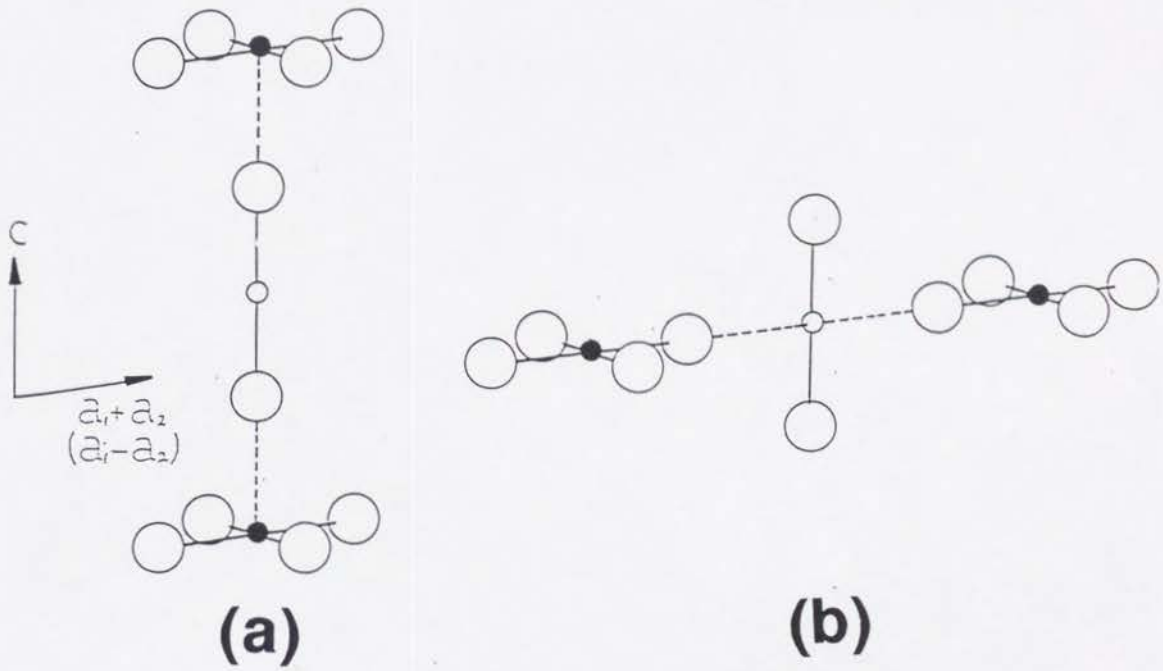

Fig.6 Two types of chains in $CsAuX_3$

due to the ligand-to-metal charge-transfer transition which was also observed at 23500 cm^{-1} for $[Au^{III}Cl_4]^-$ ion. Therefore, they thought that the 23500 cm^{-1} band must be polarized in $[Au^{III}Cl_4]^-$ plane (*i.e.* ab-plane), and that the 15500 cm^{-1} band should be the intervalence charge-transfer band polarized along the c-axis.

There was a discrepancy between their assumption and Robin's result. The author have several questions about the Yamada-Tsuchida's and Robim-Day's experimental results and

discussions about the absorption spectra in this mixed-valence system;

1) Is the dz^2 orbital of $[Au^{I}Cl_2]^-$, just as they thought, the donor orbital? Is the possibility of the dx^2-y^2 orbital of $[Au^{I}Cl_2]^-$ present as the donor orbital? If so, the donor and acceptor dx^2-y^2 orbitals of $[Au^{I}Cl_2]^-$ and $[Au^{III}Cl_4]^-$ should have a larger overlap than those in the case of Robin-Day's assumption. And the intervalence charge-transfer absorption band should be polarized in the ab-plane.

2) Is the 23500 cm^{-1} band (*i.e.* yellow color) observed for $Cs_2AgAuCl_6$ and $Cs_2AuAuCl_6$ not a LMCT band in $[Au^{III}Cl_4]^-$ but a LMCT band in $[Ag^{I}Cl_2]^-$ and $[Au^{I}Cl_2]^-$? The LMCT ($p\pi \rightarrow 6s$) band is situated in the ultraviolet region in the case of AgCl, $CsAgCl_2$, AuCl, and $[n\text{-}Bu_4N][AuCl_2]$. However, in the case that the Ag^{I} (or Au^{I}) ion is located in the Cl^- coordination octahedral site, the LMCT band might shift to the near-visible region. On the other hand, because of the higher energy level of ligand p-orbital, the LMCT band of AgBr, $[n\text{-}Bu_4N][AuI_2]$, AgI, and AuI is in fact situated in the near-visible region and the colors of the salts are yellow.

From the viewpoints of these problems and questions mentioned above, the author have investigated the absorption spectra of $Cs_2Au_2X_6$ (X=Cl,Br,I) and the polarized reflectance spectra of the single crystal $Cs_2Au_2I_6$

quantitatively for the first time.

5-4 EXPERIMENTAL

For absorption spectra, the powdered $Cs_2Au_2X_6$ (X=Cl,Br,I) were diluted with CsCl, KBr, and CsI, respectively, and then the mixtures were processed into pellets under pressure. The absorption spectra were measured at 4.2 K with a Jasco CT-100 spectrometer using a tungsten lamp for the light source. A lock-in amplifier system working with HTV R376 and R316 photomultiplliers and a PbS photoconductive cell was used for detection. The sample was placed in glass Dewar's vessel and immersed in liquid helium to cool.

The absorption spectra of solutions were measured at room temperature with a Hitachi model 356 Double Beam Spectrophotometer.

The single-crystal polarized reflectance spectra at room temperature were measured for the (110) and (001) faces of $Cs_2Au_2I_6$, with the CT-100 spectrometer, the tungsten lamp for the light source and a Glan-Thompson prism for polarizing the light. The electric vector (E) was aligned parallel to the ab-plane and the c-axis. Only as-grown surfaces were measured and typical sample dimensions were 3 × 2 × 1 mm. Samples were irradiated with the

monochromatic light and a lock-in amplifier system working with HTV R376 and R316 photomultipliers and a PbS photoconductive cell was used for detection. Data were collected with a NEC 9801VX0 computer linked to the lock-in amplifier. Detail of this system were described elsewhere.[10]

5-5 INTERVALENCE CHARGE-TRANSFER ABSORPTION SPECTRA OF $Cs_2Au_2X_6$

Figure 7 shows the solid-state absorption spectra of $Cs_2Au_2Cl_6$, $Cs_2Au_2Br_6$, and $Cs_2Au_2I_6$ at 4.2 K. Each of these mixed-valence complexes showed two strong absorption spectra in the region from visible to near-infrared, which are not observed in the spectra of the corresponding component complex ions. These two bands can be assigned to the intervalence charge-transfer transition (IVCT) from Au^{I} to Au^{III}, which is a common feature of the one-dimensional halogen-bridged mixed-valence metal complexes, namely the class-II mixed-valence compounds. In the order of $Cs_2Au_2Cl_6 \rightarrow Cs_2Au_2Br_6 \rightarrow Cs_2Au_2I_6$, the IVCT band at smaller wavenumber (IVCT-1) shifts to the lower energy, as well as the IVCT band at larger wavenumber (IVCT-2). This means that the energy difference between the electronic states of Au^{I} and Au^{III}

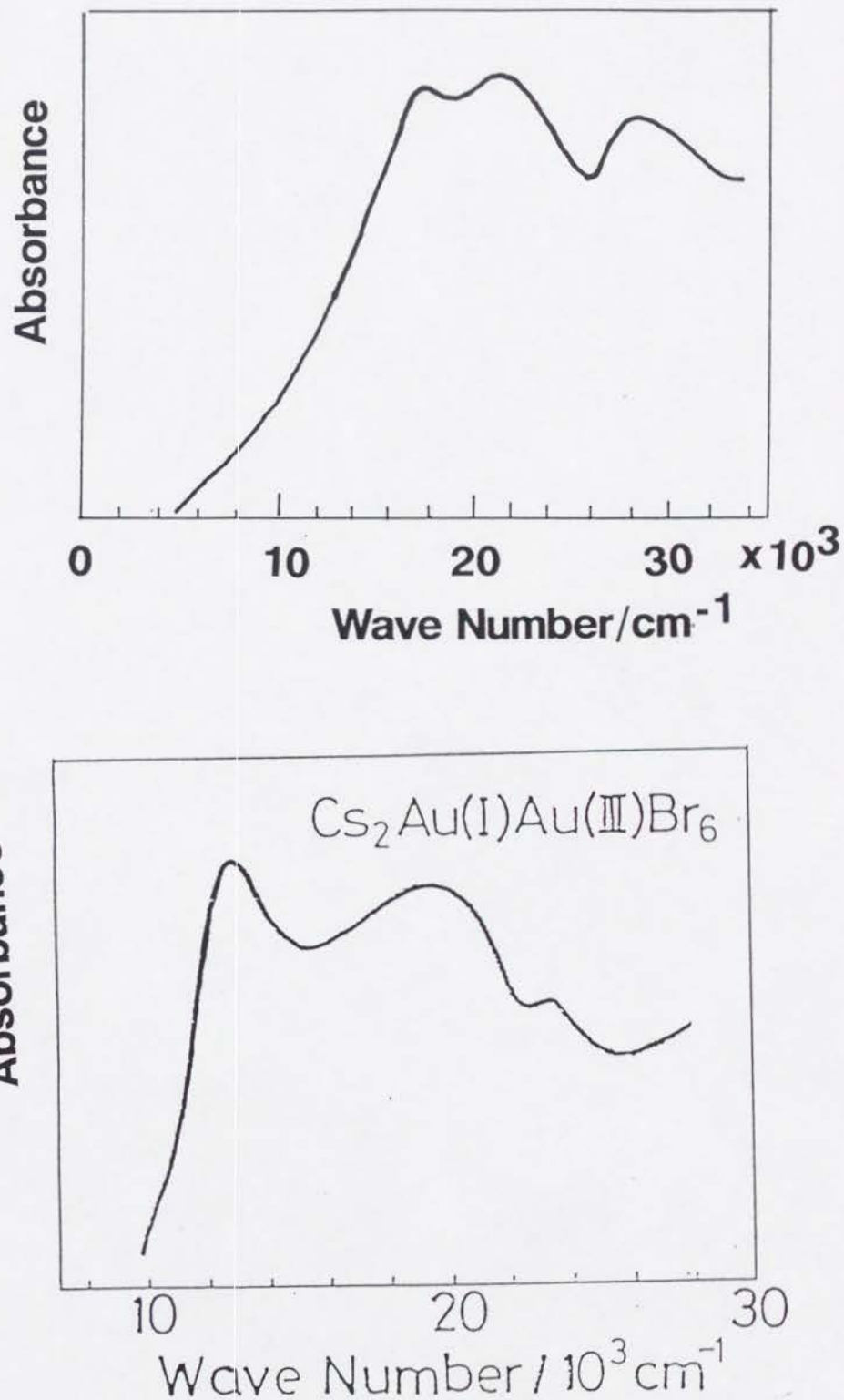

Fig.7 Absorption spectra of $CsAuCl_3$ (above) and $CsAuBr_3$ (below) (4.2 K)

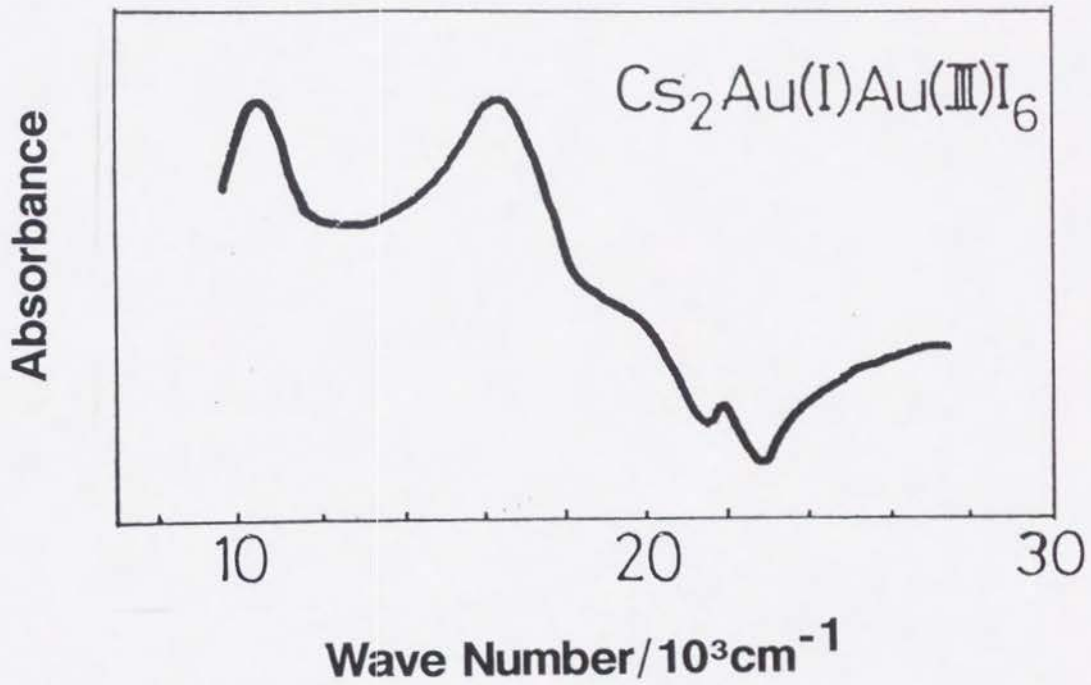

Fig.7 Absorption spectra of $CsAuI_3$ (4.2 K)

with the results of XPS and ^{197}Au Mössbauer spectroscopy studies (Chapter 3 and 4). As the covalency of $-Au^{I}-X-Au^{III}-$ networks becomes higher in the order of X=Cl<Br<I, the transfer energy between the 5d orbitals of Au^{I} and Au^{III} through the hybrid orbitals with p orbitals of the bridging halogen becomes larger. The absorption band at larger wavenumber than the two IVCT bands can be assigned to the ligand-to-metal charge-transfer transition (LMCT) from halogen $p\pi$ orbital to Au 5d orbital. The peak positions of IVCT-1, IVCT-2 and LMCT are listed in Table 1, together with the data[11] of related compounds.

Table.1 The energies of charge-transfer bands (cm^{-1}) at 4.2 K

(CM^{-1}) 4.2K

Complexes	IVCT-1	IVCT-2	LMCT
$Cs_2Au_2Cl_6$	16500	21500	28000
$Cs_2Au_2Br_6$	13000	19500	23500
$Rb_2Au_2Br_6$	18000	21000	25000
$Cs_2Au_2I_6$	10500	16300	19500
$Rb_2Au_2I_6$	12500	16500	20300
$K_2Au_2I_6$	11400 12900	16000	19100

In $Cs_2Au_2Cl_6$, the energies of the IVCT-1, IVCT-2 and LMCT bands are 16500 cm^{-1}, 21500 cm^{-1} and 28000 cm^{-1}. The spectrum obtained is not consistent with the preliminary one measured by Robin in 1962, which was described in the Robin-Day review. According to it, only one IVCT band was observed and its energy was 15500 cm^{-1}. On the other hand, the energy of LMCT was 23500 cm^{-1} and differs too greatly from the author's. Qualitative 5d-orbital energy-level diagrams for Au^{I} and Au^{III} in $Cs_2Au_2X_6$ are shown in Figure 8. The order of 5d orbital of Au^{I} is $dz^2 > dx^2-y^2 > dxz, dyz > dxy$. All these 5d orbitals are doubly occupied in the ground state. In the case of Au^{III}, that is $dx^2-y^2 > dz^2 > dxy > dxz, dyz$. Of these orbitals, all but dx^2-y^2 are doubly occupied. In general, the lowest energy transition in the electronic spectrum of $Cs_2Au_2X_6$ is expected to be dz^2 of $Au^{I} \rightarrow dx^2-y^2$ of Au^{III}. As pointed out

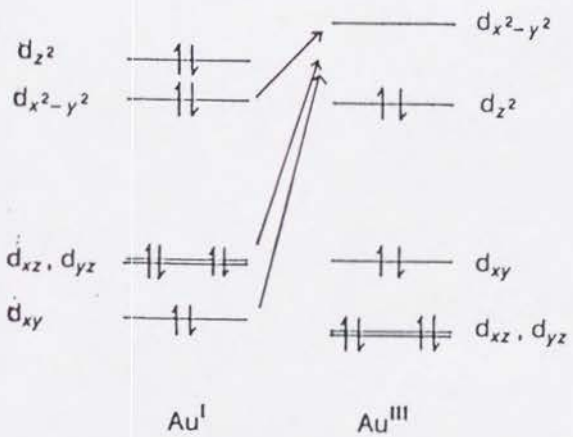

Fig.8 The 5d energy diagram of $Cs_2Au_2X_6$

by Robin and Day,[8] the dz^2 orbital of Au^{I} and the dx^2-y^2 orbital of Au^{III} are orthogonal in the c direction, while those orbitals in the a plane($\perp$ c) have a nonzero overlap. However, the overlap is considered to be very small. Therefore, the author considers that the charge-transfer interaction in $Cs_2Au_2X_6$ is mainly attributed to the larger overlap between the donor dx^2-y^2 orbital of Au^{I} and the acceptor dx^2-y^2 orbital of Au^{III} through the p orbitals of bridging halogen X. Compared with $Cs_2Au_2X_6$, the IVCT bands of $Rb_2Au_2X_6$(X=Br, I) and $K_2Au_2I_6$ is situated in the higher-energy side, which may be due to a smaller overlap integral between the dx^2-y^2 orbitals caused by their lattice distortions.

5-6 SINGLE-CRYSTAL POLARIZED REFLECTANCE SPECTRA OF $Cs_2Au_2I_6$

It is necessary and indispensable to examine whether the IVCT band at lower energy (IVCT-1) is allowed for the light polarized parallel to the c-axis or perpendicular to it. The former case means the following: As considered so far by not a few investigators, the absorption band appeared in the region from visible to near-infrared is the IVCT band from the dz^2 orbital of Au^{I} to the dx^2-y^2 orbital of Au^{III}.

The charge-transfer interaction in the Au-X networks of the c direction would be dominant. In the latter case, this absorption band can be assigned to the IVCT band from the dx^2-y^2 orbital of Au^{I} to that of Au^{III}. Fortunately, the author could synthesized single crystals of $Cs_2Au_2I_6$, which was the size suitable for the spectroscopic measurement. For $Cs_2Au_2Cl_6$ and $Cs_2Au_2Br_6$, the author has not obtained the suitable size ones. Because of the jet black color, the single crystal of $Cs_2Au_2I_6$ is not suited for transmission spectroscopic measurement. So the author has performed the single-crystal polarized reflectance spectra measurement for $Cs_2Au_2I_6$ at room temperature.

The reflectance spectra of $Cs_2Au_2I_6$ are shown in Figure 9. The reflectance for E⊥c is larger than that for E//c in the lower-energy region. This shows the absorption for E⊥c is stronger than that for E//c in this region. As the lowest-energy E⊥c reflectance peak at 1.3 eV(10500 cm^{-1}) does not appeared in the E//c reflectance spectrum and it's reflectance is large, it can be concluded that this peak is due to the IVCT from the dx^2-y^2 orbital of Au^{I} to that of Au^{III} within the Au-X networks of the ab-plane. Therefore, the absorption band IVCT-1, which observed at 1.3 eV for $Cs_2Au_2I_6$, can be assigned to the same. From the qualitative d-orbital energy-level diagram, it may be concluded that the reflectance peaks observed at 1.8 eV (14500 cm^{-1}) for the

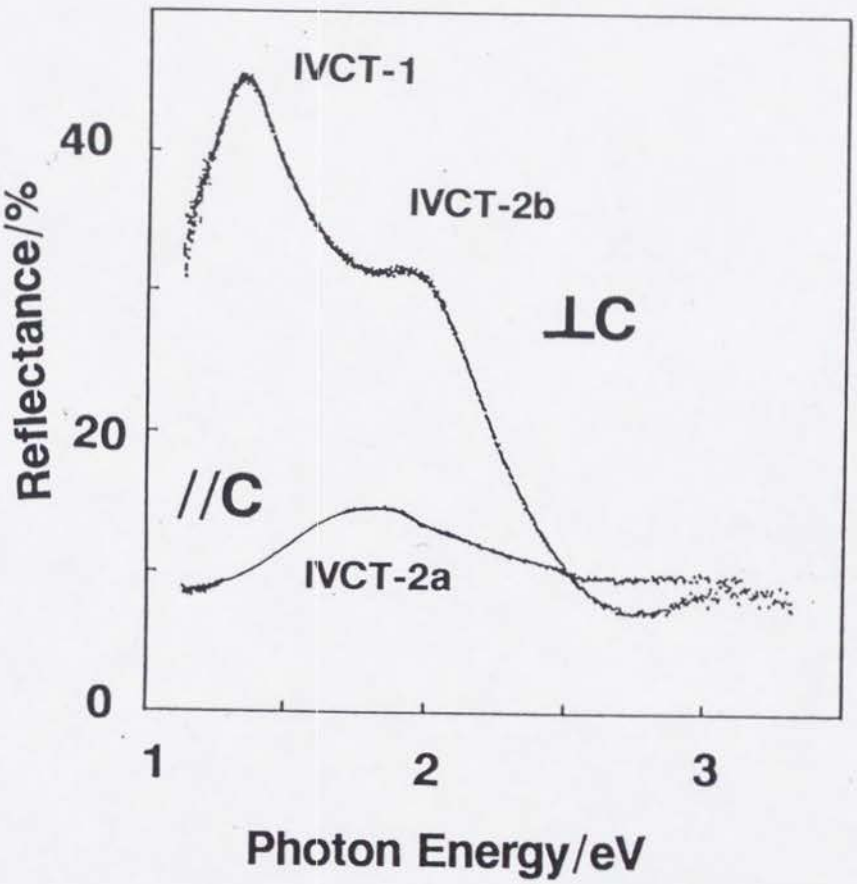

Fig.9 Reflectance spectra of $Cs_2Au_2I_6$

from the dxz and dyz orbitals of Au^{I} to the dx^2-y^2 orbital of Au^{III}. The reflection of this band is weak, which is consistent with the small overlap between those orbitals. It may be also concluded that the reflectance peaks observed at 2.0 eV (16000 cm^{-1}) for the light polarized perpendicular

to the c-axis is due to the IVCT from the dxy orbital of Au^{I} to the dx^2-y^2 orbital of Au^{III}. Therefore, the rather broader absorption band IVCT-2 consists of the two IVCT bands. One is the rather weak absorption (IVCT-2a) at lower energy (dxz, dyz of Au^{I} → dx^2-y^2 of Au^{III}) and the other is the stronger absorption (IVCT-2b) at higher energy (dxy of Au^{I} → dx^2-y^2 of Au^{III}).

Very recently N. Kojima[12] determined the selection rules of the intervalence charge-transfer transitions from group theory. For a treatment of this mixed-valence system, he considered an isolated unit consisting of seven complexes: a square-planar $[Au^{III}X_4]^-$ ion with six linear $[Au^{I}X_2]^-$ ions being adjacement to the square-planar ion in the directions of ± x, ± y, ± z axes. Table 1 shows the the selection rules of the intervalence charge-transfer transitions. Considering 5d-orbitals' splittings of Au^{I} and Au^{III} ions and overlapping integral between these orbitals, IVCT-1, IVCT-2a and IVCT-2b bands have been assigned to the followings.

IVCT-1 ; Au^{I} (dx^2-y^2) ⟶ Au^{III} (dx^2-y^2)

IVCT-2a; Au^{I} (dyz, zx) ⟶ Au^{III} (dx^2-y^2)

IVCT-2b; Au^{I} (dxy) ⟶ Au^{III} (dx^2-y^2)

According to the fact that the lowest-energy intervalence charge-transfer absorption (IVCT-1) is the transition of Au^{I} (dx^2-y^2) ⟶ Au^{III} (dx^2-y^2), we can conclude that

these orbitals play a most major role on the charge-transfer interaction. This is consistent with the results of XPS and Mössbauer spectroscopy (chapters 3 and 4).

Table 1. The selection rules of the intervalence charge-transfer transition in $Cs_2Au_2X_6$

IVCT along the c-axis	
E // c	E ⊥ c
$Au^{I}(d_{x^2-y^2}) \rightarrow Au^{III}(d_{x^2-y^2})$	$Au^{I}(d_{yz,zx}) \rightarrow Au^{III}(d_{x^2-y^2})$
IVCT in the ab-plane	
E // c	E ⊥ c
$Au^{I}(d_{yz,zx}) \rightarrow Au^{III}(d_{x^2-y^2})$	$Au^{I}(d_{z^2}) \longrightarrow Au^{III}(d_{x^2-y^2})$ $Au^{I}(d_{x^2-y^2}) \rightarrow Au^{III}(d_{x^2-y^2})$ $Au^{I}(d_{xy}) \longrightarrow Au^{III}(d_{x^2-y^2})$

5-7 RETURN TO THE PROBLEMS

Now, we will return to the problems of the previous works for $Cs_2Au_2Cl_6$ or $Cs_2AgAuCl_6$ by Robin, and Yamada and Tsuchida. The present results are in conflict with their

ones. It is doubtful that Robin examined the crystal axis by X-ray analysis, while it is sure that Yamada and Tsuchida did not. He might investigated only the dichroism of small crystals $Cs_2Au_2Cl_6$ under microscope as well as Yamada and Tsuchida did for $Cs_2AgAuCl_6$. As mentioned by them, the crystals appeared almost black (due to IVCT absorption) with the electric vector along a certain direction, and yellow (due to LMCT absorption) with the electric vector normal its direction. They considered that yellow color was due to the LMCT absorption within $[Au^{III}Cl_4]^-$ complex ion. However, though the $[Au^{I}Cl_2]^-$ complex ion is colorless, four additional ligand Cl^- ions to $[Au^{I}Cl_2]^-$ markedly lower its absorption to the visible region and this is attributed to formation of $Au^{I}Cl_6$ in $Cs_2Au_2Cl_6$. Harris and Reece[13] found the similar phenomenon for the LMCT absorption in $[Au^{III}Br_4]^-$ complex ion. Also the similar phenomenon is observed the LMCT bands in solid $Cs_2Au_2Cl_6$ and $Cs_2Au_2Br_6$, compared with the corresponding solution spectrum. This is mainly due to the change of the crystal field splitting going from the tetrahedral to octahedral site. The present results suggests that Robin, and Yamada and Tsuchida took the LMCT band from the ligand pz orbital to $5dz^2$ or 6s one of Au^{I} for the LMCT band from ligand px,y orbitals to $5dx^2-y^2$ one of Au^{III}. The former band must be polarized parallel to the c-axis, while the latter must be polarized perpendicular to it.

Consequently he thought the IVCT band to be polarized parallel to the c-axis by mistake.

Recently, Tanino, *et al.*[14] measured the reflectance spectra of polycrystalline $Cs_2Au_2Cl_6$ under pressure at room temperature (Figure 10). They observed strong IVCT bands in the visible spectral range. They also considered the IVCT band near at 2 eV, which the author abbreviates as IVCT-1, as an absorption presumably polarized parallel to the c-axis by mistake, as well as Robin, and Yamada and Tsuchida. According to their work, the low-energy reflectivity edge near 2 eV decreases continuously in energy at the extremely large rate under high pressure. So they suggested that the

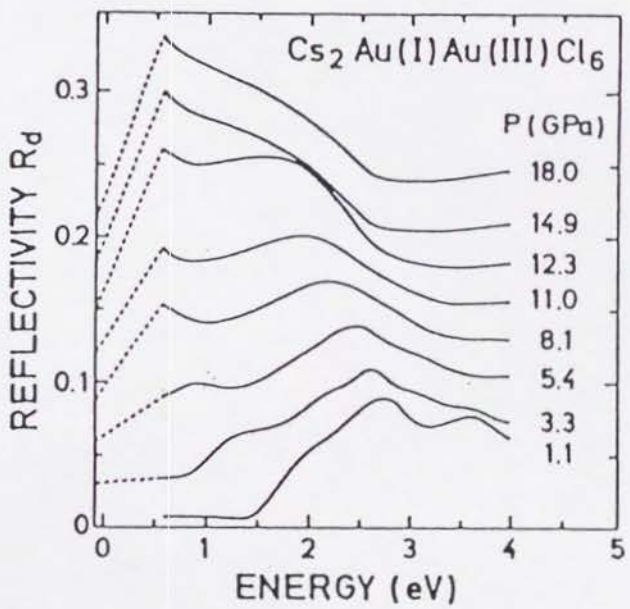

Fig.10 Reflectance spectra of polycrystalline $Cs_2Au_2Cl_6$ under high pressure[14]

electronic properties of $Cs_2Au_2Cl_6$ above 6.5 GPa are strongly anisotropic with metallic character along the c-axis only. However, from the ab polarization of IVCT-1 band observed actually by the polarized reflectance measurements, we suppose that this properties is anisotropic with metallic character in the ab plane($\perp$ c). As the pressure is increased, the bridging halogen is expected to shifts to the midpoint of Au ions. Accompanied by the movement of the halogen ions, the occupied dx^2-y^2 orbital of Au^{I} and unoccupied one of Au^{III} gradually degenerate and the difference in energy between the orbitals becomes smaller.

5-8 CONCLUSIONS

We have succeeded in solving the problem about the polarization of IVCT bands in $Cs_2Au_2X_6$. Three IVCT bands were observed for each of $Cs_2Au_2X_6$ salts. From the polarized reflectance spectra of $Cs_2Au_2I_6$, the strong absorption band at lowest energy can be assigned to be the intervalence charge-transfer transition from the dx^2-y^2 orbital of Au^{I} to that of Au^{III} within the Au-X networks of the ab-plane. This indicates that a two-dimensional correlation between Au ions is present in the charge-transfer interaction regardless of a three-dimensional perovskite structure.

References

1 W.B.Pollard, *J.Chem.Soc.*, 1920, 117, 99.

2 H.L.Wells, *Am.J.Sci.*, 1922, 4, 257.

3 S.Yamada and R.Tsuchida, *Bull.Chem.Soc.Jpn.*, 1956, 29, 421.

4 J.C.Bowles and D.Hall, *J.Chem.Soc., Chem.Commun.*, 1971, 1523: *Acta Cryst.* 1975, B31, 2149.

5 H.L.Wells, *Am.J.Sci.*, 1922, 3, 315:3.417.

6 O.K.Vetensk, *Akad.Forhamdl.*, 1882, 23

7 N.Elliott and L.Pauling, *J.Am.Chem.Soc.*, 1938, 60, 419.

8 M.Robin and P.Day, *Adv.Inorg.Chem.Radiochem.*, 1967, 10, 361.

9 M.Robin, unpublished results 1962 (in Ref.8).

10 N.Watanabe, Doctor's thesis of Kyoto Univ.(1988).

11 R.Kato, Master's thesis of Kyoto Univ.(1990).

12 N.Kojima, to be submitted for publication

13 C.M.Harris and I.H.Reece, *Nature*, 1958, 182, 1665.

14 H.Tanino, K.Syassen, Z.Wang, M.Hanfland and K.Takahashi, Proc.12th AIRAPT and 27th EHPRG Int.Conf.on High Pressure Science and Technology, Paderborn, (1989).

CHAPTER 6

Behavior of the Electrical Conductivity of the Three-Dimensional Mixed-Valence Compounds $Cs_2Au_2X_6$ (X=Cl, Br, I) Under High Pressure

6-1 INTRODUCTION

The crystal structure and mixed-valence state of $Cs_2Au_2X_6$ are similar to those of $BaBiO_3$ which is the host lattice of superconducting oxides $BaPb_xBi_{1-x}O_3$ and $Ba_{1-x}K_xBiO_3$. It can be correspondence: $Cs^+ \Leftrightarrow Ba^{2+}$, $Au^+, Au^{3+} \Leftrightarrow Bi^{3+}, Bi^{5+}$, $X^- \Leftrightarrow O^{2-}$. So, the compounds $Cs_2Au_2X_6$ are interesting from the viewpoints of the researches on superconducting materials.

In the case of $Cs_2Au_2Cl_6$, R.Keller *et al.*[1] reported a strong continual increase in the electrical conductivity by nearly nine orders of magnitude from ambient pressure to 12 GPa and a gradual semiconductor-to-metal transition at about

6 GPa has been interpreted as evidence for the overlap of the filled $5d_{z^2}$ band of Au^{I} and the empty $5d_{x^2-y^2}$ band of Au^{III}. Being stimulated by killer *et al.*'s work, several studies on $Cs_2Au_2Cl_6$ under high pressure have been done. In 1979, W. Denner *et al.* measured[2] its crystal structure under high pressures. According to them, with increasing pressure the Cl atom shifts gradually toward the midpoint of the Au atoms that is attained at 5.2 GPa. Therefore, they have described that the Au sites become indistinguishable and the valence state of Au is Au^{II} above 5.2 GPa. However, ^{197}Au Mössbauer spectra[3] and Raman spectra[4] of $Cs_2Au_2Cl_6$ under high pressures have shown that the Au^{I} and Au^{III} sites are still clearly distinguishable even above 5.2 GPa. As mentioned above, the elucidation of the Au valence state of $Cs_2Au_2Cl_6$ under high pressures has not yet been achieved. Turning to $Cs_2Au_2Br_6$ and $Cs_2Au_2I_6$, little work has been reported on physical properties under high pressure.

Being stimulated by these problems, we have intended to elucidate the Au mixed-valence state of $Cs_2Au_2X_6$. In this chapter, we report the behavior of the electrical resistivities of $Cs_2Au_2X_6$ (X=Cl,Br,I) under high pressures and discuss the Au valence state.

6-2 EXPERIMENTAL

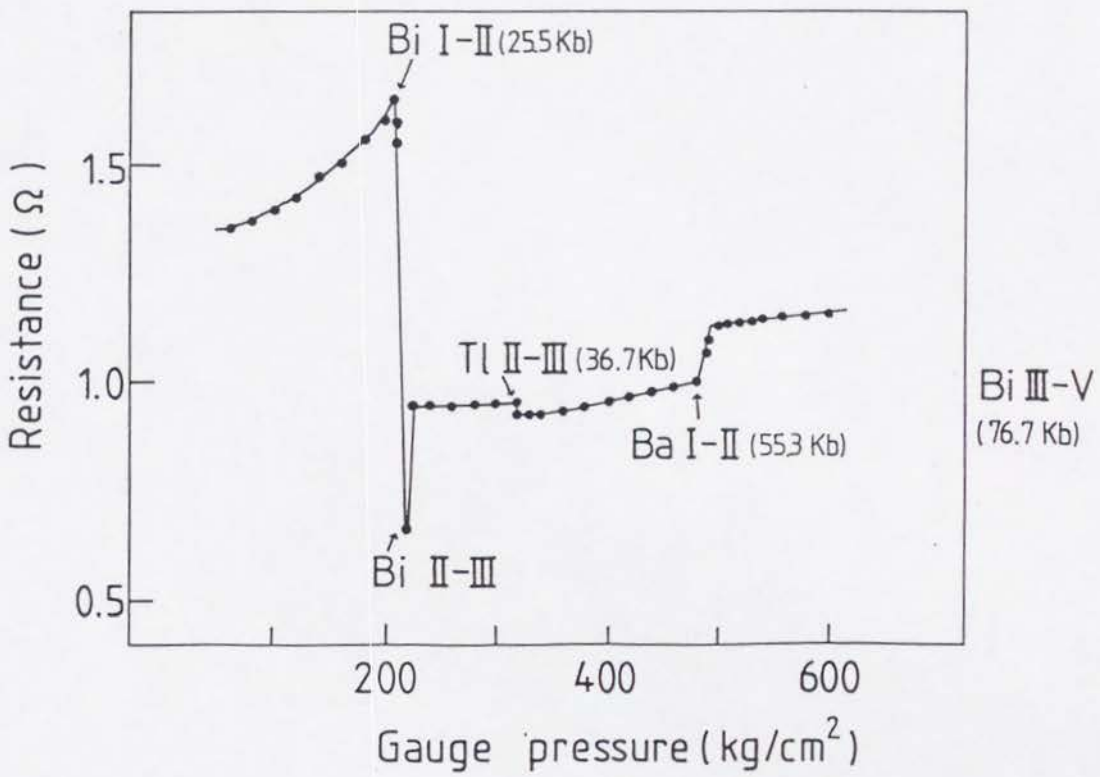

Fig.1 Calibrations of pressure

High pressures were generated by a 1200 ton cubic anvil having an edge of 10 mm using pyrophyllite and talc as a pressure medium. Sharp changes in the electrical resistivity of Bi_{I-II} (2.55 GPa), Tl_{II-III} (3.67 GPa), Ba_{I-II} (5.53 GPa), and Bi_{III-V} (7.67 GPa) were used to calibrate the pressure of the sample cell. One of the calibrations is shown in Figure 1. The d.c. electrical resistivity measurements were performed on polycrystalline samples with quasi-four-probe method which was applied at the sample or the ends of the upper and lower anvils. The sample was covered with Pt plates to guarantee a good contact. The sample was heated by an internal manganine resistance heater and its temperature was measured by Alumel-Chromel thermocouple. Two types of the sample assembly used for resistivity measurements under high pressure are shown in Figure 2. The detailed high-pressure apparatus is described elsewhere.[5]

6-3 BEHAVIOR OF ELECTRICAL RESISTIVITY UNDER HIGH PRESSURE

Figure 3 shows the behavior of the electrical resistivities of the compounds $Cs_2Au_2X_6$ under quasi-hydrostatic pressures at room temperature (r.t.). When the pressure is applied up to 7.0 GPa, the resistivities of $Cs_2Au_2Cl_6$ and $Cs_2Au_2Br_6$ decrease rapidly by nearly ten

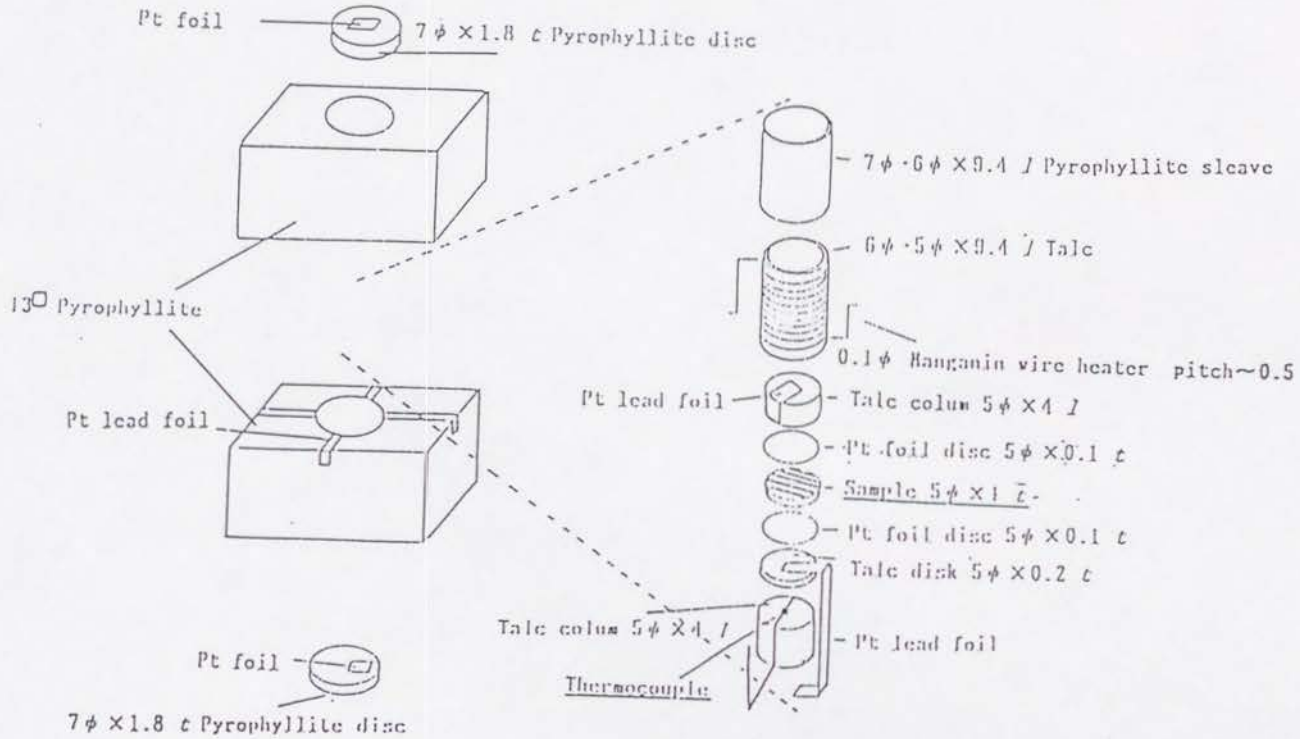

Fig.2a Sample assembly used for measurements of resistivity under high pressures Older-type cell of two-probe method

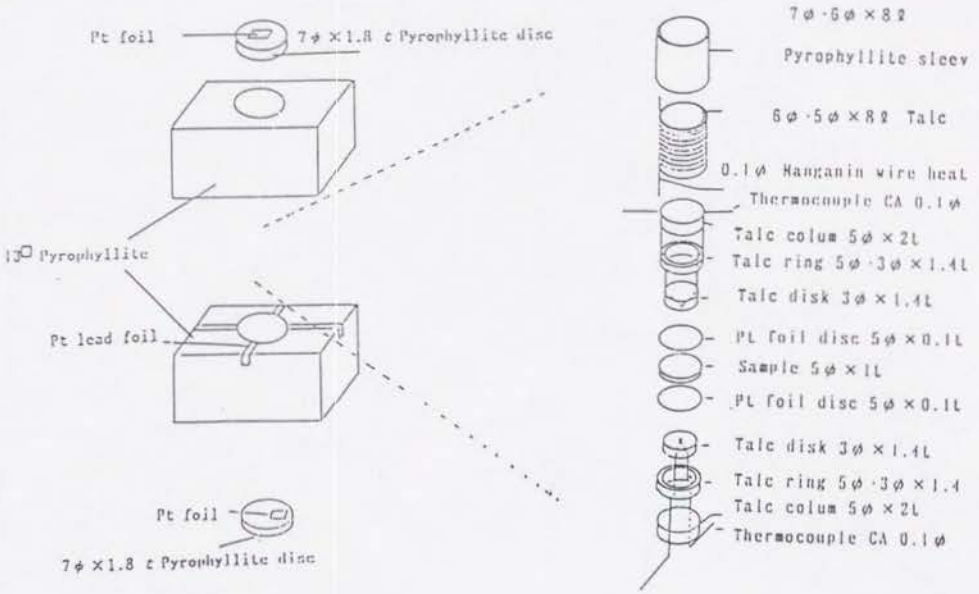

Fig.2b Sample assembly used for measurements of resistivity under high pressures Newer-type cell of quasi-four-probe method

orders of magnitude down to the semimetal region of 4.8×10^{-2} Ω cm and 7.2×10^{-3}Ω cm, respectively. In the case of $Cs_2Au_2I_6$, it decreases rapidly from 2.2×10^{7}Ω cm down to 6.9×10^{-3}Ω cm between ambient pressure (a.p.) and 5.4 GPa, then increases above 5.4 GPa. The resistivity minimum was not observed for $Cs_2Au_2Cl_6$ and $Cs_2Au_2Br_6$ in the pressure region of 0-7 GPa where our pressure vessel can generate. In the pressure region of 2-5.5 GPa, the electrical conductivity increases in the order of X=Cl<Br<I. This behavior can be explained by an increase of the transfer energy between Au 5d orbitals through halogen *p* orbitals in this order.

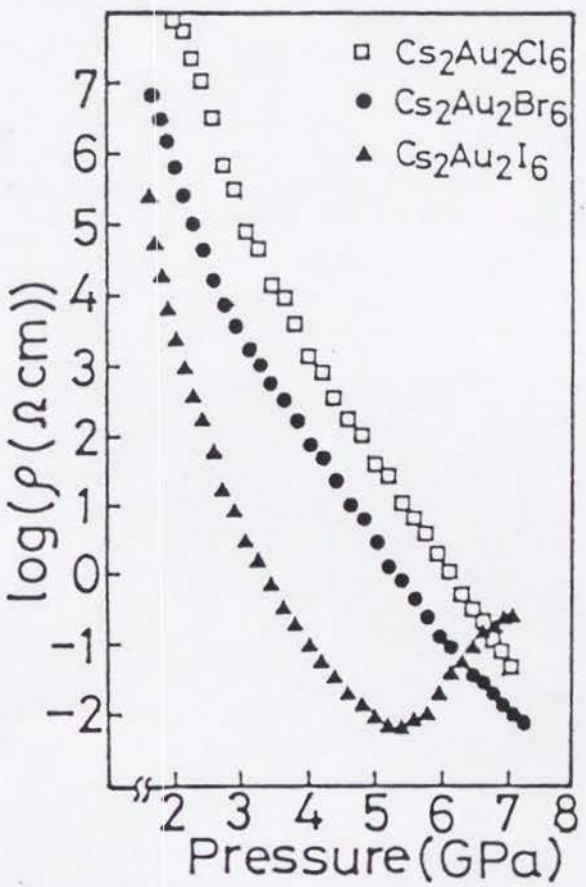

Fig.3 Electrical resistivities of $Cs_2Au_2X_6$ (X=Cl,Br,I) as a function of pressure at r.t.

6-4 BEHAVIOR OF ENERGY GAP UNDER HIGH PRESSURE

Figure 4 shows the energy gap Eg of $Cs_2Au_2X_6$ at the temperatures above r.t. as a function of pressure. The energy gap was obtained by a least-squares fit to the usual equation $\sigma = \sigma_0 \exp(-Eg/2kT)$. The energy gaps of $Cs_2Au_2Cl_6$, $Cs_2Au_2Br_6$, and $Cs_2Au_2I_6$ decrease linearly with increasing pressure. The decrease of the energy gap can be explained mainly by the decrease of the difference between the site energies of Au^{I} and Au^{III}, which is due to the halogen anions' shifting to the midpoint of Au cations, and secondarily by the broadening of the bands near the Fermi energy. Average pressure coefficients $\Delta Eg/\Delta P$ are found to be -1.6×10^{-5}, -1.3×10^{-5}, and -3.5×10^{-5} for $Cs_2Au_2Cl_6$, $Cs_2Au_2Br_6$, and $Cs_2Au_2I_6$, respectively. The absolute coefficient decreases in the order of $Cs_2Au_2I_6$ > $Cs_2Au_2Cl_6$ > $Cs_2Au_2Br_6$, which implies that the bridging Br^- anion is the hardest to shift to the midpoints of Au cations with increasing pressure.

The energy gaps are estimated by extrapolation as zero at 7.5 GPa, 7.2 GPa, and 4.5 GPa, respectively. From these results, $Cs_2Au_2I_6$ was found to undergo a pressure-induced semiconductor-to-metal transition at 4.5 GPa, and $Cs_2Au_2Cl_6$ and $Cs_2Au_2Br_6$ are expected to undergo a pressure-induced semiconductor-to-metal transition at 7.5 GPa and 7.2 GPa.

respectively.

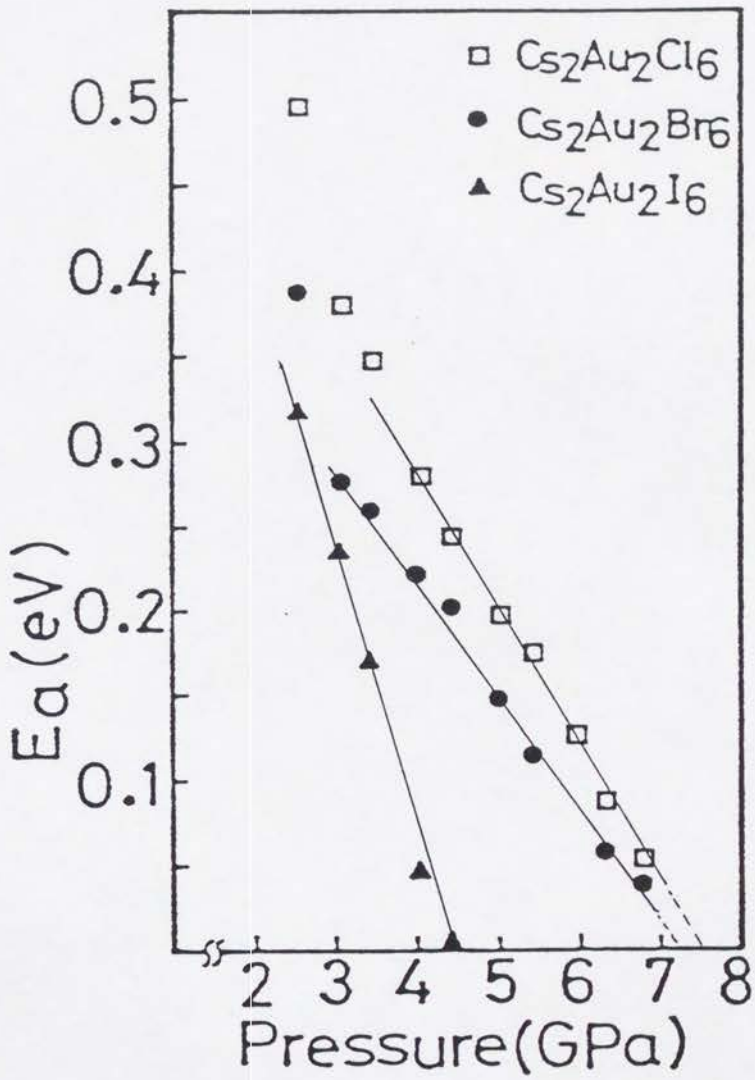

Fig.4 Activation energies of $Cs_2Au_2X_6$ (X=Cl,Br,I) as a function of pressure.

In connection with these results, the following should be mentioned. In the case of $Cs_2Au_2Cl_6$, there are two differences between our results and those of Keller *et al.*:

(1) our energy gap observed is ten times as large as theirs

(2) our critical pressure (7.5 GPa) where the energy gap becomes zero is higher than theirs (~6 GPa).

According to Keller *et al.* the $\log\rho$ versus $1/T$ plots are not linear over any large temperature range. They estimated the energy gap of $Cs_2Au_2Cl_6$ at the low temperatures while we did it above room temperature, which are responsible for the above mentioned differences. Recently, Tanino, *et al.*[4] have reported optical reflectance spectra of $Cs_2Au_2Cl_6$ under high pressure. The optical gap energy E_{OP} observed at r.t. is compatible with twice the energy gap Eg ($=2E_{th}$) which we measured for the activation energy of conduction. In general within the following simple relation has been derived within the high-temperature limit.

$$E_{th} \simeq E_{OP}/4$$

A qualitative agreement was found between the values of E_{th} deduced from optical measurements and the observed activation energy of conduction, E_{th}. Moreover the optical energy gap at r.t. of $Cs_2Au_2Cl_6$ below 4 GPa extrapolates to a zero gap energy at 6.5 GPa, which is consistent with our result (6.6 GPa) of electrical conductivity measurements. From

good agreements between our and Tanino *et al*'s results, the difference in energy gap between our and Keller *et al*'s measurements result from the difference in the temperature range where the energy gap was estimated.

Keller *et al*. reported that the energy gap of $Cs_2Au_2Cl_6$ became zero near at 6 GPa and observed the resistance minimum for it at 11 GPa. Recently, Tanino *et al*. have observed[4] two resonant Raman modes peaks for $Cs_2Au_2Cl_6$ under pressures up to at least 8 GPa (Figure 5), which are assigned to stretching vibrations of the bridging chlorines about the Au^{I} and Au^{III} atoms. This shows that two different Au species are still present well above 5 GPa, in accordance with Mössbauer studies, but at variance with X-ray diffraction results. They also have observed a discontinuous increase of the reflectivity at 0.6 eV for $Cs_2Au_2Cl_6$ near at 11 GPa. Tanino *et al*. attribute it to a structural phase transition. We note that a resistance curves for $Cs_2Au_2Cl_6$ reported by Keller *et al*. showed a slight resistance minimum at about 11 GPa. We guess from other workers' results the followings. Even at 7 GPa in the case of $Cs_2Au_2Cl_6$, the Cl^- ions are still in a nonsymmetric positions between Au ions and the Au^{I} and Au^{III} states are distinguishable. These result in non-degenerate d-bands near the Fermi energy. However the disappearance of the band gap of $Cs_2Au_2Cl_6$ derives from the small overlap of the Au^{I} valence band with the Au^{III}

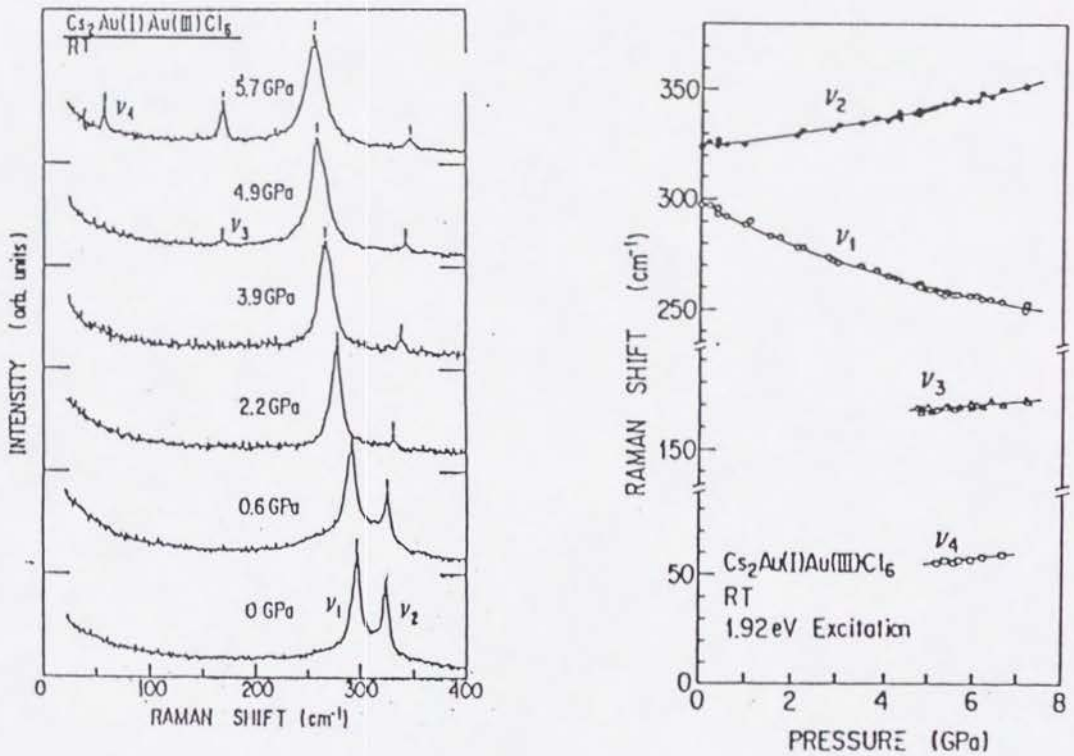

Fig.5 Raman spectra and line frequencies of $Cs_2Au_2Cl_6$ under high pressure.[4]

conduction band. This case is considered to be semimetal state where the carrier concentration is small. At the pressure of 11 GPa where the reflectivity at 0.6 GPa increases discontinuously, the Cl^- ions come to be situated at the midpoints of Au ions and the valence state of Au is +Ⅱ. The d-bands near Fermi energy must be completely degenerate and half-filled. Therefore the carrier concentration is expected to increase considerably, which is consistent with the increase of the reflectivity.

But strange to say, the resistivity curves of $Cs_2Au_2Cl_6$ show a resistance minimum at the same pressure of 11 GPa. This behavior is puzzel for us. The fact that the resistance minimum was observed at 5.5 GPa for $Cs_2Au_2I_6$ indicates that the valence state of Au would come to be +II at this pressure.

In the case of $Cs_2Au_2I_6$, a gradual semiconductor-to-metal transition occurs at about 4.5 GPa in the sense of $d\sigma/dT$. In the pressure region where the activation energy become zero, the halogen ions presumably shift toward the midpoint of the Au^{I} and Au^{III} sites and then the filled $5d_{x^2-y^2}$ band of Au^{I} and the empty $5d_{x^2-y^2}$ band of Au^{III} overlap each other, which is responsible for the gradual semiconductor-to-metal transition. As shown in Figure 6, the resistivity becomes to be metallic above 4.5 GPa.

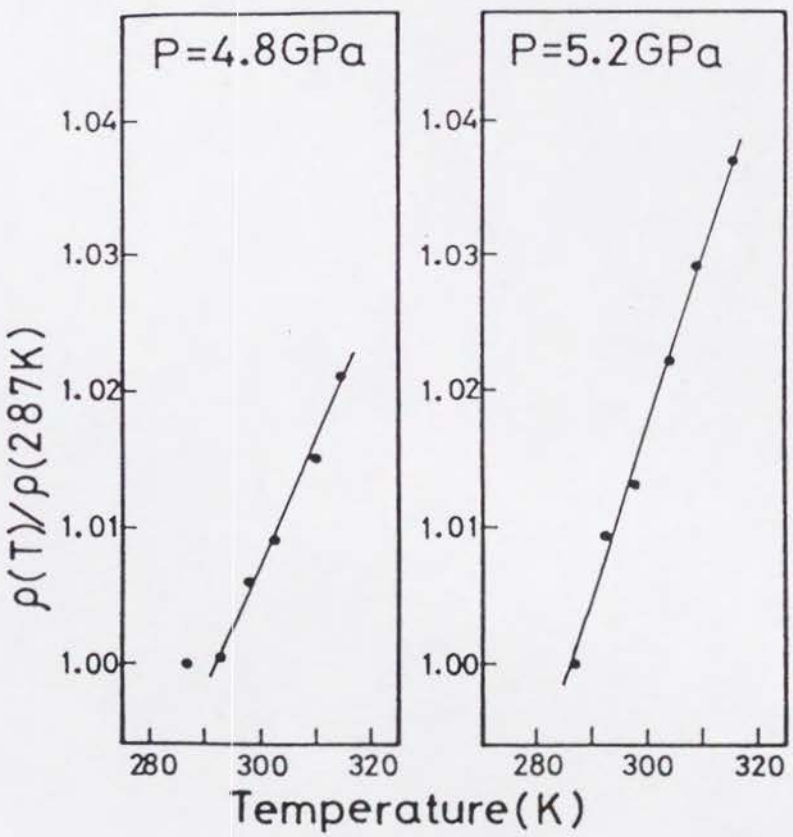

Fig.6

However in the case of $Cs_2Au_2I_6$, as shown in Figure 7, when the temperature is increased at 6.5 GPa, the resistivity decreases and a steep drop occurs at about 330 K and then it increases linearly above 420 K, which implies that $Cs_2Au_2I_6$ has two metallic phsaes and a metal-to-metal transition occurs at P=6.5 GPa and T~ 330 K. In the cooling

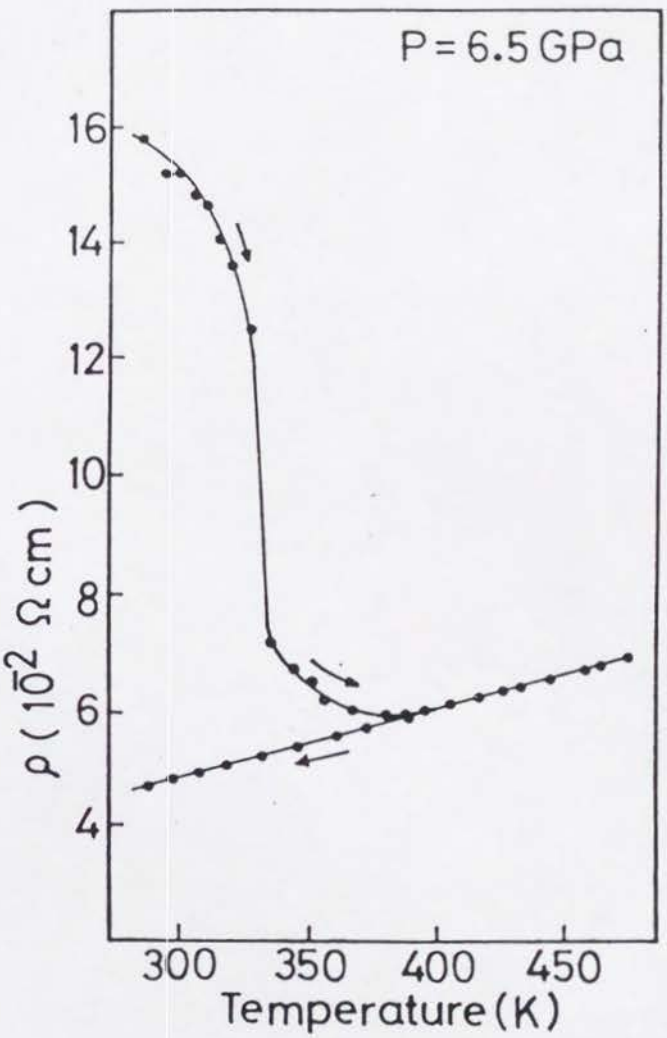

Fig.7 Temperature dependence of the electrical resistivity of $Cs_2Au_2I_6$ at P=6.5 GPa. The sample is first heated up to 480 K, then cooled down to room temperature.

process, the electrical resistivity decreases linearly with temperature cooled down to r.t. This fact implies that the second metallic phase appeared at P=6.5 GPa and T>330 K can be stable at P=6.5 GPa and T=r.t. in the cooling process. Moreover, this metallic phase could be obtained as a metastable phase at r.t. and a.p. by decreasing temperature and pressure after increasing pressure up to 6.5 GPa and temperature up to 480 K. However the resistivity gradually increases from $\sim 5\times 10^{-2}\Omega$ cm to $\sim 10^{7}\Omega$ cm in an hour at a.p.

Figure 8(b) shows the X-ray powder pattern of this metastable phase of $Cs_2Au_2I_6$, which implies that the crystal structure of the second metallic phase appeared at P=6.5 GPa and T>330 K is a cubic perovskite structure (*Pm*3*m*). In this phase, it is considered that the Au valence state is Au^{II} and the degenerate $5d_{x^2-y^2}$ and $5d_{z^2}$ bands are three-quarters filled. The DSC measurement for this metastable phase shows an exothermic anomaly at about 350 K on heating between r.t. and 370 K, while it dose not show any anomaly on cooling between r.t. and 370 K. As shown in Figure 8(c), the X-ray pattern after annealing the metastable phase of $Cs_2Au_2I_6$ at 370 K is assigned to the tetragonal perovskite structure. From these results, it is concluded that the metastable cubic phase of $Cs_2Au_2I_6$ changes itself into normal tetragonal perovskite phase at about 350 K.

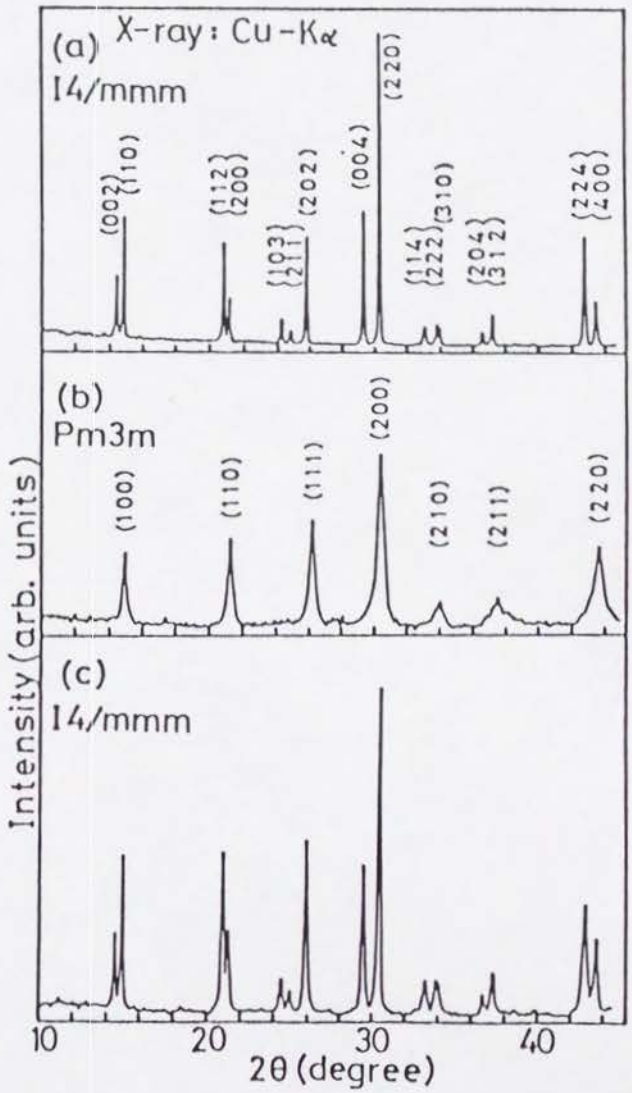

Fig.8 X-ray powder patterns of $Cs_2Au_2I_6$ at r.t. and a.p. (a) X-ray pattern before applying pressures. (b) X-ray pattern of the metastable phase obtained by decreasing temperature and pressure after increasing pressure up to 6.5 GPa and increasing temperature up to 480 K. (c) X-ray pattern after annealing the metastable phase at 370 K.

6-6 CONCLUSIONS

Electrical resistivity of the three-dimensional Au mixed-valence compounds $Cs_2Au_2X_6$ (X=Cl,Br,I) was investigated under quasihydrostatic pressures up to 7.0 GPa and temperatures between room temperature and 480 K. In the case of $Cs_2Au_2I_6$, a semiconductor-to-metal transition (P=4.5 GPa, T=room temperature) and a metal-to-metal transition (P=6.5 GPa, T$\sim$330 K) were observed. The latter metallic phase could be obtained at room temperature and ambient pressure as a metastable phase, whose structure was found to be a cubic perovskite structure from the X-ray diffraction pattern. The Au valence state of the metallic phases is expected to be +Ⅱ.

References

1 R.Keller, J.Fenner and W.B.Holzapfel, *Meter.Res.Bull.*9 (1974),1363.

2 W.Denner, H.Schulz and H.D'Amour, *Acta Cryst.*A35 (1979) 360.

3 J.Stanek, *J.Chem.Phys.*76 (1982) 2315.

4 H.Tanino, K.Syassen, Z.Wang, M.Hanfland and K.Takahashi, Proc.12th AIRAPT and 27th EHPRG Int.Conf.on High Pressure Science and Technology, Paderborn, (1989).

5 J.Osugi, K.Shimizu, K.Inoue and K.Yasunami, *Rev.Phys.Chem. Jpn.*34 (1964) 1.

CHAPTER 7

Consecutive Phase Transitions of the 3-D Mixed-Valence Compex $Cs_2Au_2I_6$ under High Pressure

7-1 INTRODUCTION

Since the discovery of superconductivity in the perovskites $La_{2-x}Ba_xCuO_4$[1] and $YBaCu_3O_7$[2] there have been a large number of materials researches for high-temperature superconductors. A large number of new perovskite-type oxides have been synthesized and some of them exhibit superconductivity. It is well known that the breakthrough of Bednorz and Müller in discovering superconductivity in the $La_{2-x}Ba_xCuO_4$[1] system was inspired in part by their knowledge of the superconducting properties of $BaPb_{1-x}Bi_xO_3$[3]. In the $BaPb_{1-x}Bi_xO_3$ system, the bismuth valence state has been considered very important factor for the comprehension of

its physical properties. The insulating state of its parent compound $BaBiO_3$ was explained by the charge disproportionation of the bismuth cations (+Ⅳ into +Ⅲ and +Ⅴ) which couples to lattice deformation or the stabilization of a commensurate charge-density wave (CCDW)[4]. On the other hand, a large number of perovskite-type halides ABX_3 and A_2BX_4 (A=alkali metal; B=metal; X=F,Cl,Br,I) have been known. However, among the perovskite-type halides, only a few compounds exhibit mixed valency.

$CsAuX_3$ (X=Cl,Br,I) is known as a rare three-dimensional halogen-bridged mixed-valence system in which the three-dimensional MX-networks are orthogonal to each other. This system exhibits the $Au^{I}(5d^{10})$-$Au^{III}(5d^{8})$ mixed valency. As shown in Figure 1, the crystal structure of $Cs_2Au_2Cl_6$ is a distorted perovskite structure with tetragonal space group $I4/mmm$[5,6]. It can be characterized by a breathing-mode-type atomic distortion of $AuCl_6$ octahedra. The $Au^{I}Cl_6$ octahedra are contracted in the c direction, while $Au^{III}Cl_6$ ones are elongated in this direction. This distortion is analogous to the mixed-valence bismuth oxide $BaBiO_3$ which is the parent compound of Cu-free superconductors $Ba_{1-x}(K \text{ or } Rb)_xBiO_3$[7] and $BaPb_{1-x}Bi_xO_3$[3]. Our very recent single crystal X-ray analysis of $Cs_2Au_2I_6$[8] shows that this complex belongs to $I4/mmm$ with a=8.284(1), C=12.092(2)Å, and Z=2 and is isostructural with $Cs_2Au_2Cl_6$. The mixed-valence state of

$Cs_2Au_2X_6$ may be regarded as the result of a CCDW or an on-site bipolaronic (insulator) state as well as that of $BaBiO_3$.

From another structural point of view, an anisotropy is present in the three-dimensional $-Au^{I}-X-Au^{III}-X-$ networks. In the c-direction is $\cdots X-Au^{I}-X\cdots Au^{III}\cdots$ and in the a_1a_2 plane $\cdots Au^{I}\cdots X-Au^{III}-X\cdots$. This anisotropy reflects the co-ordination forms and the valence states of Au. We have systematically studied the anisotropic charge-transfer interaction in the three-dimensional MX-networks of $Cs_2Au_2X_6$ by X-ray photoelectron spectroscopy (Chapter 3)[9] and ^{197}Au Mössbauer spectroscopy (Chapter 4).[10]

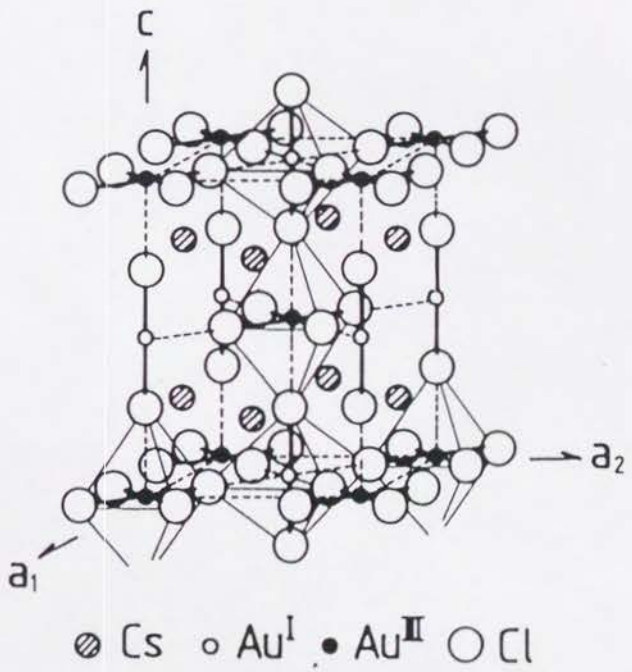

Fig. 1. Crystal structure of $Cs_2Au_2Cl_6$ [5, 6]. The crystal structure of $Cs_2Au_2I_6$ is isostructural with $Cs_2Au_2I_6$ [8].

Now, high-pressure experiments have proved to be of great interest in revealing the properties of various materials. The application of pressure is a useful tool which can alter physical properties owing to the consequent changes in the lattice parameters, energy-band structure and the energy of the various interactions between electrons or between electron and phonon.

We have recently shown[11] that $Cs_2Au_2I_6$ exhibits a pressure-induced semiconductor-to-metal (phase Ⅰ-to-phase Ⅱ) transition at 4.5 GPa and room temperature (r.t.) which has not been found for one-dimensional halogen-bridged mixed-valence metal complexes. It was also found that $Cs_2Au_2I_6$ undergoes a metal-to-metal (phase Ⅱ-to-phase Ⅲ) transition at 6.5 GPa and T～330 K. The resistivity of $Cs_2Au_2I_6$ at r.t. decreases rapidly by nine orders of magnitude down to the region of semimetal from ambient pressure (a.p.) to 5.5 GPa, and then increases from 5.5 GPa to 7.1 GPa. Many complexes of gold, whose empirical formulae suggest the presence of the Au^{II} state, have been shown to be Au^{I}-Au^{III} mixed-valence species and little is known as a true Au^{II} polynuclear complex. Therefore it is interesting whether the valence state of Au in the high-pressure metallic phases is +Ⅱ or not.

From the following interests, we have performed the structure analysis of $Cs_2Au_2I_6$ under high pressure;

(1) the mechanism of the metallization,

(2) the relationship between the electron system and the lattice system under high pressure,

(3) the origin of the minimum in the pressure-resistance curve near 5.5 GPa, and

(4) the valence states of Au in the high-pressure metallic states.

7-2 EXPERIMENTAL

$Cs_2Au_2I_6$ was prepared by the same method as described inthe paper[9] and recrystallized from concentrated HI solution. The single crystals obtained in this manner were crushed and pulverized for powder X-ray diffraction measurements.

The structure analysis of $Cs_2Au_2I_6$ was performed by energy-dispersive X-ray diffraction using the high-temperature and high-pressure apparatus, called MAX80[12], with synchrotron radiation(SR). SR was supplied by the accumulation ring (6.5 GeV,30 mA) for the TRISTAN main ring in the National Laboratory for High Energy Physics (KEK). The pressure vessel is a cubic anvil type which compresses a boron-epoxy cube with a teflon or a boron nitride sample capsule. It can generate a pressure of 7 GPa and a temperature of 1800 K. The anvils used were made of tungsten

carbides having 6 mm on edge of square face. As a fluid pressure-transmitting medium in the teflon capsule, ethanol or fluorinert (No.FC70) was used. Diffracted X-ray was detected by a handy solid-state detector (pure Ge) mounted on the arm of the goniometer. The mean measuring time was about 17 min. The pressure was determined by the lattice constants of NaCl. The position and intensity of each diffraction peak were obtained by least-squares Gaussian fitting to its profile. The lattice parameters were determined by least-squares fits to the measured positions of reflections where $2\theta = 2.9 \sim 4.3^{\circ}$.

7-3 PRESSURE DEPENDENCE OF THE LATTICE CONSTANTS

The diffraction patterns of $Cs_2Au_2I_6$ were measured at various pressures up to 6.8 GPa. The crystal system at the pressure range of 0-6.8 GPa and at r.t. was tetragonal. Figure 2 shows the observed lattice constants of a and c. Figure 3 shows the observed relative volume with respect to that at a.p.(V_o = 829.81 $\AA^3$). As seen in Figure 2, a gradual contraction of the c axis was observed with increasing pressure up to 5.5 GPa. At the pressure of about 5.5 GPa, the lattice constant of c increases discontinuously. This indicates the Au-Au distance elongates along the c-axis.

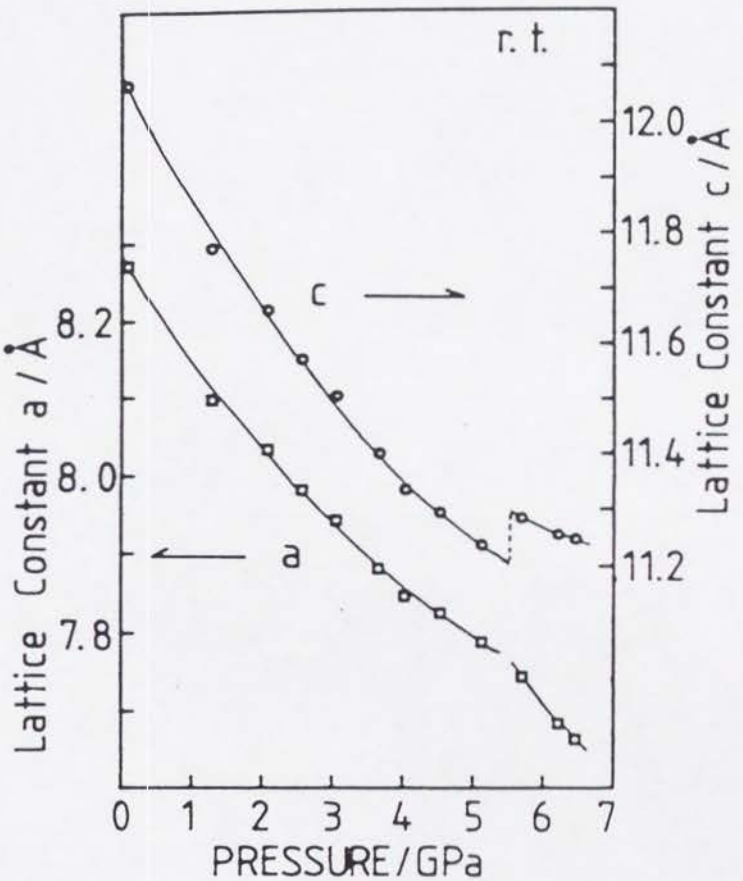

Fig. 2. Pressure dependence of the lattice constants of $Cs_2Au_2I_6$.

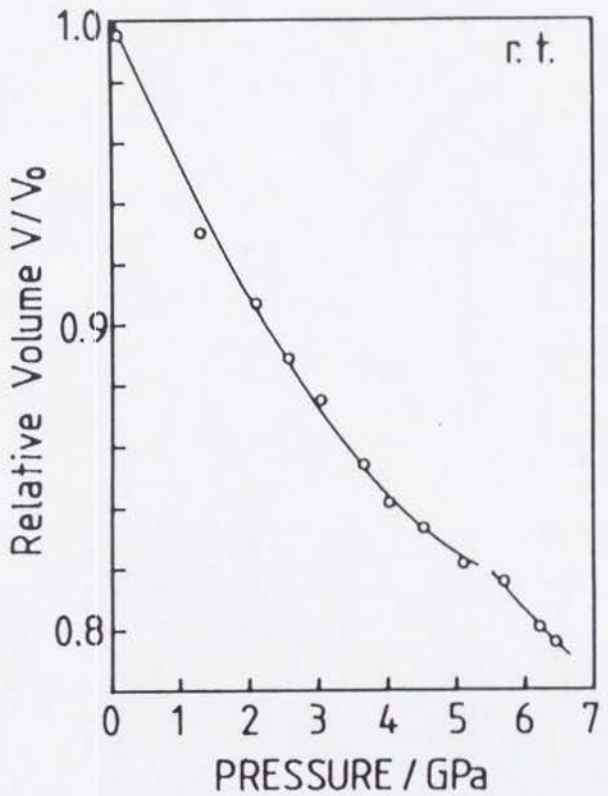

Fig. 3. Pressure dependence of the volume of $Cs_2Au_2I_6$. The volume is normalized by that at a.p.

Above this transition pressure, rather slower gradual contraction of c axis was observed. Also seen in Figure 2 is a gradual contraction of the a axis with increasing pressure. Above 5.5 GPa, however, rather faster contraction was observed. In the case of the relative volume shown in Figure 3, an appreciable discontinuous jump was not observed near the transition point. However, as described below, the transition at 5.5 GPa was found to be a first-order transition. This transition takes place when V/V_o becomes 0.82.

7-4 PRESSURE-INDUCED JAHN-TELLER TRANSFORMATION AT 5.5 GPa

Figure 4 displays the key reflections 004 and 220 of the tetragonality in the region of the high-pressure metallic state (phase Ⅱ) observed at several pressures in a process of compression around the transition pressure, where 2θ = 3.56°. The new diffraction peak marked with the triangle ▽ indicating the appearance of the high-pressure phase (phase Ⅱb) was observed at 5.7 GPa and the 004 reflection in the low-pressure phase (phase Ⅱa) diminished at 6.5 GPa. The reflection index of phase Ⅱb can be based on the tetragonal lattice, as well as that of phase Ⅱa. The coexistence of two phases seen at 5.7 GPa and 6.2 GPa is due to the nature of

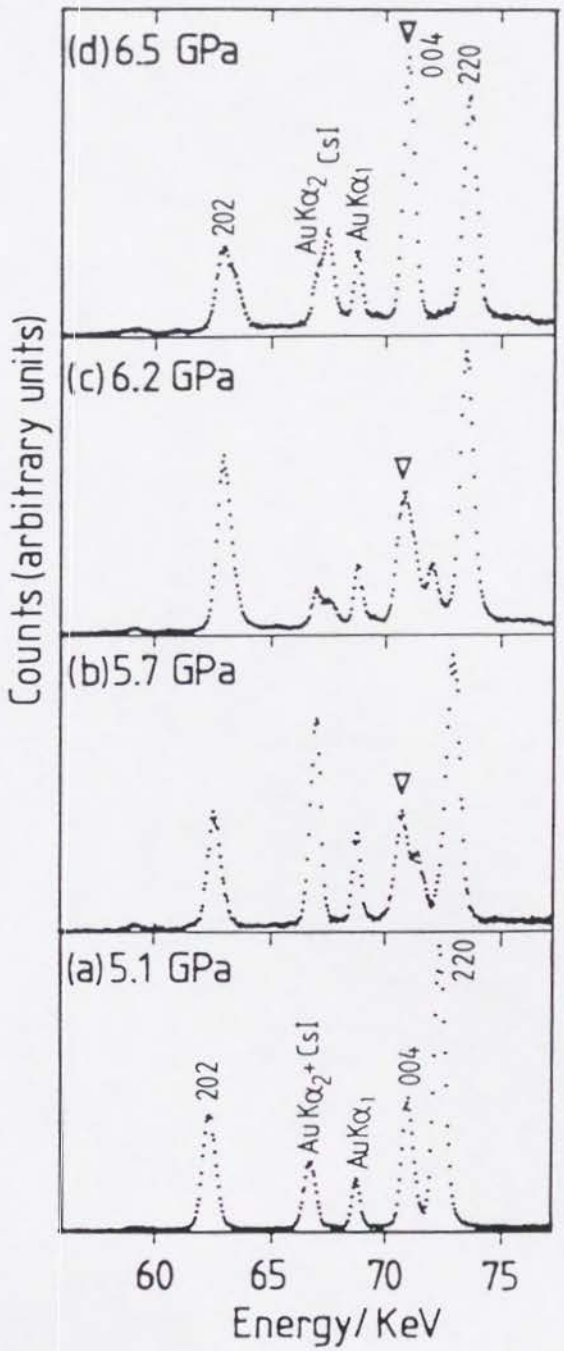

Fig. 4. The energy-dispersive X-ray diffraction profiles for the metallic phase II of $Cs_2Au_2I_6$ (a) at 5.1, (b) at 5.7, (c) at 6.2 and (d) at 6.5 GPa. Here $2\theta = 3.56°$.

the first-order phase transition, as well as the pressure distribution in the sample, which is expected to be small for the pressure-transmitting medium ethanol. For energy-dispersive X-ray diffraction method, Bragg's law is

$$Ed = hc/2\sin\theta = \text{constant}.$$

Hear E is the peak energy, d is the interplanar spacing, h is Plank's constant, c is the velocity of light and θ is the Bragg angle. Therefore, the fact that the new 004 peak appears in the lower-energy side of the 004 reflection of low-pressure phase shows that the Au-Au distance along the c-axis elongates discontinuously at the pressure of about 5.5 GPa. Consequently, $Cs_2Au_2I_6$ undergoes a pressure-induced first-order tetragonal-to-tetragonal phase transition at about 5.5 GPa and r.t. This transition would relate to the resistance minimum observed at about 5.5 GPa[11]. The resistance minimum[13] and the discontinuous increase of the reflectivity at 0.6 eV[14] observed for $Cs_2Au_2Cl_6$ at about 10~11 GPa might be due to the similar phase transition.

7-5 REALIZATION of A RARE GOLD-II VALENCE STATE UNDER HIGH PRESSURE

Figure 5 shows the axial ratio $\sqrt{2}a/c$ observed in the whole pressure region as a function of pressure. The ratio $\sqrt{2}a/c$

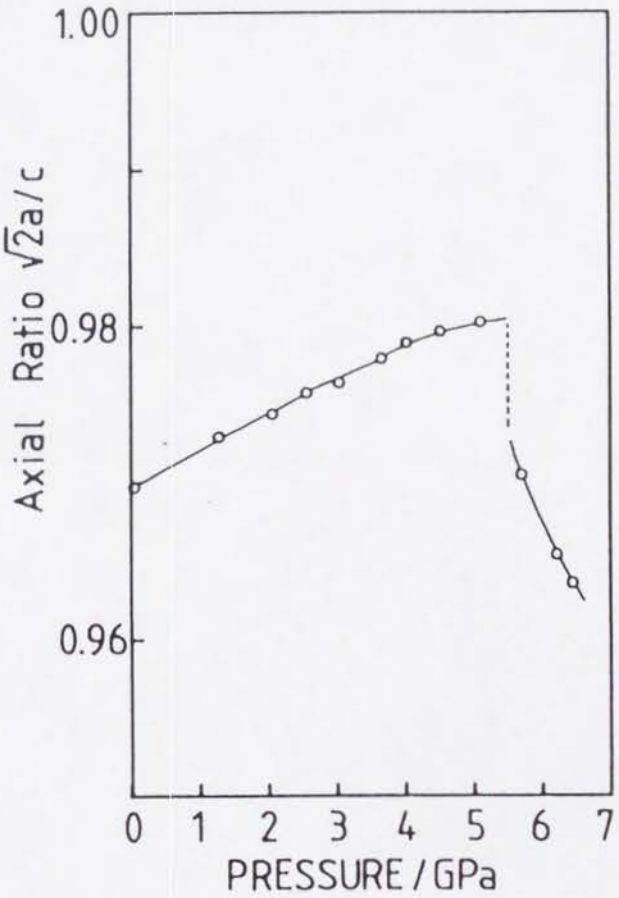

Fig. 5. Pressure dependence of the axial ratio $\sqrt{2}a/c$ of $Cs_2Au_2I_6$.

indicates the distortion of the tetragonal lattice. The cubic lattice is realized at $\sqrt{2}$ a/c = 1. The axial ratio $\sqrt{2}$ a/c increases from 0.969 up to 0.980 between a.p. and 5.1 GPa, while it decreases rapidly from 0.970 down to 0.964 between 5.7 GPa and 6.5 GPa. This change implies that the structural

anisotropy decreases from a.p. to about 5.5 GPa and increases inversely from about 5.5 GPa to 6.5 GPa. In other words, as pressure is increased, the 3-D correlation between the Au ions becomes stronger below about 5.5 GPa and the 2-D correlation becomes stronger above about 5.5 GPa. With increasing pressure, the charge-transfer interaction between Au^{I} and Au^{III} through the bridging iodine is expected to become stronger (*i.e.* the intersite transfer energy of electron becomes stronger) and therefore the difference in the oxidation states between Au^{I} and Au^{III} would become smaller. Consequently, the structural anisotropy in this mixed-valence system is expected to decrease. However, if the valence state of Au becomes +II ($5d^{9}$), the lowering in symmetry of AuI_6 octahedra can be caused by the Jahn-Teller transformation. Hence, with increasing pressure both the valence states of Au^{I} and Au^{III} approach the Au^{II} state that is co nsidered to be attained at 5.5 GPa. We note the pressure dependence of the ratio $\sqrt{2}a/c$ in $Cs_2Au_2I_6$ is very different from that in $Cs_2Au_2Cl_6$[15,16].

The X-ray powder diffraction of $Cs_2Au_2I_6$ at a.p. shows the crystal structure (I4/mmm) having a $\sqrt{2}a \times \sqrt{2}a \times 2c$ supercell. The geometrical difference between $Au^{I}I_6$ and $Au^{III}I_6$ octahedra produces weak superlattice reflections [e.g.(103), (211)] in the diffraction profile. When the bridging iodine is situated at the midpoint between Au ions, $\sqrt{2}a \times \sqrt{2}a \times 2c$ sup

ercell reflections diminish. In this case, it belongs to the space group P4/mmm of a perovskite structure having an a × a × c unit cell. The (103) and (211) superlattice reflections were observed to some appreciable extent up to the transition point of 5.5 GPa. But with increasing pressure up to this point, the intensities of (103) and (211) tended to decrease. This implies the bridging iodine shifts to the symmetrical position between the Au^{I} and the Au^{III} sites with increasing pressure. However in the present work, it could not be concluded whether the diffraction pattern of the high-pressure metallic state (phase Ⅱb) is the body-centered tetragonal Bravais lattice (I4/mmm) or the primitive tetragonal Bravais lattice (P4/mmm), because of the partial decomposition due to the partial dissolution of $Cs_2Au_2I_6$ into the transmitting medium ethanol;

$$Cs_2Au_2I_6 \longrightarrow 2CsI + 2Au + 2I_2.$$

In the case of using BN powder as a solid pressure-transmitting medium for the analysis of the phase Ⅲ described below, the decomposition did not take place. Above 5.5 GPa, the reflection peak (111) of solid iodine was located at the energy position[17] where, if exists, the superlattice peak (103) of $Cs_2Au_2I_6$ lies. However the appreciable peak (211) was not observed above 5.5 GPa. In order to obtaining more detailed structure of phase Ⅱb, further X-ray studies are indispensable.

7-6 CUBIC PHASE AND METASTABLE PHASE

The diffraction pattern of the high-pressure and high-temperature metallic state (phase Ⅲ) at 6.8 GPa and 440 K is satisfactorily explained by the space group Pm3m with a=5.370(5)Å. Figure 6 shows the diffraction patterns observed at 6.8 GPa and at several temperatures in a process of heating. As temperature is increased, the intensities of the (002),(112), and (004) reflections decrease without the change in their energy positions. At 440 K these reflections diminish completely. The reflections due to the interplanar spacing in the a_1a_2 plane ($\perp$ c-axis) remain unchanged in this process. This shows the Au-Au distance along the c-axis contracts discontinuously and becomes equal to that in the a_1a_2 plane at the transition temperature. From mentioned above, $Cs_2Au_2I_6$ undergoes a temperature-induced first-order tetragonal-to-cubic phase transition at 6.8 GPa and T$\sim$ 350 K. This phase transition can be interpreted as follows. In the high temperature, due to the entropy term the free energy of the cubic phase is lower than that of the distorted one. Therefore, as the temperature is raised, the Jahn-Teller distorted phase undergoes a transformation of crystal lattice into the cubic phase. In this phase Ⅲ,

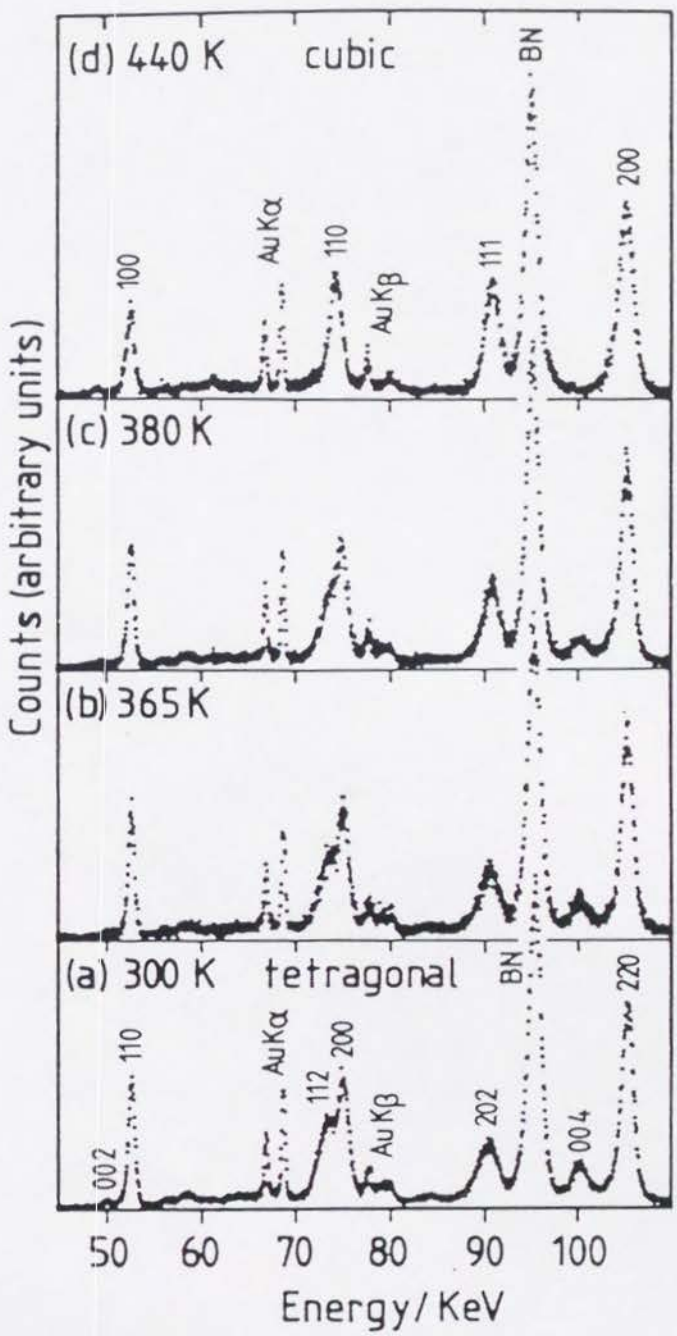

Fig. 6. The energy-dispersive X-ray diffraction profiles for $Cs_2Au_2I_6$ at 6.8 GPa in a process of heating (a) at 300, (b) at 365, (c) at 380 and (d) at 440 K. Here $2\theta = 2.51°$.

it is concluded that the oxidation state of Au^{II} is realized.

The crystal structure after decreasing temperature down to r.t. at 6.8 GPa is assigned to the same space group Pm3m with a=5.373(3)Å [Figure 7(a)], and moreover, the structure after the release of pressure at r.t. is also assigned to Pm3m with a=5.871(12)Å [Figure 7(b)] which is close to the value (5.858 A) of $a/\sqrt{2}$ in the tetragonal phase of $Cs_2Au_2I_6$ at a.p. and r.t. After increasing temperature up to 380 K at a.p. and decreasing it down to r.t., the structure of this sample was the original tetragonal space group I4/mmm [Figure 7(c)]. Consequently, the metastable cubic phase converts into the stable tetragonal phase by heating. In fact, the metastable cubic phase showed a broad exothermic peak in the differential-scanning-analysis (DSC) curve near 335 K (Figure 8). From the above mentioned results, it is concluded that the phase Ⅱ b-to-phase Ⅲ transition is a first-order tetragonal-to-cubic phase transition and the phase Ⅲ can be obtained as a metastable phase.

Figure 9 shows the schematic variation in the crystal field splitting of e_g orbital accompanied by the shift of bridging iodine to the midpoint between the Au^{I} and Au^{III} sites and by the tetragonal-to-cubic phase transition. At the pressure of 4.5 GPa where the energy gap becomes zero, the occupied $5dx^2-y^2$ band of Au^{I} (valence band) and the

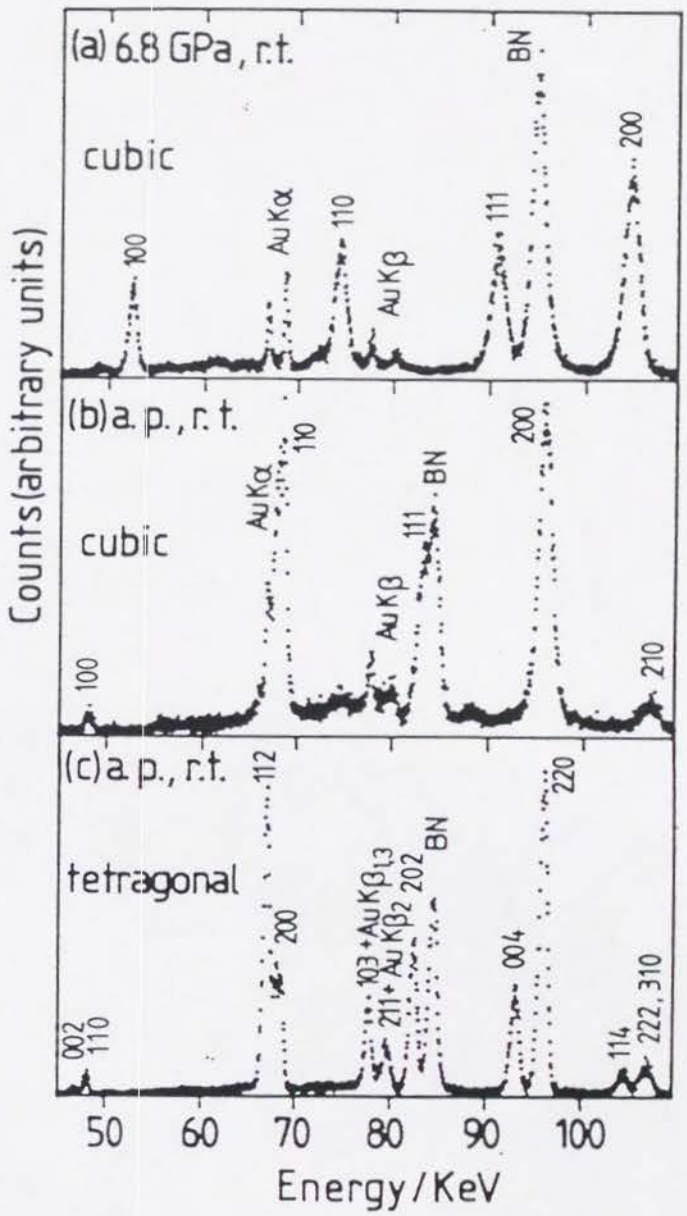

Fig. 7. The energy-dispersive X-ray diffraction profiles for $Cs_2Au_2I_6$ (a) after decreasing temperature down to r.t. at 6.8 GPa, (b) after the release of pressure at r.t., and (c) after heating the sample of (b) up to 380 K and cooling it down to r.t. at a.p. Here $2\theta = 2.51°$.

unoccupied $5dx^2-y^2$ band of Au^{III} (conduction band) overlap a little each other, which is responsible for the semiconductor-to-metal transition. In the pressure region of 4.5-5.2 GPa the bridging iodine is not located yet at the midpoint of the distance between the two golds, because of the existence of the discernible superlattice reflections. This implies that $Cs_2Au_2I_6$ is still a mixed-valence and semimetal state. At the pressure of 5.5 GPa, the bridging iodine becomes situated at the midpoint and then $5dx^2-y^2$ bands of Au^{I} and Au^{III} degenerate and the conduction band is half-filled. It is interesting from the viewpoint of the two-dimensionality, the AuI_2 sheets of the a_1a_2 plane in which holes exist are analogous to the superconductively active CuO_2 sheets. In this case, on account of the valence state of Au is + II (d^9), $Cs_2Au_2I_6$

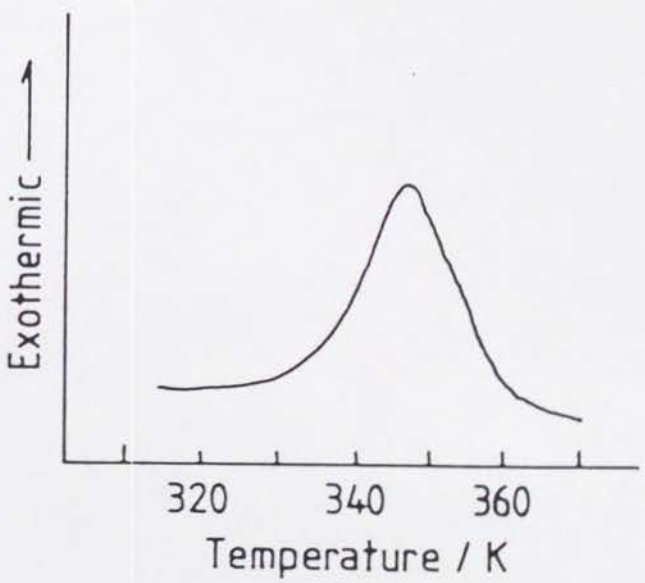

Fig. 8. Differential-scanning-analysis (DSC) curve for $Cs_2Au_2I_6$ after the release of pressure at r.t.

undergoes 'band Jahn-Teller' transition. This transition would be electronically driven by a high density of states at the Fermi energy, in which case a lowering of the lattice symmetry could open a gap at the Fermi energy, thereby lowering the free energy of the system. This transition might cause the increase of the resistivity in $Cs_2Au_2I_6$ observed above 5.5 GPa[11]. In the phase Ⅲ, it is considered that the conduction band is a three quarters-filled degenerate e_g band. Such successive transitions as mentioned above can be seen in Figures 10(a)-(d), which show the schematic projections of networks of AuI_6 octahedra.

7-7 INCONSISTENCIES BETWEEN HIGH-PRESSURE STUDIES OF $Cs_2Au_2Cl_6$

In connection with above mentioned results, we will refer to the inconsistencies between the studies about the mixed-valence state of $Cs_2Au_2Cl_6$ under high pressures. According to the high-pressure X-ray analysis[16] for $Cs_2Au_2Cl_6$, the bridging chlorine becomes located at the midpoint of the distance between the two golds at the pressure of 5.2 GPa and thereby the valence state of Au^{II} is realized at this pressure. But this conclusion appears doubtful. The resistance minimum is observed at about 11 GPa for

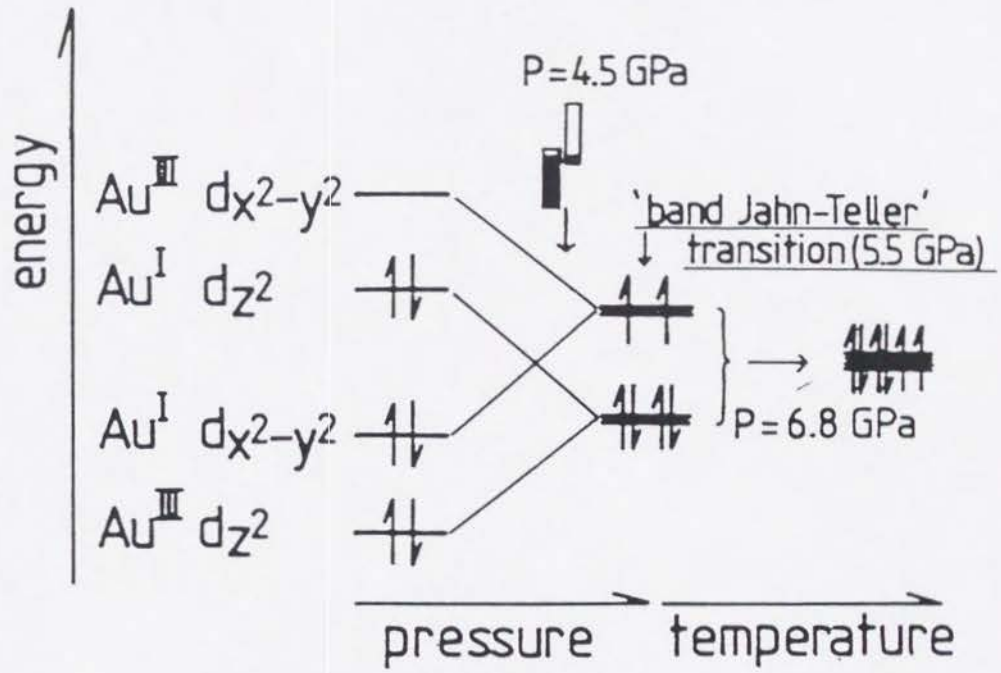

Fig. 9. Schematic variation in the crystal field splitting of e_g orbital accompanied by the shift of the bridging iodine to the midpoint of distance between the two golds and by the tetragonal-to-cubic phase transition.

$Cs_2Au_2Cl_6$[13], which is analogous to that observed at about 5.5 GPa for $Cs_2Au_2I_6$[11]. We suggest that $Cs_2Au_2Cl_6$ undergoes the same phase transition at about 11 GPa as does $Cs_2Au_2I_6$ at 5.5 GPa. In fact, discontinuous jump in the optical reflectivity of $Cs_2Au_2Cl_6$ is observed at about

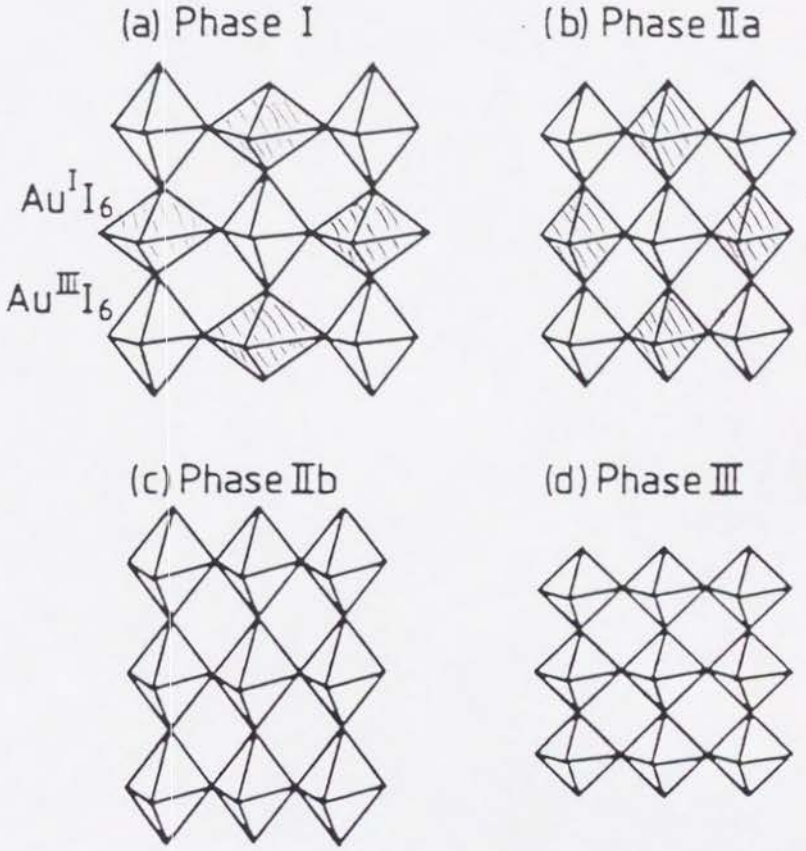

Fig. 10. Schematic projections of networks of AuI_6 octahedra (a) at a.p. in the phase I ($0 < P < 4.5$ GPa), (b) just below 5.5 GPa in the phase IIa ($4.5 < P < 5.5$ GPa), (c) just above 5.5 GPa in the phase IIb (P 5.5 GPa), and (d) in the phase III ($P = 6.8$ GPa, $T > 350$ K).

this pressure, which is considered to be due to some phase transition[14]. From these experimental results for $Cs_2Au_2Cl_6$ and our present work for $Cs_2Au_2I_6$, the valence state of Au^{II} in $Cs_2Au_2Cl_6$ would be achieved at the pressure of about 11 GPa. In order to promote a better understanding of the correlations between the mixed-valence state and the crystal structure, Raman, ^{197}Au Mössbauer, electrical conductivity at low temperatures using a single crystal[18], and band-structure calculation[19] for $Cs_2Au_2X_6$ (X=Cl,Br,I) under high pressure are indispensable and in progress.

7-8 CONCLUSIONS

We have shown that insulating mixed-valence complex $Cs_2Au_2I_6$ transforms gradually to a metallic state between ambient pressure and 4.5 GPa at room temperature. Also shown that $Cs_2Au_2I_6$ undergoes a metal-to-metal transition in a process of increasing temperature at 6.5 GPa. The present energy-dispersive X-ray diffraction study has revealed that $Cs_2Au_2I_6$ undergoes a pressure-induced first-order tetragonal-to-tetragonal phase transition at about 5.5 GPa and room temperature. At the transition pressure, the Au-Au distance elongates along the c-axis, which is due to the 'band Jahn-Teller' transition. The Au^{II} valence state

is considered to be realized at this pressure. This phase transition would relate to the minimum in the pressure-resistance curve near 5.5 GPa, previously reported. It was also found that $Cs_2Au_2I_6$ undergoes a first-order tetragonal-to-cubic phase transition at 6.8 GPa and T~50 K.

References

1. J. G. Bednorz and K. A. Müller, *Z. Phy.* B64, 189 (1986).
2. M. K. Wu, J. R. Ashburn, C. J. Torng, P. H. Hor, R. L. Meng, L. Gao, Z. J. Huang, Y. Q. Wang, and C. W. Chu, *Phy. Rev. Lett.* 58, 908 (1987).
3. A. W. Sleight, J. L. Gillson, and P. E. Bierstad, *Solid State Commun.* 17, 27 (1975).
4. D. E. Cox and A. W. Sleight, *Solid State Commun.* 19, 969 (1976).
5. N. Elliott and L. Pauling, *J. Am. Chem. Soc.* 60, 1846 (1938).
6. J. C. M. Tindemans-v. Eijndhoven and G. C. Verschoor, *Mater. Res. Bull.* 9, 1667 (1974).
7. L. F. Mattheiss, E. M. Gyorgy, and D. W. Johnson, Jr., *Phys. Rev.* B37, 3745 (1988).

   R. J. Cava, B. Batlogg, J. J. Krajewski, R. Farrow, L. W. Rupp, Jr., A. E. Wnite, K. Short, W. F. Peck, and T. Kometani, *Nature* (London) 332, 814 (1988).
8. N. Matsushita, H. Kitagawa, and N. Kojima, to be submitted for publication.
9. H. Kitagawa, N. Kojima, and T. Nakajima, *J. Chem. Soc., Dalton Trans.*, 3115 (1991)

10. H. Kitagawa, N. Kojima, and H. Sakai, *J. Chem. Soc., Dalton Trans.*, **3211** (1991)

11. N. Kojima, H. Kitagawa, T. Ban, F. Amita, and M. Nakahara, *Solid State Commun.* 73, 74. (1990).

12. O. Shimomura, *Physica*, 139 & 140B, 292 (1986).

13. R. Keller, J. Fenner, and W. B. Holzapfel, *Mater. Res. Bull.* 9, 1363 (1974).

14. H. Tanino, K. Syassen, Z. Wang, M. Hanfland, and K. Takahashi, Proc. 12th AIRAPT and 27th EHPRG Int. Conf. on High Pressure Science and Technology 17-21 July, Paderborn, F. R. Germany (1989).

15. P. Day, C. Vettier and G. Parisot, *Inorg. Chem.* 17, 2319 (1978).

16. W. Denner, H. Schulz, and H. D'Amour, *Acta Cryst.* A35, 360 (1979).

17. K. Takemura, S. Minomura, O. Shimomura, Y. Fujii, and J. D. Axe, *Phys. Rev.* B26, 998 (1982).

18 H. Kitagawa, N. Kojima, H.Takahashi and N.Mori, to be submitted for publication.

19 M. Shirai, personal communication.

CHAPTER 8

Electrical Conductivity and Its Anisotropy of Single Crystal $Cs_2Au_2I_6$ Under High Pressures and Low Temperature

8-1 INTRODUCTION

In 1974 R.Keller, *et al.* measured[1] the resistivity of the mixed-valence compound $Cs_2Au_2Cl_6$ at quasihydrostatic pressures up to about 12 GPa and temperatures down to about 10 K. They found a resistivity drop of about 9 decades and a semiconductor-to-metal transition at about 6 GPa. The semiconductor-to-metal transition was confirmed by a disappearance of energy gap. They estimated the energy gap at low temperatures below 150 K. However, even at 11 GPa a positive temperature coefficient $d\sigma/dT$ was observed in the region above 150 K. They explained this effect by the

additional contributions from thermally excited charge carriers. From this effect they suggested that the overlap of the Au^{I} valence band with the Au^{III} conduction band was still very small even at 11 GPa (*i.e.* semimetallic state). They considered that this overlapping bands were corresponding to the dz^2 band of Au^{I} and the dx^2-y^2 band of Au^{III}.

In the Chapter 6 we have shown, from the measurement of electrical conductivity of polycrystalline $Cs_2Au_2I_6$ pellet, that $Cs_2Au_2I_6$ exhibits a pressure-induced semiconductor-to-metal transition at 4.5 GPa and room temperature. Considering the anisotropy of the crystal structure in $Cs_2Au_2I_6$, we need measure the electrical conductivity using single crystals.

In the preceding chapter we will show that $Cs_2Au_2I_6$ undergoes a pressure-induced first-order phase transition at 5.5 GPa and room temperature. As the pressure is increased up to the transition pressure the geometries of $Au^{I}I_6$ and $Au^{III}I_6$ octahedra become more equivalent, and when those are equivalent and the electronic structure of Au approaches a d^9 valence state, the lowering in symmetry of AuI_6 octahedra is caused by the Jahn-Teller effect. Just below the transition pressure, the valence of Au atoms is considered to be vigorously fluctuating. Above the transition pressure electron-phonon interaction in this system, which should be

strong, can occur owing to the Jahn-Teller effect, while those owing to the mixed-valence effect below the transition pressure. Above the transition pressure, moreover, there is a possible effects of magnetism (S=1/2) in the $CsAuI_3$ system. It is interesting to explore the possible interactions between itinerant electrons and the effects mentioned above, and to explore the possibility of superconductivity in this system under high pressures.

From these reasons we have performed electrical conductivity experiments on single crystals $Cs_2Au_2I_6$ under hydrostatic high pressures and low temperatures.

8-2 EXPERIMENTAL

Figure 1 shows a schematic cross-sectional view of the high-pressure cryostat which has a Be windows for X-ray examination. The cubic-anvil dies were placed between the end of a pair of pressure transmitting columns. The anvils used were made of tungsten carbides having 4 mm on edge of square face. The backup block and the retaining die were hardened steels. Teflon sheets acting as lubricants and as electrical insulators were in place between anvil and die. In Figure 2 the internal configuration of a gasket with a Teflon cell is shown. We used a fluid pressure medium, a

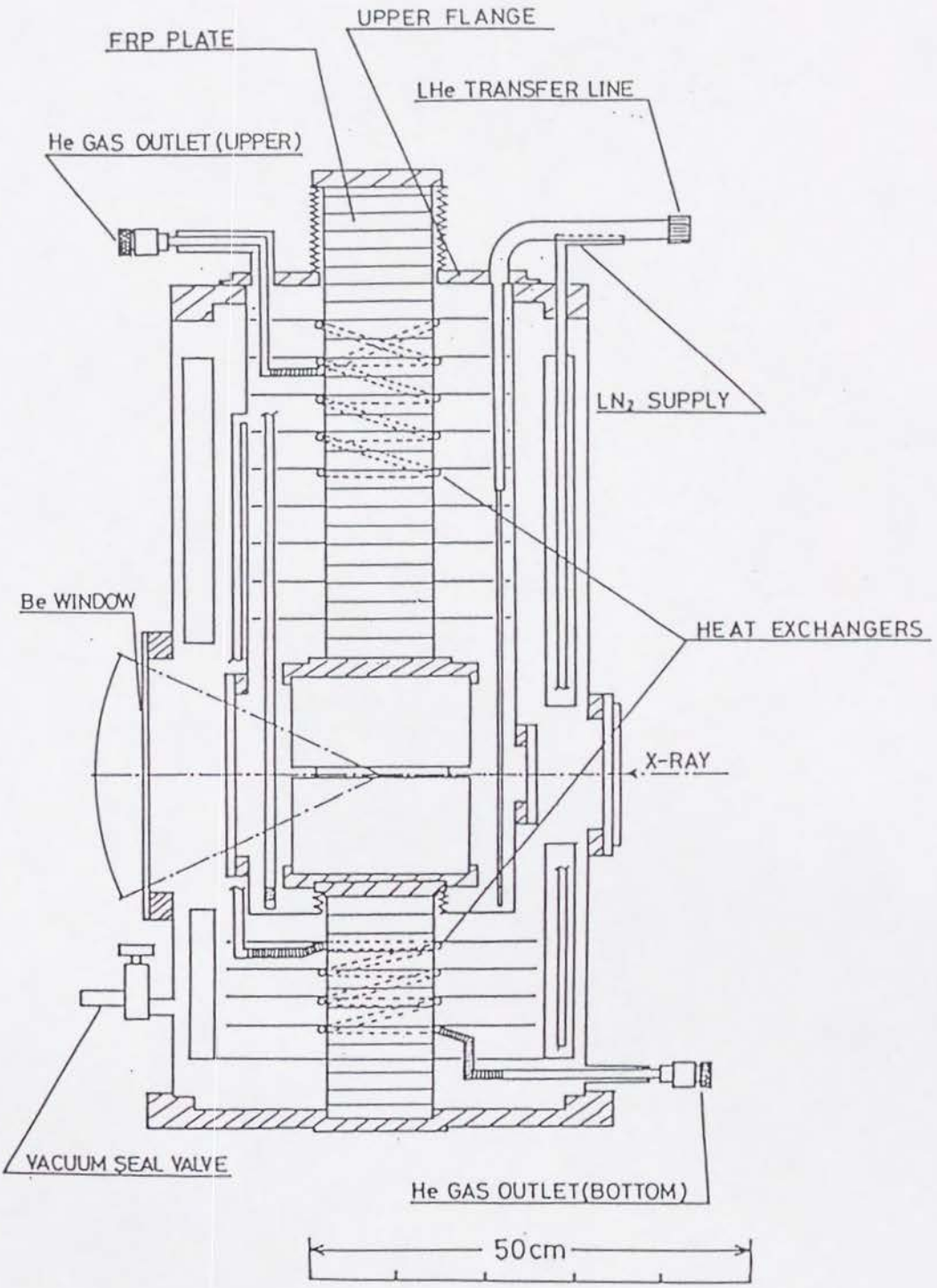

Fig.1 Cross-sectional view of high pressure cryostat

mixture of Fluorinert No.FC70 and No.FC77 (Sumitomo 3M Ltd.). The electrical resistivity was measured by the standard dc four probe technique. As electrical leads, 20μm in diam. gold wires (Mitsubishi Metal Corporation, Type MGM, 99.99%Au) were used with gold paint (Tokuriki Kagaku No.8560) contact on the surface of the specimen and connected to thin gold ribbons attached to backup blocks. We obtained a pressure calibration curve by the phase transitions of bismuth I-II(2.55 GPa), II-III(2.7 GPa), and III'-V(7.7 GPa). For experiments below room temperature, the force applied to the anvil was controlled not to change during the measurements upon cooling and heating runs after it was changed at room temperature. Judging from the differences of the resistivity or the dielectric constant of samples at room temperature between before and after the cooling run, the pressure below room temperatures was estimated to be kept constant within 3%. The temperature was measured with a calibrated Pt(Co) resistance thermometer placed near the sample. The heating rate was about 0.3 K/min. Typical size of single crystals used was 0.4 × 0.4 × 0.8 mm. In this way, the high-pressure apparatus works at pressures up to 8 GPa and at low-temperatures down to 4.2 K under reasonably hydrostatic conditions and without any damages in the single crystals. Detail of this system were described elsewhere.[2]

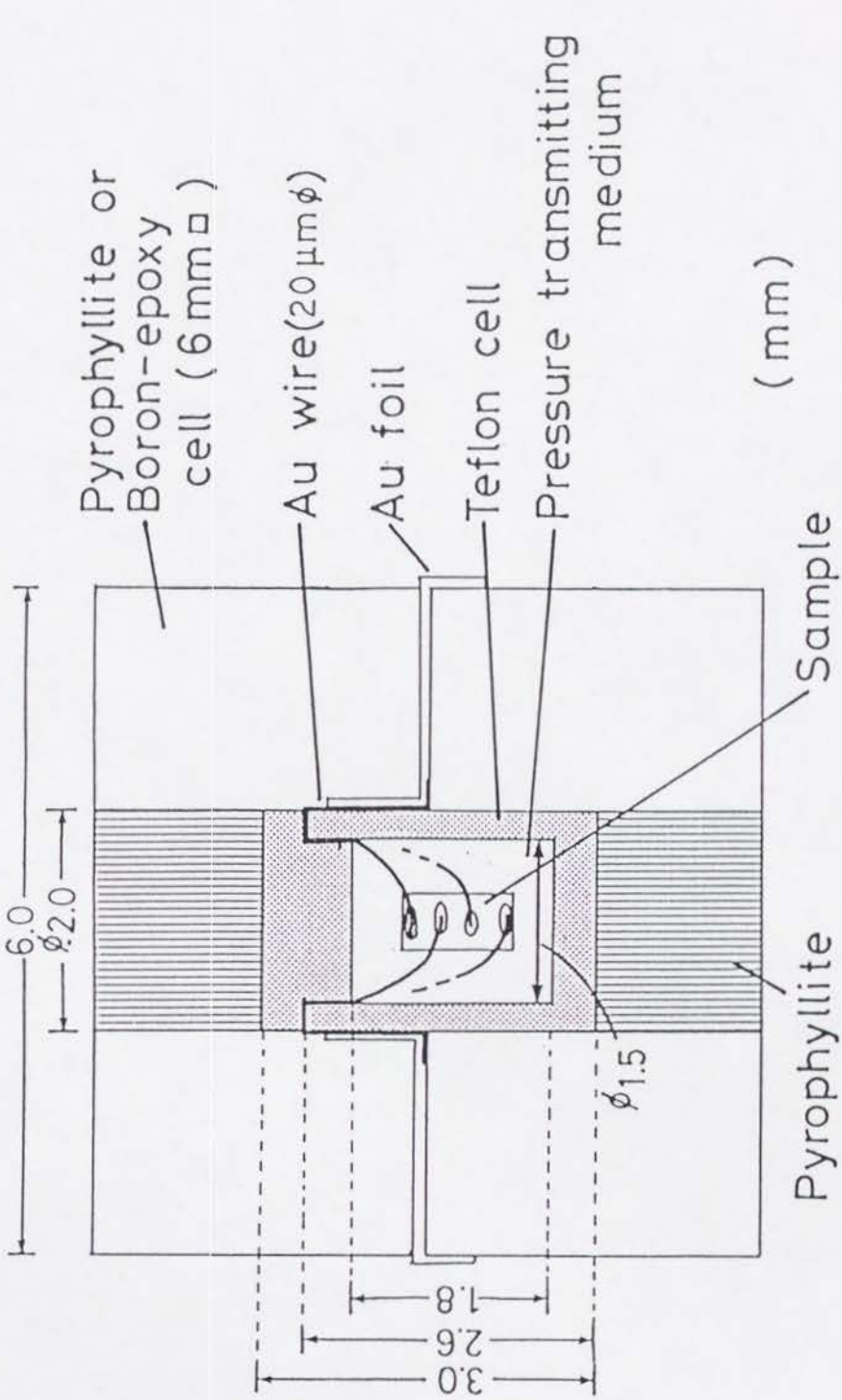

Fig.2 Internal configuration of gasket with Teflon cell

8-3 PRESSURE DEPENDENCE OF THE RESISTIVITY AT ROOM TEMPERATURE

Figure 3 shows the pressure dependence of the resistivity parallel and perpendicular to the c-axis at room temperature. As the pressure is increased, the insulating mixed-valence complex $Cs_2Au_2I_6$ transforms gradually to a metallic state. The resistivity at room temperature decreases by ten orders of magnitude down to the region of metal from ambient pressure to 5.0 GPa. On the other hand, just above 5.0 GPa, each of //c and $\perp$c resistivities increases rapidly by four orders of magnitude up to 3Ω·cm. Also in the process upon decreasing pressure (Figure 4), the drastic change of resistivity($\perp$c) were reproduced completely. This reproducibility indicates highly hydrostatic conditions and no damages in the single crystal. In the region of 0-2 GPa the resistivity ($\perp$c) is smaller than that //c. However above 2 GPa, an apparent anisotropy in the resistivity was not observed at room temperature. The drastic resistance jump around 5 GPa can be related to the structural phase transition observed at 5.5 GPa. The energy-dispersive X-ray diffraction study (Chapter 7) has revealed that $Cs_2Au_2I_6$ undergoes a pressure-induced first-order tetragonal-to-tetragonal phase transition at about 5.5 GPa and room temperature. At the transition

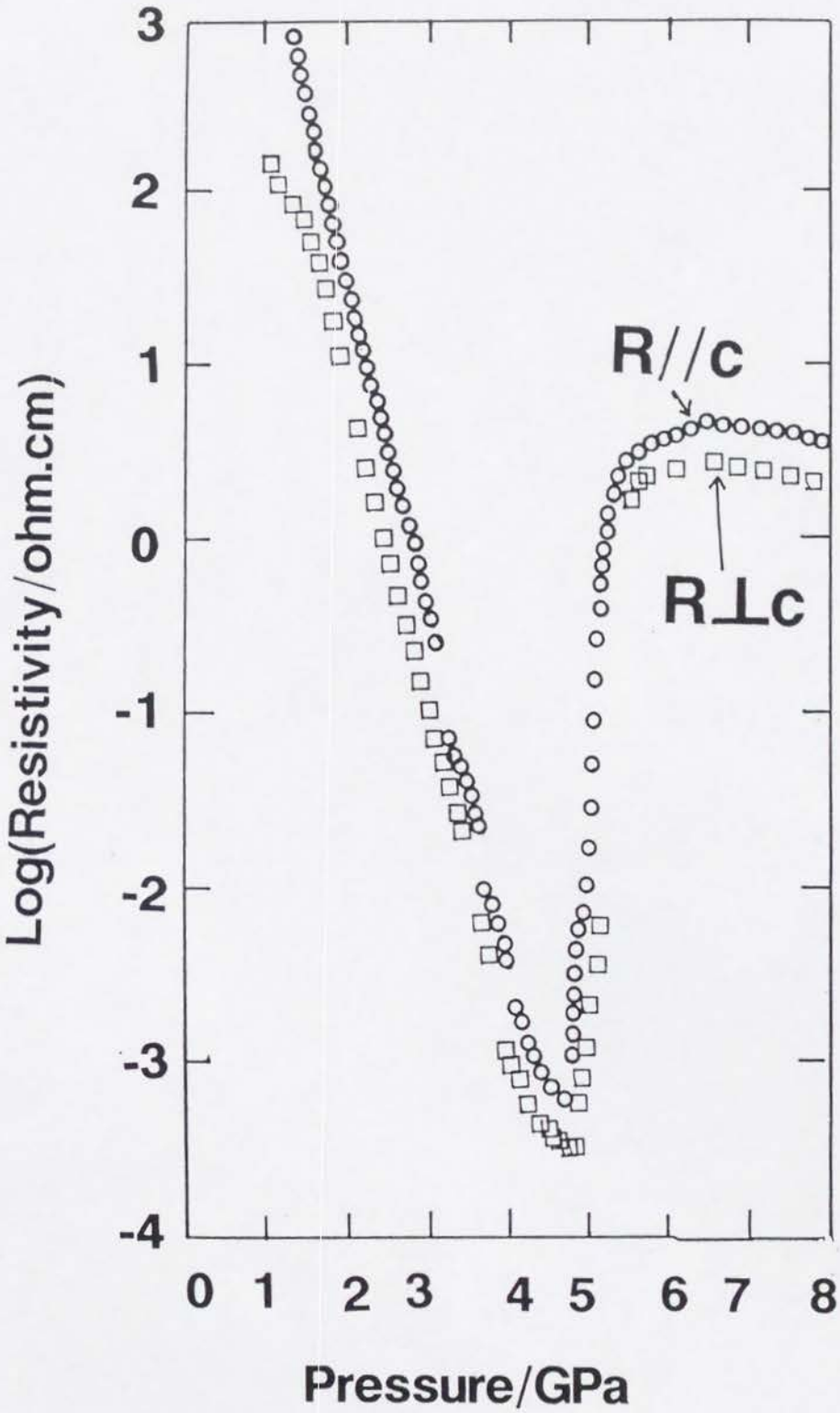

Fig.3 Pressure dependence of the resistivity parallel and perpendicular to the c-axis at room temperature.

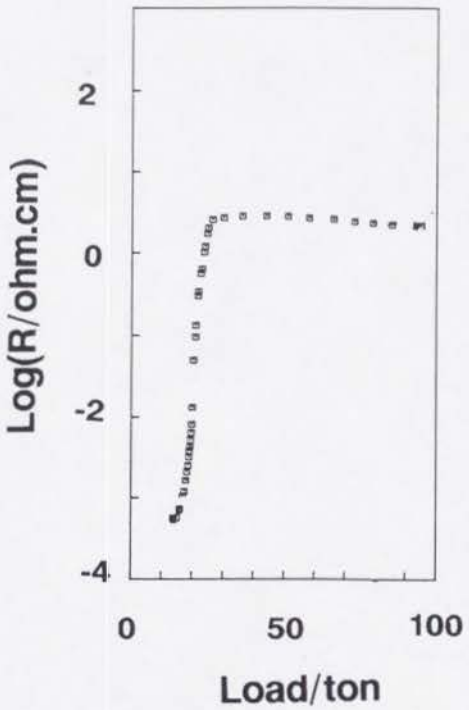

Fig.4 Pressure dependence of the resistivity perpendicular to the c-axis on decreasing pressure at room temperature

pressure, the Au-Au distance elongates along the c-axis. There is a small difference in the transition point of pressure between the measurements of electrical conductivity and X-ray analysis, which is due to the error in the pressure calibrations. The followings are considered to be responsible for the drastic resistance jump around 5 GPa. One is a "band Jahn-Teller" transition. This transition is electronically driven by a high density of states at the Fermi energy, in which case a lowering of the lattice

symmetry could open a gap at the Fermi energy, thereby lowering the free energy of the system. Such a band Jahn-Teller transition occurs in the Chevrel-phase superconductors,[3] giving rise to a transition from a metallic superconducting state to a semimetallic or semiconducting state which has been observed by varying pressure or composition. Another is a CDW transition. According to the very recent band-structure calculation using the APW method by M.Shirai,[4] the Fermi surface of the hypothetical primitive tetragonal Bravais lattice (*P4/mmm*) has a strong nesting feature for q=(π ,π ,π).

8-4 TEMPERATURE DEPENDENCE OF ELECTRICAL RESISTIVITY BELOW 5.5 GPa

Figure 5 shows the temperature dependence of electrical resistivity perpendicular to the c-axis for $Cs_2Au_2I_6$ at various pressures. The resistivity anomalies were observed. Under the pressure of 3.8 GPa, the resistivity peak and shoulder lie at 200 K and 235 K, respectively. The resistivity decreases monotonically with temperature down to 20 K and increases in reverse below 20 K. The resistivity under the temperature range of 100-200 K is proportional to T^2. The broad peak and the shoulder in ρ near 200 K is

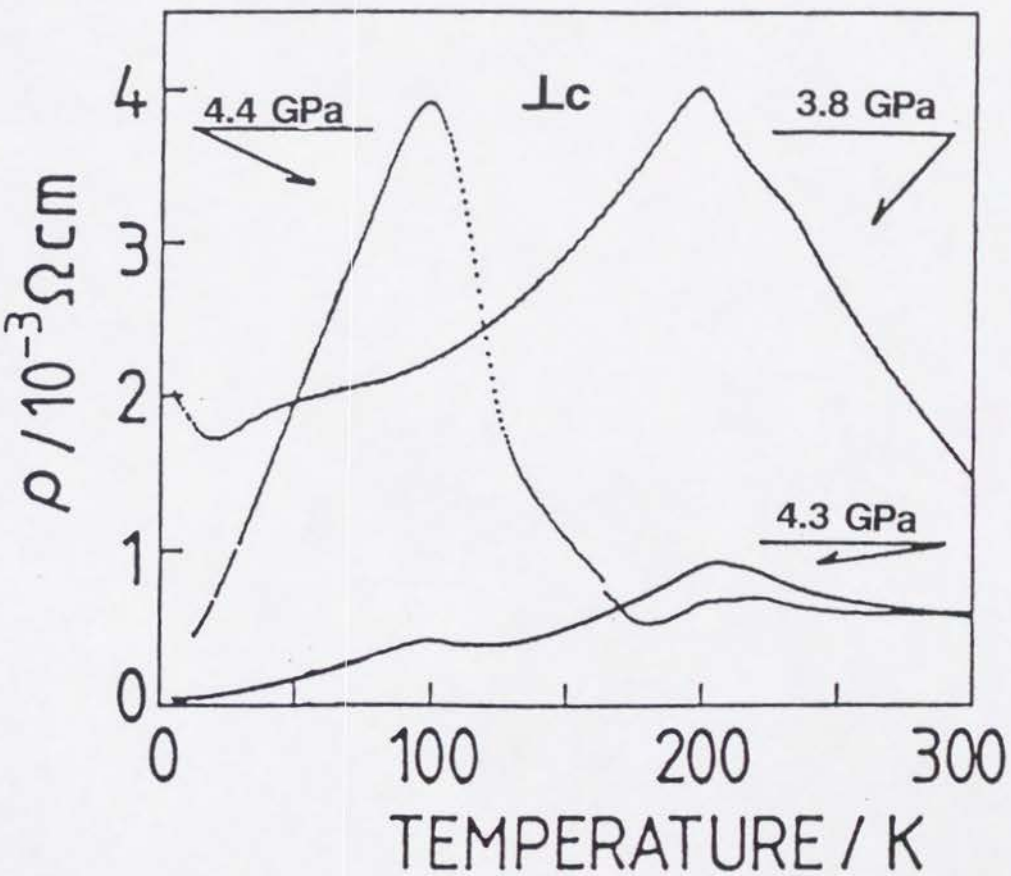

Fig.5 Temperature dependence of electrical resistivity perpendicular to the c-axis for $Cs_2Au_2I_6$

reduced with increasing pressure up to 5.0 GPa. However the peak and shoulder temperatures do not change with increasing pressure. On the other hand near 100 K, a new resistivity anomaly was observed at 4.3 GPa. This anomaly is rapidly and strongly induced with increasing pressure up to 5.0 GPa. This behavior implies the linkage to the resistance jump and the phase transition just above 5.0 GPa. This peak temperature also do not change with increasing pressure. In the low temperature region below 50 K, the resistivities at 4.5 and 5.0 GPa are not proportional to T^6 but to $T^{1.7}$ and $T^{1.4}$, respectively. This shows that the temperature dependence of electrical resistance at very low temperature can not be explained by a simple electron-phonon interaction in homogeneous three-dimensional solids. Electron-electron interactions and the Umklapp process in electron-phonon interaction may be considered in addition to the anisotropical lattice dynamics. The deviations from the T^6 law in polyvalent metals and transition metals have been explained in consideration of these effects.

The observed peak of resistivity does not show any sharp structure which might be an indication of a phase transition. If the peaks of the resistivity is associated with CDW transition the sluggish change of the resistivity must reflect fluctuations, which are not compatible with metallic behavior of resistivity below the peak temperature. In a low-

dimensional material most parts of the Fermi surface vanish at the CDW transition and it becomes non-metallic behavior below the peak temperature. In a three-dimensional system, however, the Fermi surface can not vanish completely at the CDW transition. At the transition where the Fermi surface is partially vanishing, the anisotropy of resistivity is expected to decrease below the transition temperature because the more anisotropic parts of the Fermi surface vanish. The surviving Fermi surface is less anisotropic and transport properties are more isotropic compared with those of the normal state. In order to examine the anisotropy of the resistivity, the electrical resistivity parallel to the c-axis was also measured.

The resistivity anomalies illustrated in Figures 6 and 7 were observed parallel to the c-axis as well as perpendicular to it. The behavior of these anomalies against the pressure is similar to those perpendicular to the c-axis. Under the pressure of 3.0 GPa, metallic behavior of the resistivity was observed in the temperature range of 100-200 K. The resistivity anomaly, which was observed for the resistivity of $\perp$ c under 3.8-4.4 GPa, was observed also for that of //c under this pressure. Below 100 K the resistivity increases slowly. Also under 3.5 GPa the anomaly near 200 K was observed. At this pressure the temperature region, where $Cs_2Au_2I_6$ indicates metallic behavior, extends to lower

temperature. The resistivity increases below 40 K but decreases below 7.5 K. The origin of this decreasing is not clear. At 4.0 GPa $Cs_2Au_2I_6$ indicated metallic behavior to the low temperature of 4.2 K. A small resistivity shoulder lie at the higher-temperature side of the anomaly of 200 K. Under 4.1 GPa a new anomaly was observed at 220 K while the anomaly at 200 K diminished. The coexistence of the anomaly at 200 K and the shoulder at 220 K under 4.0 GPa implies the nature of the first-order transition. A new anomaly was induced near 100 K at 4.2 GPa. Above 4.4 GPa the anomaly at 220 K diminished and that around 100 K was enhanced. A new giant anomaly, which lied as a shoulder near 120 K at 4.4 GPa, was observed at 130 K under 4.5 GPa. The temperature dependence of the resistivity at 4.7 GPa is shown in Figure 8. The lack of the upper side in the resistivity curve around 130 K is due to a mistake under the measurement that the voltagemeter was set at the lower voltage range than the suitable one. This anomaly was rapidly and strongly enhanced by one hundred times up to the transition point of 5.5 GPa, which implies the linkage to the resistance jump and the phase transition of 5.5 GPa.
In the low temperature region below 50 K, each of the resistivities at 4.5 and 5.0 GPa is proportional to $T^{1.6}$.

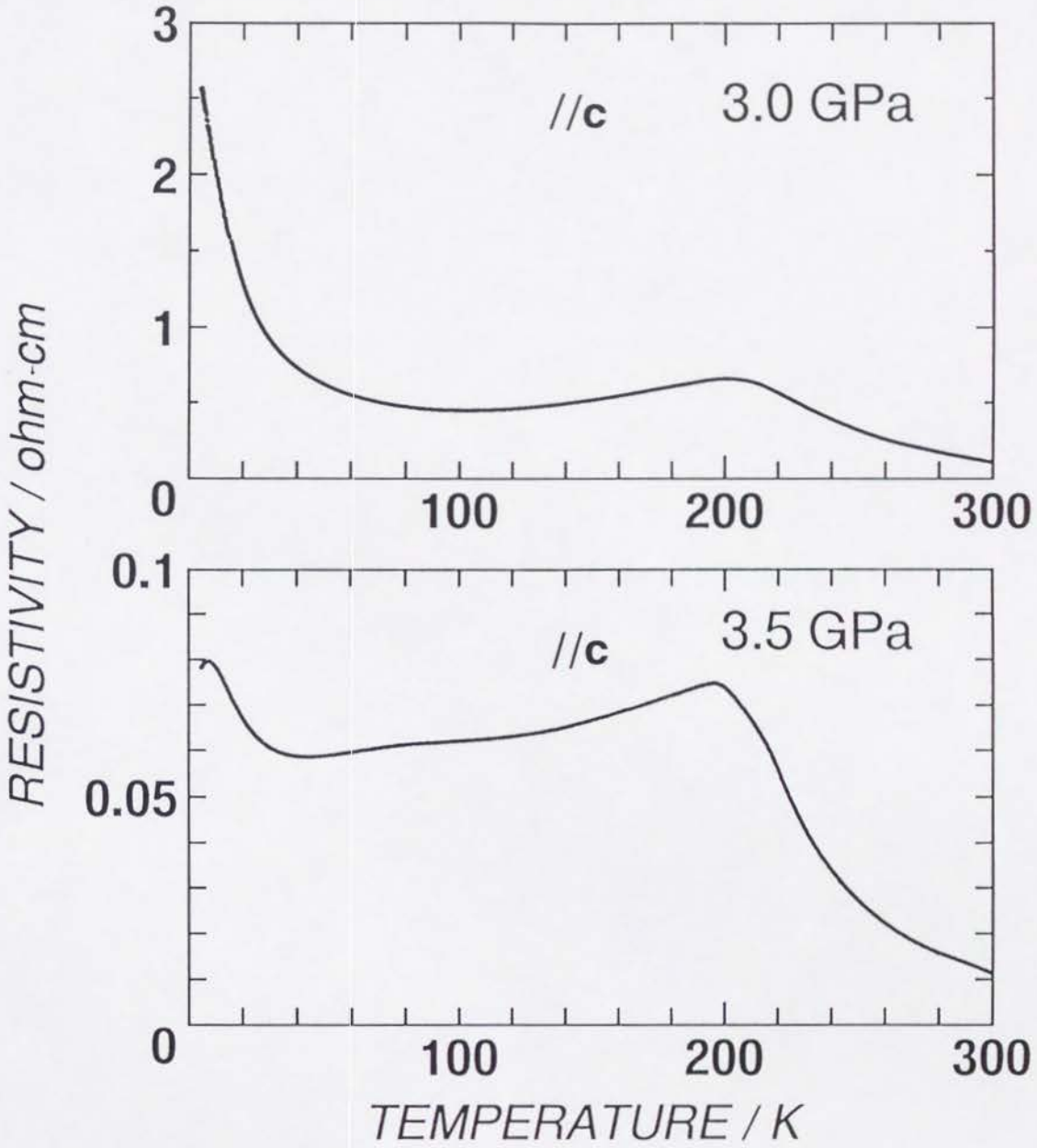

Fig.6 Temperature dependence of the electrical resistivity parallel to the c-axis below 4.0 GPa

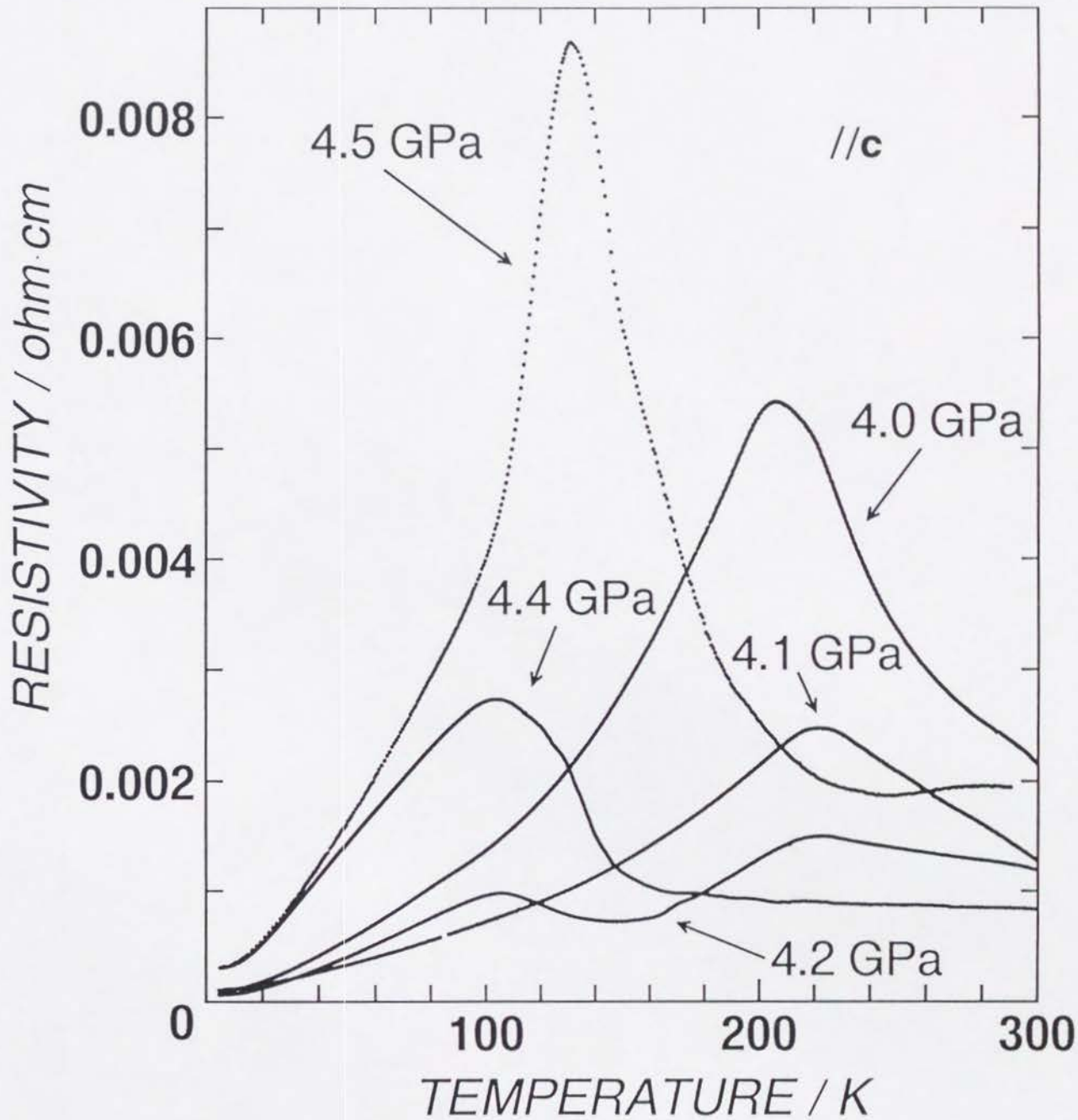

Fig.7 Temperature dependence of the electrical resistivity parallel to the c-axis between 4.0 and 4.5 GPa

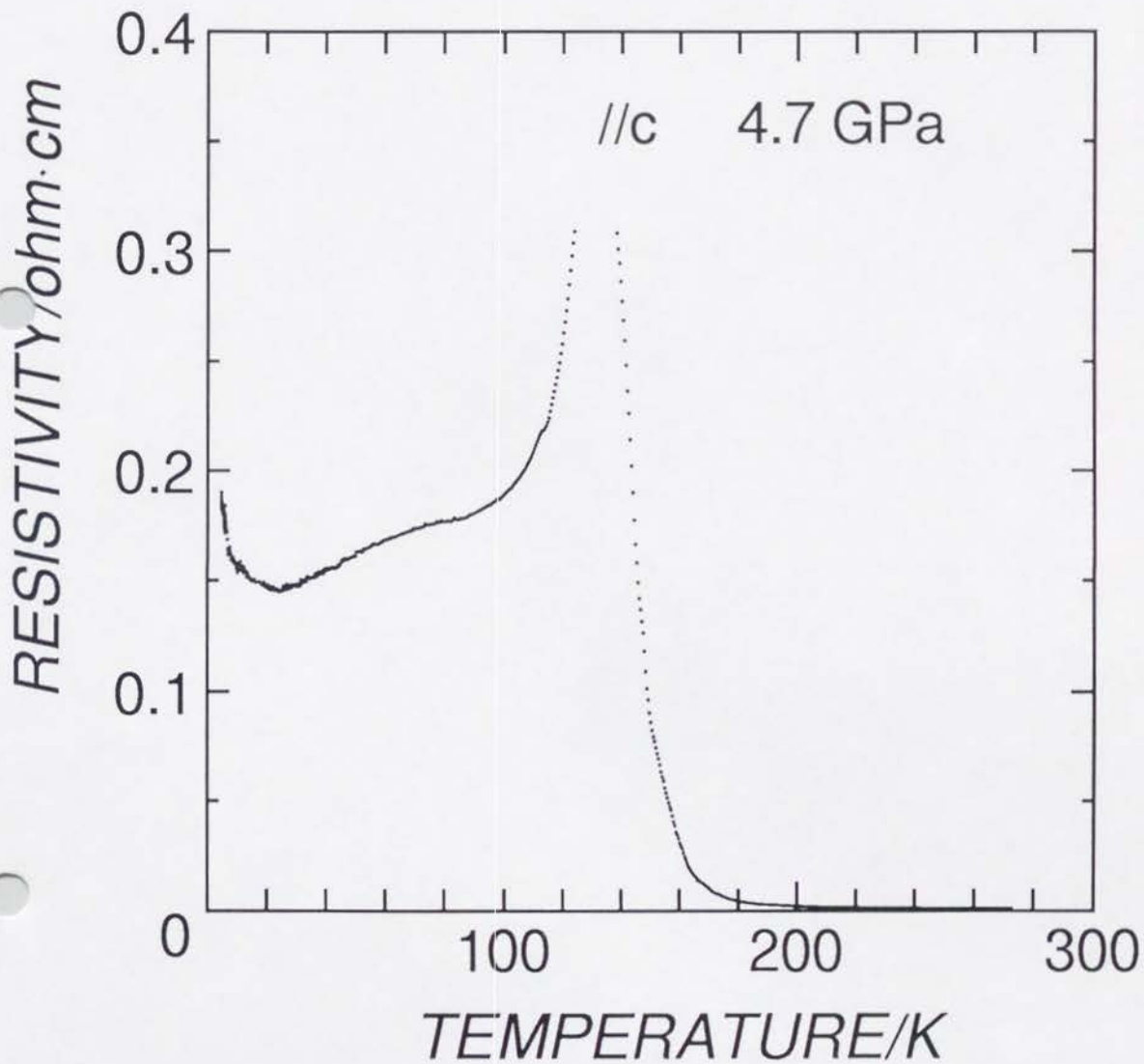

Fig.8 Temperature dependence of the electrical resistivity parallel to the c-axis at 4.7 GPa

8-5 TEMPERATURE DEPENDENCE OF ELECTRICAL RESISTIVITY ABOVE THE TRANSITION OF 5.5 GPa

Figure 9 shows the temperature dependence of the electrical resistivity parallel and perpendicular to the c-axis at the pressure above 5.5 GPa. At the pressure of 5.5 GPa where the first-order structural phase transition occurs, the resistivity at room temperature become larger by four orders of magnitude than that below the transition pressure and the resistivity increases with decreasing temperature. However, as can be seen in Figure 9, the behavior of the conduction is not activation type. From the coefficient $d(\log\sigma)/d(1/T)$, we estimate the temperature dependence of an apparent energy gap Eg, as shown in Figure 10. The apparent energy gap is not constant throughout the experimental temperature. And the $Eg(\perp c)$ is almost equal to 0 below 120 K. These might mean that this high-pressure phase is unusual semimetal where the carrier concentration is dependent on the temperature.

We have not yet determined the source of the anomalous peaks observed in electrical resistivity of $Cs_2Au_2I_6$ under high pressure and low temperature. The variety of the measurements under high pressure (>3 GPa) and low temperature was very small and the method is limited to special one. However, in order to reveal the origin of the resistivity

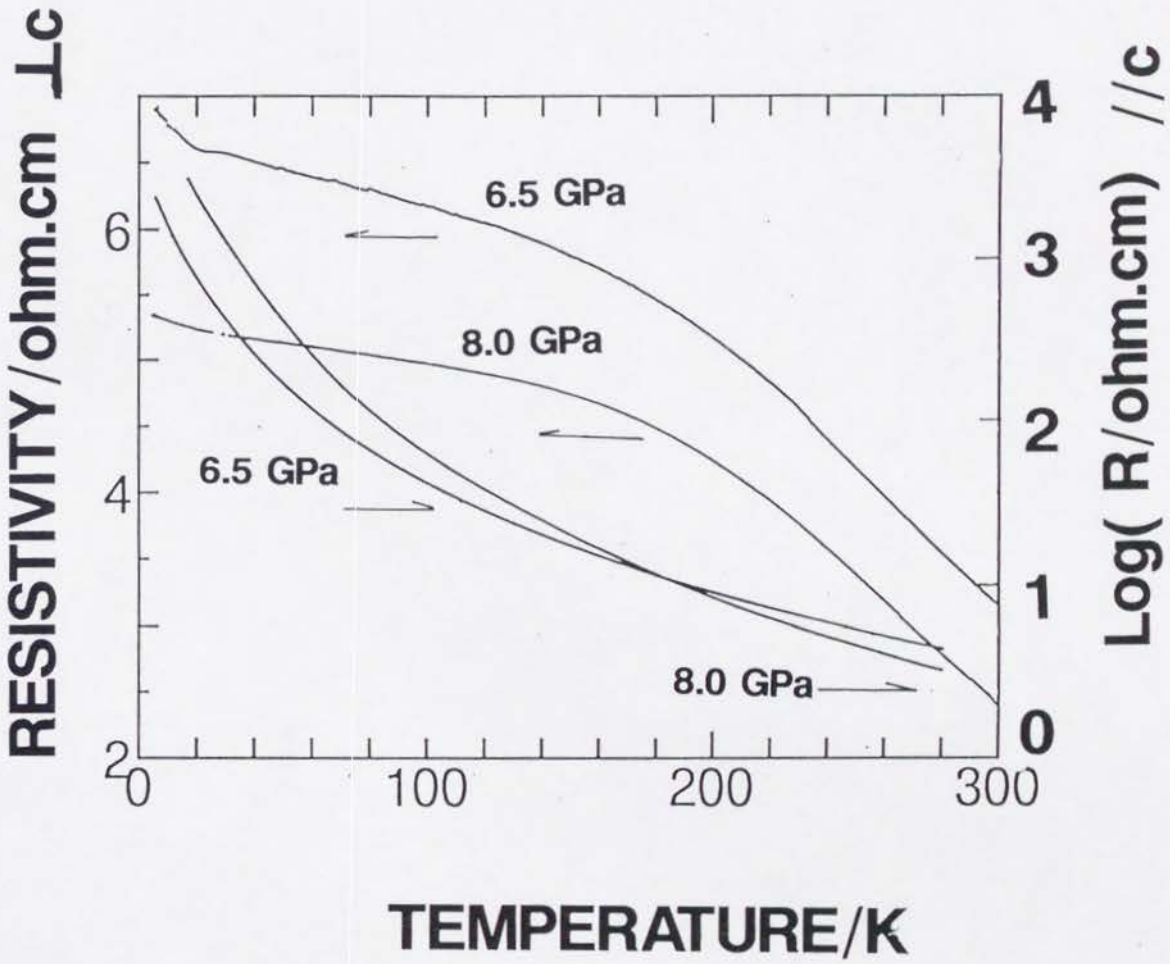

Fig.9 Pressure dependence of the electrical resistivity parallel and perpendicular to the c-axis above 5.5 GPa

anomalies, the followings are possible. It is well known that an anomaly associated with CDW is easily suppressed by doping impurities, as observed in $NbSe_3$ and in many dichalcogenides. It is necessary to investigate the effect of impurity on the resistivity anomaly. It is also well known that in a CDW system depinned CDW under high electric fields can contribute to conductivity. We need to measure the electric field and frequency dependences of conductivity associated with resistivity anomalies in $Cs_2Au_2I_2$ in order to reveal whether the anomalies are due to the dynamical response of a collective mode or not. Moreover the X-ray diffuse scattering measurement using a diamond anvil cell, will reveal whether the resistivity anomalies are associated with the CDW formation or not. The X-ray single crystal analysis will reveal whether the resistivity anomalies are associated with some structural phase transition or not. The resonance Raman spectroscopy will afford the information about the phonon energies and the soft modes associated with the phase transition. The ^{197}Au Mössbauer spectroscopy will provide the visual information about the mixed-valence state and the magnetic order. If the magnetic fluctuation is present under high pressure and low temperature, the line-width of Mössbauer spectra might reflect it. The reflectance spectra can afford an information about charge carriers. Recent APW band structure calculations for the hypothetical high-

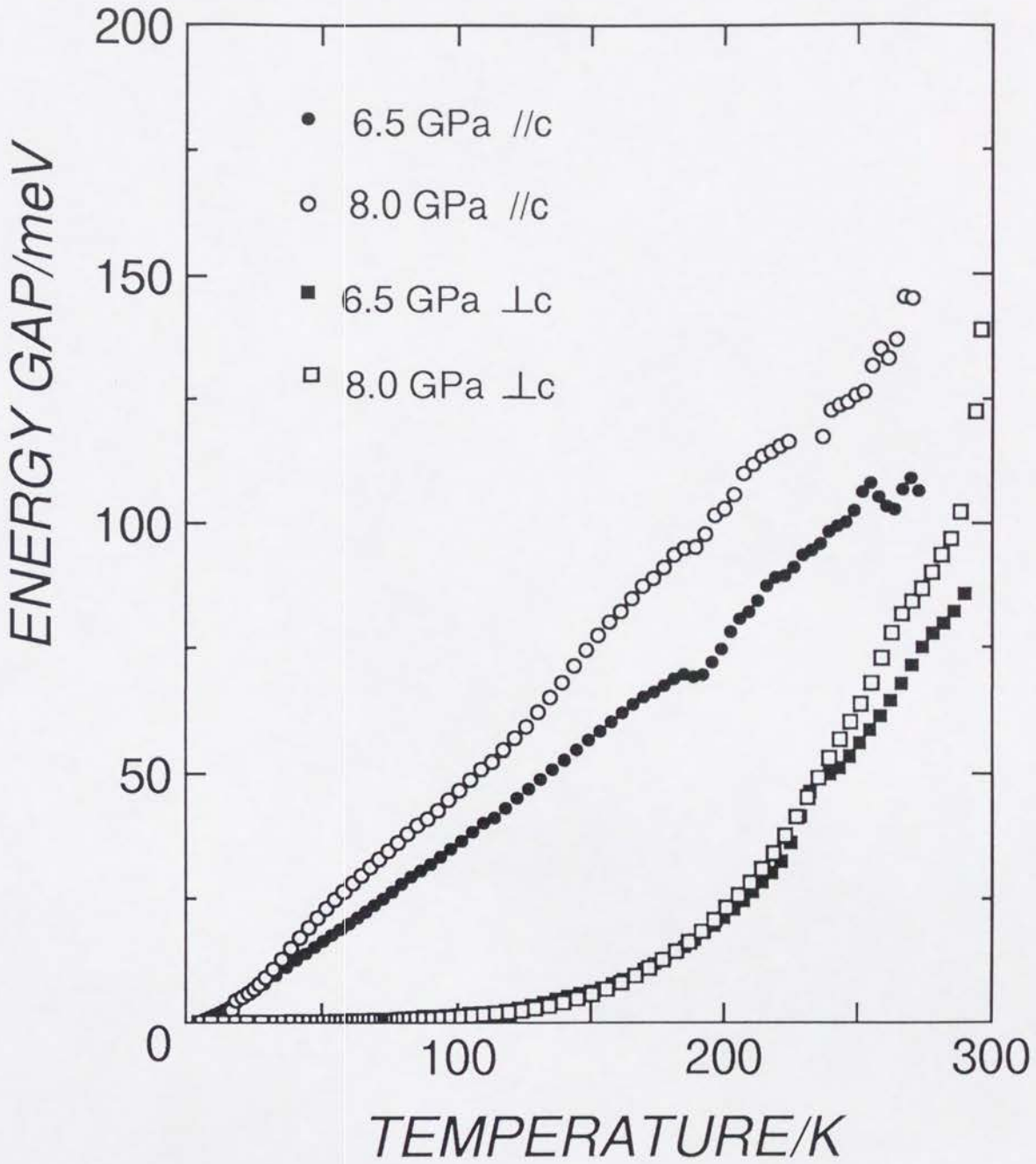

Fig.10 Temperature dependence of apparent energy gap *Eg*

pressure phases will useful some informations.

8-6 CONCLUSIONS.

We have observed strongly pressure-dependent resistivity anomalies of $Cs_2Au_2I_2$ under hydrostatic pressure condition. We have also observed drastic resistance jump around 5 GPa which may be associated with the "band Jahn-Teller" transition or the CDW transition. Further studies are required in $Cs_2Au_2X_2$ (X=Cl,Br,I) to establish the nature of the probable phase transitions at low temperature and high pressure.

References

1 R.Keller,J.Fenner and W.B.Holzapfel, *Mater.Res.Bull.*, 9 (1974) 1363.

2 N.Mori,H.Takahashi and Y.Miyane, *Kotaibutsuri* 25 (1990) 185.

3 R.Baillif,A.Dunand,J.Muller and K.Yvon, *Phys.Rev.Lett.*47 (1981) 672

4 M.Shirai, personal communication (1990).

CHAPTER 9

General Conclusions

The mixed-valence states in $Cs_2Au_2X_6$ (X=Cl,Br,or I) have been systematically studied. Each conclusion of the present studies is described in the end of each chapter.

According to the present studies, the mixed-valence state, 2-D charge-transfer interaction, electronic and crystal structures, electrical conductivity, and phase transitions under high pressure in this system have been clarified. However not a few properties under high pressure remain unexplained and unexplored. In order to reveal the origin of the resistivity jump at 5.5 GPa, the giant anomaly at 130 K, and other anomalies, the scattering mechanism, concentration, and sign of conduction carrier, magnetism, and phonon structure under high pressure, we need to measure the electric field and frequency dependences of conductivity, the X-ray diffuse scattering, the X-ray single crystal diffraction, the resonance Raman spectra, the reflectance spectra, and ^{197}Au Mössbauer spectra under high pressure. On the other hand the superconductivity was not observed

for $Cs_2Au_2I_6$ under up to 8 GPa and down to 4.2 K. Very recently Valma[1] proposed a theoretical model with negative *U* effect, which gives insulating behavior near half-filling and superconductivity farther from it in agreement with the properties of $Ba(PbBi)O_3$ and $(BaK)BiO_3$, as shown in Figure 1. From this model the replacement of Cs or Au with Ba or Hg is considered to be significant chemical decoration for the modifying the band filling.

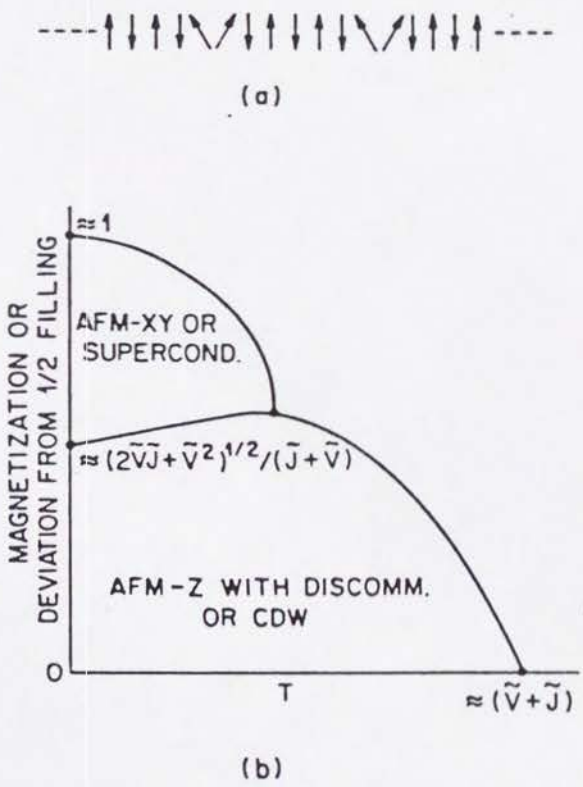

FIG. 1. (a) Schematic picture of the ground state of the anisotropic anitferromagnetic Heisenberg model at fixed magnetization for low magnetization. A down spin corresponds to a doubly occupied site, an up sign to a vacant site, and a tilted spin to a linear combination of the two in the original model. (b) Schematic phase diagram.

Recently $Cs_2Ag^{I}Ag^{III}Cl_6$ was synthesized[2], which is isomorphous with $Cs_2Au_2X_6$. We strongly desire the materials researches based on these mixed-valence systems. The author shall be happy to have a lot of researches (especially theorist) who become interested in this system and have lots of suggestions and discussions.

References

1 C.M.Varma, Phys.Rev.Lett. 61 (1988) 2713.

2 J.Bill, K.Lerch and W.Laqua, Z.anorg.allg.Chem. 589 (1990) 7.